ANALYSIS AND BEHAVIOUR OF COUPLED NON-LINEAR SHEAR WALLS

Vladimir Gocevski

A Thesis

in

The Department

of

Civil Engineering

Presented in Partial Fulfillment of the Requirements
for the degree of Master of Engineering at
Concordia University
Montreal, Quebec, Canada

August 1977

ABSTRACT

ANALYSIS AND BEHAVIOUR OF COUPLED NON-LINEAR SHEAR WALLS

Vladimir Gocevski

This study formulates an approximate method and presents results of an investigation of coupled non-linear shear walls. Symmetric T-section shear wall structures are subjected to lateral loading increasing monotonically up to overall collapse.

Non-linear behaviour is assessed by the introduction of an elasto-plastic continuum to model connecting beams. Plastic hinges are permitted to develop progressively up to and including overall collapse. The latter may include base hinges in the walls as well as total or partial yielding of the connecting medium. Attention is directed toward identifying properties of geometry and strength for the coupled system, as well as beam and system ductility requirements at overall collapse.

Additional parameters have also been investigated. These include moment-axial force interaction in the walls and effect of the loading pattern. The latter consists of a triangularly-distributed load together with a concentrated load at the top of the structure.

RESUME

ANALYSE ET COMPORTEMENT DES MURS DE REFEND NON-LINEAIRE

Vladimir Gocevski

Cette étude développe une méthode approximative d'analyse pour les murs de refend non-linéaires. Les structures des murs de refend symétriques de section en T sont chargées de forces latérales augmentant de façon uniforme jusqu'à la rupture totale.

Le comportement non-linéaire est, par la suite, étudié en introduisant, dans le modèle mathématique du système, un milieu élasto-plastique continu et homogène. Le développement progressif des rotules plastiques est ensuite permis jusqu'à la rupture totale. Ce dernier peut inclure, non seulement des rotules dans le bas des murs de refend, mais aussi la rupture totale ou partielle du milieu de liaison. Une attention spéciale est portée sur l'identification de la corrélation des propriétés de géométrie, de résistance, et de la ductilité des poutres et des murs de refend.

L'étude détaillée d'autres paramètres a aussi été effectuée. Ceci inclut l'action réciproque des moments-forces axiales dans les murs et l'influence de la manière de chargement. Ce dernier consiste d'un chargement, croissant uniformément de façon triangulaire avec une force concentrée au sommet de la structure.

ACKNOWLEDGEMENTS

The author wishes to express his sincere thanks to his supervisor, Dr. O. A. Pekau, for his help and guidance, as well as for his encouragement and valuable advice during the course of this study and the writing of this thesis.

Many thanks as well to Dr. K. M. Ashraful Alam, structural engineer at Hatch, Ouellette and Associates, for helpful suggestions and discussions that have contributed to this work.

Thanks are also due to Mr. Noah Steward for the typing of this thesis.

Finally, the author would like to give special thanks to his wife and family for their patience and fortitude in foregoing the normal fruits of life during this period.

TABLE OF CONTENTS

ENGLISH - INTERNATIONAL SYSTEM (SI)

CONVERSION FACTORS

The list below gives the conversion factors for all Imperial units used in this study.

TO CONVERT	TO	MULTIPLY BY
inches (in.)	millimetres (mm)	25.4
feet (ft)	metres (m)	0.3048
square inches (sq. in.)	square millimetres (mm^2)	645.16
square feet (sq ft)	square metres (m^2)	0.0929
pound-force (lbf)	newton (N)	4.4482
kip (k)	newton (N)	4448.2
pound-force-inch (lbf-in.)	newton-metre (Nm)	0.1130
pound-force-foot (lbf-ft)	newton-metre (Nm)	1.3558
kip/inch (k/in)	kilonewton/metre (KN/m)	175.1
pound-force/square inch (psi)	newton/square metre (N/m^2)	6895

LIST OF TABLES

LIST OF FIGURES

LIST OF SYMBOLS

Symbols are defined where they first appear in the text. Those symbols which appear often in the text are defined below.

A_1, A_2 = cross-section area of wall 1 and 2, respectively

d_1, d_2 = width of wall 1 and 2, respectively

E = modulus of elasticity

H = overall structure height

h = story height

I_1, I_2 = cross-section moment of inertia for wall 1 and 2, respectively

$I_o = I_1 + I_2$

I_b = coupling beam moment of inertia

$M_o(\xi)$ = total cantilever moment produced by the external lateral load

$M(\xi)$ = bending moment on an arbitrary cross-section through both walls

$M_1(\xi)$, $M_2(\xi)$ = bending moments in walls 1 and 2, respectively

M_u = ultimate bending moment

P_u = ultimate compression force

p = percent of tensile reinforcement

p_b = value of p producing balanced condition

$q(\xi)$ = distributed shear in the lamina

q_η, q_ζ = distributed shear in the lamellae at η and ζ

q_u = ultimate coupling shear capacity of connecting beams

s = clear span of the coupling beams

$T(\xi)$ = axial force generated in walls

T_η, T_ζ = values of $T(\xi)$ at η and ζ, respectively

t = shear wall thickness

V = total base shear

W = triangular component of the lateral load (non-linear behaviour)

W_e = triangular component of the lateral load (elastic behaviour).

W_y = value of triangular component of lateral load at the onset of yielding

W_u = triangular component of the ultimate lateral load

x = distance measured from top of the structure

Z = a stiffness parameter

α = geometric stiffness parameter

γ = a stiffness parameter

$\delta_e(\xi)$ = elastic wall deflection

$\delta_{e_{TOP}}$ = value of δ_e at the top of the structure

$\delta(\xi)$ = lateral deflection of walls

$\delta'(\xi)$

$\delta''(\xi)$ } = components of the total deflection $\delta(\xi)$

$\delta'''(\xi)$

δ_y = value of $\delta(\xi)$ at the onset of yielding

δ_{TOP} = top deflection of the structure.

η, ζ = boundary coordinates for inelastic shear distribution

$\theta(\xi)$ = laminar rotation

$\theta_w(\xi)$ = elastic wall rotation

θ_y = yield rotation of coupling beams

θ_p = plastic component of laminar rotation

λ = coefficient related to stiffness parameter

μ_b = rotation ductility factor of connecting beams

μ_s = system displacement ductility factor

ξ = non-dimensional distance from top of structure = x/H

ξ_0 = position of the critically situated lamina

ϵ = dummy variable

ρ = ratio between the horizontal point load applied at the top and the lateral triangular load

ψ = a stiffness parameter

CHAPTER I

INTRODUCTION

1.1 General

The current philosophy of earthquake-resistant design is that a structure should be able to withstand major earthquake excitation without collapse, even though a certain amount of structural damage is incurred. This requirement can be met economically by introducing shear wall elements which, if properly designed, provide ductile behaviour vital to such aseismic design. However, to arrive at this requires knowledge of the non-linear behaviour of the structure.

Very often, windows, doors and service ducts require openings in exterior and interior shear walls. These openings normally occur in vertical rows throughout the height and are separated by either connecting beams which form part of the wall, or floor slabs. The terms often used to describe such walls are coupled shear walls, pierced shear walls and shear walls with openings.

Theories for the analysis of shear walls were fully formulated beginning in the 1960's, and three basic techniques exist: (a) continuum approach, (b) frame analysis, and (c) finite element analysis.

1.2 Previous Investigations

The results of earlier works on elastic analysis of coupled shear walls as well as future trends were reviewed in 1966 [1][†], where the emphasis is given on the continuum approach. This technique was first applied to the analysis of coupled shear walls by Beck [2] but was fully developed by Rosman [3]. While it has many limitations, this approach is sufficiently accurate to illustrate the basic behaviour of coupled wall systems.

A computer technique for the analysis of multistory shear walls considering a frame with finite joints was used by MacLeod [4] and Candy [5], while several investigators [6,7,8] have solved the problem using the finite element method.

An early study by Winokur and Glück [9] introduced inelastic analysis by assuming a complete collapse mechanism for the structure where all coupling beams have formed hinges at their ends while the two walls yield at their base. The solution is based on ultimate strength.

Paulay [10] presented an elasto-plastic analysis of coupled shear walls assuming that the collapse mechanism is formed when plastic hinges have developed at the ends of 95 percent

---

[†] Numbers in square brackets refer to the list of references given at the end of this report.

of all coupling beams and one hinge has developed at the base of each of the two walls. Using the continuous connection method he included the effect of cracking of both the connecting beams and piers by arbitrarily reducing their stiffness, although the manner of cracking is still not accurately known.

Glück's [11] elasto-plastic procedure, in which plastic hinges at the ends of the coupling beams may develop over only a part of the structure, assumed that the two walls behave elastically. He assumed the lateral ultimate capacity to be governed by yield limitation of the coupling continuum in the middle zone of the structure. The upper and lower zone laminae in this continuum approach were taken to behave elastically and the shear distribution was obtained from the governing differential equation and the compatibility conditions at the boundary of three zones.

Elveholy and Robinson [12] presented a finite difference method for elastic and inelastic analysis of coupled shear walls where the effect of cracking of the reinforced concrete elements and gravity load were included in the analysis.

The recent work by Nayor and Coull [13] presented a stepwise linear elastic-plastic analysis based on the wide-column frame analogy where the walls and beams are represented by

line members of corresponding stiffness. The analysis provides the possibility of following the structural behaviour from working to ultimate load range.

1.3 Scope of Present Study

The methods using the continuum approach [10, 11] may in some cases not be applicable in practice. Because a plastic hinge at the base of one of the walls can occur before the limit of rotational ductility of the beams is reached, Glück's ultimate load capacity of the system may not exploit the true load capacity of the structure. Also the topmost coupling beam may not reach its elastic limit before one of the walls yields; hence, Paulay's analysis may not be valid in some cases. The latter analysis, furthermore, does not examine structural behaviour between the occurrence of the first plastic hinge and yielding of the top beam.

The analysis using the finite difference method or the column-frame analogy is connected with computer work and hand procedure is not feasible. Thus these methods may not be useful for fast analysis important for office purposes.

The elasto-plastic analysis presented in this study uses the continuum approach and attempts to follow the history of lateral load response considering all possible cases which may occur. Overall collapse may include base hinges in the walls as well as total or partial yielding of the connecting continuum. The assumed loading pattern consists

of an upper triangular load with concentrated force at the top of the structure. Equations expressing shear distribution among the coupling beams, as well as rotations, and the system lateral deflections are derived. Beam and system ductility requirements at overall failure are obtained as functions of wall coupling shear strength. The importance of system geometry on ductility requirements and moment-axial force interaction relations for the walls are also examined. Finally, the effect of concentrated load at the top of the structure on connecting beam and overall ductility requirements is examined.

The analysis and investigation reported herein is organized in the following manner:

The elastic formulation of the continuum method which forms the basis for the proposed elastic-plastic procedure employed in this investigation is presented in Chapter II.

The assumptions made for the non-linear behaviour and the derivation of governing equations are described in Chapter III. Also a step-by-step calculation of load displacement response, definition of ductility factors and an illustrative example of non-linear analysis are presented in this chapter.

The influence of the moment-axial force interaction in the walls on overall behaviour is presented in Chapter IV. Here,

rectangular and "T" section walls are examined under moment combined with axial tension or compression forces.

In Chapter V non-linear structural behaviour according to different stiffness parameters and coupling beam strengths are discussed and results of a parametric study are presented in detail.

Finally, general conclusions are listed in Chapter VI.

CHAPTER II

ELASTIC ANALYSIS

2.1 Introduction

The analysis which is presented in this chapter is restricted to elastic behaviour of a coupled shear wall structure. The development is carried out for a homogeneous, isotropic, linearly elastic material. This analysis has received extensive attention and is available in the literature. The elastic formulation is provided here in order to make clear the continuum method, since the latter provides the basis for the proposed elastic-plastic procedure employed in the present investigation.

2.2 Governing Equation

Figure 1 shows the structure and the assumed loading pattern. The latter approximates the pseudo-static forces of current seismic building codes. The coupling beams formed by the vertically arranged openings in the structure are replaced, for purpose of analysis, by a continuous connection. This connection has the same stiffness from story to story as provided by connecting beams which have moment of inertia I_b and occur at spacing h, the story height. This continuous connection can be imagined as laminae of height dx and stiffness $I_b(\frac{dx}{h})$ extending one after the other along the whole height H, as shown in Figure 2(a). By consideration

of equilibrium and compatibility conditions, the following governing differential equation† of the second order is established:

$$\frac{d^2T(\xi)}{d\xi^2} - \alpha^2 T(\xi) = -\gamma \frac{M_o(\xi)}{H} \tag{2.1}$$

where:

$$\alpha^2 = \left(\frac{1}{A_1} + \frac{1}{A_2} + \frac{\ell^2}{I_o}\right) \frac{12\, I_b H^2}{hs^3} \tag{2.2}$$

$$\gamma = \frac{12\, I_b \ell H^3}{hs^3 I_o} \tag{2.3}$$

and $\xi = \frac{x}{H}$, ℓ = span between shear wall centroidal lines, s = clear span of connecting beams, I_o = sum of moments of inertia (I_1 and I_2) of walls 1 and 2, $T(\xi)$ = axial force at ξ, and $M_o(\xi)$ = cantilever moment produced by the external lateral load.

Solving Eq. (2.1) for the appropriate boundary conditions at the top and bottom, the general solution becomes:

$$T(\xi) = \frac{2\gamma W_e}{\alpha^4} \left[C\sinh\alpha\xi - \cosh\alpha\xi - \xi + 1 - \frac{\alpha^2}{2}\left(\frac{\xi^3}{3} - \xi^2 - \rho\xi\right)\right] \tag{2.4}$$

in which: W_e = sum of the distributed load, ρ = ratio of top point load to the sum of the triangular load, and:

$$C = \tanh\alpha + \frac{2 - \alpha^2(1 + \rho)}{2\alpha \cosh\alpha} \tag{2.5}$$

† Complete derivation of differential equation is given in Appendix A.

Once the distribution of the force $T(\xi)$ has been determined, $q(\xi)$, the shear force per unit height, is defined by:

$$q(\xi) = \frac{dT(\xi)}{Hd\xi} \tag{2.6}$$

which gives:

$$q(\xi) = \frac{2\gamma W_e}{H\alpha^4}\left[C\alpha\cosh\alpha\xi - \alpha\sinh\alpha\xi - 1 - \frac{\alpha^2}{2}(\xi^2 - 2\xi - 0)\right] \tag{2.7}$$

For various forms of lateral loading solutions, in the form of graphs and tables, are available in the literature.

2.3 Laminar Rotation

The meaning of laminar rotation θ is defined in Figure 3. It may be noted that the angle between the axis of the beam, or lamina, and the axis of the wall do not remain at right angles after loading. This effect would be emphasized further by the contribution of shear distortions during elastic performance and by hinge rotations after yielding of laminae.

By evaluating the elastic wall rotation and axial deformation, it may easily be shown that the laminar rotation at any height is given by:

$$\theta = \theta_b - \theta_t \tag{2.8}$$

where θ = total laminar rotation, θ_b = elastic rotation due to wall bending, and θ_t = elastic rotation due to wall axial deformations.

Rotations θ_b and θ_t are obtained from simple strength of materials; namely,

$$\theta_b = \frac{H}{EI_o}\frac{\ell}{s}\int_\xi^1 [M_o(\xi) - \ell T(\xi)]d\xi \tag{2.9}$$

$$\theta_t = \frac{H}{sE}\left(\frac{1}{A_1} + \frac{1}{A_2}\right)\int_\xi^1 T(\xi)d\xi \tag{2.10}$$

Substituting the above expressions for θ_b and θ_t into Eq. (2.8) results in:

$$\theta = \frac{H\ell}{sEI_o}\left\{\int_\xi^1 M_o(\xi)d\xi - \ell\int_\xi^1 T(\xi)d\xi\right\} - \frac{H}{sE}\left(\frac{1}{A_1} + \frac{1}{A_2}\right)\int_\xi^1 T(\xi)d\xi \tag{2.11}$$

where, if appropriate load functions corresponding to the triangular and point loads of Figure 1 are substituted into $M_o(\xi)$ and the integrals evaluated, the rotation becomes:

$$\theta = W_e K_1\left\{\left(K_2 - \frac{\alpha^2}{2}\right)\left[\frac{1}{4} - \frac{\xi^3}{3} + \frac{\xi^4}{12} + \frac{\rho}{2}(1 - \xi^2)\right] - \frac{C}{\alpha}(\cosh\alpha - \cosh\alpha\xi) + \frac{1}{\alpha}(\sinh\alpha - \sinh\alpha\xi) - \frac{1}{2}(\xi^2 - 2\xi + 1)\right\} \tag{2.12}$$

where:

$$K_1 = \frac{2\gamma h\ell^2}{EI_o\alpha^4 s}\left[1 + \frac{I_o}{\ell^2\left(\frac{1}{A_1} + \frac{1}{A_2}\right)}\right] \tag{2.13a}$$

$$K_2 = \frac{H\alpha^4}{2\gamma\ell\left[1 + \frac{\frac{I_o}{\ell^2}}{\left(\frac{1}{A_1} + \frac{1}{A_2}\right)}\right]} \qquad (2.13b)$$

The distribution of laminar rotation θ along the height of the structure is shown in Figure 4.

It is of importance, for further analysis, that the maximum value of laminar rotation, denoted by θ_{max}, and the corresponding ordinate, denoted by ξ_o, be determined. Differentiation of θ with respect to ξ gives:

$$\frac{d\theta}{d\xi} = W_e K_1 \{(K_2 - \frac{\alpha^2}{2})[\frac{\xi^3}{3} - \xi^2 - \rho\xi] + C\alpha\sinh\alpha\xi - \cosh\alpha\xi - \xi + 1\} \qquad (2.14)$$

which, when set to zero at $\xi = \xi_o$, results in:

$$W_e K_1 \{(K_2 - \frac{\alpha^2}{2})[\frac{\xi_o^3}{3} - \xi_o^2 - \rho\xi_o] + C\alpha\sinh\alpha\xi_o - \cosh\alpha\xi_o - \xi_o + 1\} = 0 \qquad (2.15)$$

The solution of the above equation defines the coordinate, or position, of the lamina with maximum rotation. The Newton-Raphson method was used to evaluate ξ_o. By substituting the value of ξ_o into Eq. (2.12) the maximum rotation, θ_{max}, of the "critically situated lamina" [10] is obtained.

2.4 Lateral Deflection

Considering the assumptions made in the derivation of

differential Eq. (2.1) (see also Appendix A), the elastic wall rotation, $\theta_w(\xi)$, is obtained as:

$$\theta_w(\xi) = \frac{H}{EI_o}\left[\int_\xi^1 M_o(\xi)d\xi - \ell\int_\xi^1 T(\xi)d\xi\right] \qquad (2.16)$$

Substituting the appropriate forms for $M_o(\xi)$ and $T(\xi)$, corresponding to the load pattern of Figure 1, into Eq. (2.16) and integrating with respect to ξ the elastic wall lateral deflection, δ_e, obtained from:

$$\delta_e = H\int_\xi^1 \theta_w(\xi)d\xi \qquad (2.17a)$$

becomes:

$$\begin{aligned}\delta_e = W_e K_3\{K_4[&\frac{11}{60} + \frac{\rho}{3} - \frac{\xi}{4} + \frac{\xi^4}{12} - \frac{\xi^5}{60} - \frac{\rho}{2}(\xi - \frac{\xi^3}{3})] - \\ &- \frac{c}{\alpha}[(1-\xi)\cosh\alpha - \frac{1}{\alpha}(\sinh\alpha - \sinh\alpha\xi)] + \\ &+ \frac{1}{\alpha}[(1-\xi)\sinh\alpha - \frac{1}{\alpha}(\cosh\alpha - \cosh\alpha\xi)] - \\ &- \frac{1}{2}(\frac{1}{3} - \frac{\xi^3}{3} + \xi^2 - \xi)\}\end{aligned} \qquad (2.17b)$$

where:

$$K_3 = \frac{2\gamma H^2 \ell}{EI_o\alpha^4}$$

$$K_4 = \frac{H\alpha^4}{2\gamma\ell} - \frac{\alpha^2}{2}$$

In particular, the deflection at the top of the structure (i.e., $\xi = 0$) is:

$$\delta_{e_{TOP}} = W_e K_3 \{K_4 [\frac{11}{60} + \frac{\rho}{3}] - \frac{C}{\alpha}[\cosh\alpha - \frac{1}{\alpha}\sinh\alpha] + \frac{1}{\alpha}[\sinh\alpha - \frac{1}{\alpha}(\cosh\alpha - 1)] - \frac{1}{6}\} \quad (2.18)$$

For rapid evaluation of deflections, curves representing the above equations can be produced. By analysing Eqs. (2.17) and (2.18), it can be concluded that such curves will hold for any shape of wall, so that cross walls acting as flanges may be incorporated in the analysis. Glück [11], as well as Coull and Choudhury [14], has provided charts for evaluation of top deflection of coupled shear wall systems. Both, upper triangular as well as uniformly distributed lateral, loads are considered.

The preceding elastic analysis, briefly presented, provides a necessary background for the non-linear analysis formulated in the following chapter.

CHAPTER III

ELASTO-PLASTIC ANALYSIS

3.1 Introduction

In many tall buildings shear walls will provide the majority, if not all, of the required strength for lateral loading resulting from wind and earthquake effects. For wind loading, generally, the governing design criterion is deflection. It is usually found that the strength requirement is not difficult to be satisfied, using appropriate load factors specified by codes. Hence, for those areas where wind load is the only source of lateral load on a multistory building elastic analysis, discussed in the preceding chapter, is adequate to assess the behaviour of the structure.

Only in exceptional cases will it be possible to resist earthquake-generated forces within the elastic range of behaviour. When large seismic excitations are encountered, the coupling beams, as well as the walls, are subjected to extensive yielding. Hinge formation will depend upon relative stiffness and strength of the components. The collapse mechanism can include partial [11] or full plastification of the laminae [9,10], with large ductility demand imposed upon the coupling system.

The ultimate state of the structure may consist of the following types of failure:

1. Complete collapse mechanism, where: (a) almost all of the coupling beams including the topmost yield before plastic hinges are formed at the base of each of the two walls, or (b) a plastic hinge is formed at the base of one of the walls before yielding of the topmost coupling beam and formation of a plastic hinge at the base of the second wall; and,

2. Incomplete collapse mechanism where: (a) failure is governed by rotational capacity of the coupling beams in which case plastic hinges in the coupling beams may develop over only a part of the structure while the two walls behave elastically, or (b) plastic hinges are formed at the base of each of the walls accompanied by yielding of coupling beams in only the middle portion of the structure.

Glück's elasto-plastic procedure [11], in which plastic hinges at the ends of the coupling beams may develop over only a part of the structure, assumed that the two walls behave elastically. Here, failure was governed by yield limitation of the coupling continuum in the middle zone. The laminae in the upper and lower zones behave elastically and the shear distribution in these elastic zones was obtained from the governing differential equation and compatibility condition at the boundaries of these zones.

In some cases the above approach is not applicable. As the

results of this study will show, a coupled shear wall structure with relatively stiff walls and a strong coupling system forms a plastic hinge at the base of one of the walls before the limit of rotational ductility of the critically situated lamina is reached. To assume ultimate load capacity of the system corresponding to laminar ductility capacity may not exploit the true load capacity of the structure. Hence, Glück's assumption limits his results to the class of structures with relatively strong walls and a weak coupling system.

Paulay's elasto-plastic step-by-step procedure [10] assumed that the collapse mechanism is formed when plastic hinges have developed at ends of almost all of the coupling beams and one hinge exists at the base of each of the two walls. He assumed that 95 percent of the coupling beams are always yielded before the ultimate state of the structure is attained.

Because the topmost coupling beam may not reach its elastic limit before one of the walls yields, Paulay's analysis may not be valid in some cases. This limitation is characteristic for relatively tall buildings with slender shear walls. Also this analysis cannot be used in examining structural behaviour between time of occurrence of the first plastic beam hinge and yielding of the top of the structure.

The purpose of this chapter is to establish an elastic-plastic procedure which attempts to examine the complete

history of response of the structure to lateral load. Formation of partial collapse mechanisms at various stages of incremental loading is permitted until ultimate strength of the structure is reached.

3.2 General Assumptions for Non-Linear Behaviour

The basic assumptions made in the analysis are:

1. While the coupling beams have reached their ultimate coupling shear capacity q_u, in the middle zone shown in Figure 2(b), the shear distribution in the remaining elastic beams (in the upper and the lower zones) follows the same pattern as that obtained by elastic analysis. The corresponding axial force in the walls is obtained from equilibrium for the assumed shear distribution. Overall equilibrium is maintained by adjusting the external load as explained in Section 3.4.2.

2. A plastic hinge at the base of one of the walls may occur, while coupling beams yield over only a portion of the height. This happens when one of the walls attains its moment-axial force capacity. Thereafter, this wall continues to participate as part of the system following its moment-axial force interaction relationship.

3. One all laminae reach their ultimate capacity the wall

with the plastic hinge at its base is considered to be an ineffective cantilever.

4. Overall collapse is defined in this analysis to occur when the second wall hinge is formed, with total or partial yielding of the connecting continuum.

3.3 Derivation of Governing Equations

While the structure carries a code prescribed equivalent static design load of the form shown in Figure 1, the coupling beams and wall 1 are assumed to have cracked. Cracking caused by flexure and shear is responsible for a considerable loss of stiffness in the affected parts, causing a geometrically symmetrical structure to become structurally asymmetrical. Such loss of stiffness may be as much as 85 percent [10].

The next increment of loading brings the critically situated lamina (at ξ_o obtained from Eq. (2.15)) to its elastic limit. This load stage, defined as W_y, terminates the linear elastic behaviour of the structure. Plastic hinges at both ends of the lamina are developed, and the corresponding laminar rotation, θ_y, represents a ductility factor† of unity. All laminae below and above ξ_o possess rotations less than θ_y, therefore ductility factor μ_b is less than one.

Further load increase will cause other coupling beams to enter the plastic range, and the shear distribution is

† For definition of ductility factor, see Section 3.5.

assumed as shown on Figure 2(b).

The solutions* for bending moment and axial force distribution, as well as rotation and deflection, must be developed separately for the three zones of Figure 2(b). Boundary coordinates η and ζ define the plastic region and, together with the remaining elastic zones, yield the shear distribution for non-linear action.

3.3.1 Upper Zone -- $(0 \leq \xi \leq \eta)$

The coupling beams behave elastically, therefore the differential equation defined in the elastic analysis is assumed to be valid. The general solution expressing the laminar shear distribution is defined by Eq. (2.7) and the axial force by Eq. (2.4). Thus, the coupling effect represented by $\ell T(\xi)$ is known and $M(\xi)$, the bending moment on an arbitrary cross-section through both walls, is obtained as:

$$M(\xi) = M_o(\xi) - \ell T(\xi) \qquad (3.1)$$

where:

$T(\xi)$ = axial force generated in walls.

Since both walls must have the same deflection throughout the entire height H, total bending moment is assigned proportional to moments of inertia. Therefore, $M_1(\xi)$ and $M_2(\xi)$,

* Details for the derivation of expressions presented in final form in this chapter are contained in Appendix B.

the bending moments in walls one and two become, respectively:

$$M_1(\xi) = \frac{I_1}{I_o} M(\xi) \qquad (3.2a)$$

$$M_2(\xi) = \frac{I_2}{I_o} M(\xi) \qquad (3.2b)$$

By substituting into Eqs. (3.1) and (3.2) $T(\xi)$ from Eq. (2.4) and the following external moment resultant for the loading condition of Figure 1:

$$M_o(\xi) = WH[\xi^2 - \frac{\xi^3}{3} + \rho\xi] \qquad (3.3)$$

where W is the distributed load for non-linear behaviour, the moment on wall one is:

$$M_1(\xi) = \frac{I_1}{I_o} W\{H[\xi^2 - \frac{\xi^3}{3} + \rho\xi] - \frac{2\gamma\ell}{\alpha^4}[C\sinh\alpha\xi - \cosh\alpha\xi - \xi + 1 - \frac{\alpha^2}{2}(\frac{\xi^3}{3} - \xi^2 - \rho\xi)]\} \qquad (3.4)$$

with C defined by Eq. (2.5). A similar equation expresses the moment acting on wall 2.

The coupling beam rotation, as well as wall deflection at any section, is defined after evaluating wall rotations and axial deformations, by:

$$\theta(\xi) = \frac{\ell H}{s} \int_{\xi}^{1} \frac{M(\xi)m(\xi)}{EI_o} d\xi - \\ - \frac{H}{sE} \left(\frac{1}{A_1} + \frac{1}{A_2}\right) \int_{\xi}^{1} T(\xi)p(\xi)d\xi \qquad (3.5)$$

where $m(\xi)$ and $p(\xi)$ are virtual moment and axial force, respectively.

Substituting corresponding expressions for $M(\xi)$, $T(\xi)$, $m(\xi)$ and $p(\xi)$ into Eq. (3.5) leads to:

$$\theta(\xi) = \frac{H\ell}{sEI_o} \left\{ \int_{\xi}^{1} M_o(\xi)d\xi - \ell \int_{\xi}^{1} T(\xi)d\xi \right\} - \\ - \frac{H}{sE} \left(\frac{1}{A_1} + \frac{1}{A_2}\right) \int_{\xi}^{1} T(\xi)d\xi \qquad (3.6)$$

for which:

$$\int_{\xi}^{1} T(\xi)d\xi = \int_{\xi}^{\eta} T(\xi)d\xi + T_\eta(1 - \eta) + \\ + Hq_u\left[-\frac{1}{2}(\zeta^2 - \eta^2) + \zeta - \eta\right] + \qquad (3.7) \\ + \int_{\zeta}^{1} T(\xi)d\xi - T_\zeta(1 - \zeta)$$

where notation for axial force at boundary points is:

$$T_\eta = T(\xi) \quad , \quad \xi = \eta \quad ; \quad T_\zeta = T(\xi) \quad , \quad \xi = \zeta$$

and, as before, q_u indicates ultimate laminar shear capacity per unit height, and T_η and T_ζ are obtained from Eq. (2.4), with elastic load W_e replaced by inelastic load W obtained from Eq. (3.38).

After integration beam end rotations are given by:

$$\theta(\xi) = \dot{W}\frac{H^2\ell}{sEI_o}\left[\frac{1}{4} + \frac{\xi^4}{12} - \frac{\xi^3}{3} + \frac{\rho}{2}(1 - \xi^2)\right] -$$

$$- \left[\frac{H\ell^2}{sEI_o} + \frac{H}{sE}\left(\frac{1}{A_1} + \frac{1}{A_2}\right)\right]\left\{\frac{2\gamma W}{\alpha^4}\left\{\frac{C}{\alpha}(\cosh\alpha\eta - \cosh\alpha\xi) - \right.\right.$$

$$- \frac{1}{\alpha}(\sinh\alpha\eta - \sinh\alpha\xi) - \frac{\alpha^2}{2}\left[\frac{1}{12}(\eta^4 - \xi^4) - \right. \qquad (3.8)$$

$$- \frac{1}{3}(\eta^3 - \xi^3) - \frac{\rho}{2}(\eta^2 - \xi^2) + \eta - \xi -$$

$$\left.\left. - \frac{1}{2}(\eta^2 - \xi^2)\right\} + C_1 + C_2\right]$$

where:

$$C_1 = T_\eta(1 - \eta) + Hq_u(\zeta - \eta)\left[\frac{1}{2}(\zeta - \eta) + (1 - \zeta)\right] -$$

$$- T_\zeta(1 - \zeta) \qquad (3.9)$$

$$C_2 = \frac{2\gamma W}{\alpha^4}\left\{\frac{C}{\alpha}(\cosh\alpha - \cosh\alpha\zeta) - \frac{1}{\alpha}(\sinh\alpha - \sinh\alpha\zeta) + \right.$$

$$+ \frac{\alpha^2}{2}\left[\frac{1}{4} + \frac{\zeta^4}{12} - \frac{\zeta^3}{3} + \frac{\rho}{2}(1 - \zeta^2)\right] + \qquad (3.10)$$

$$\left. + \frac{1}{2}(1 + \zeta^2 - 2\zeta)\right\}$$

E is concrete modulus of elasticity, and W = distributed load for non-linear behaviour given by Eq. (3.38).

The deflection at any arbitrary section can be found from elementary strength of materials as:

$$\delta(\xi) = H\int_\xi^1 \theta_w(\xi)d\xi \qquad (3.11)$$

It is convenient to treat the solution of Eq. (3.11) as a combination of external load and coupling effects.

The load shown in Figure 1 will produce lateral deflection of the coupled shear wall system. The axial force generated in the walls by this load will, through coupling effect expressed as $\ell T(\xi)$, tend to oppose the lateral load deflection. The effect of the elasto-plastic shear distribution shown in Figure 2(b) can be considered as two additional and separate contributions to deflection: (1) a component associated with the elastic shear distribution $q(\xi)$ and, (2) a component due to missing portion $(q - q_u)$ indicated in Figure 5. Defining deflection components associated with these three force conditions by $\delta'(\xi)$, $\delta''(\xi)$ and $\delta'''(\xi)$, respectively, the deflection at any height of the structure is found to be;

$$\delta(\xi) = \delta'(\xi) - \delta''(\xi) \pm \delta'''(\xi) \qquad (3.12)$$

From strength of materials:

$$\delta'(\xi) = \frac{WH^3}{EI_o} \int_{\xi}^{1} (\varepsilon^2 - \frac{\varepsilon^3}{3} + \rho\varepsilon)(\varepsilon - \xi)d\varepsilon \qquad (3.13)$$

$$\delta''(\xi) = \frac{H^2\ell}{EI_o} \int_{\xi}^{1} T(\xi)(\varepsilon - \xi)d\varepsilon \qquad (3.14)$$

$$\delta'''(\xi) = (\xi - \eta)\frac{H^2\ell}{EI_o}\{\int_\eta^\zeta [T(\xi) - T_\eta - Hq_u(\xi - \eta)]d\xi + C_3(1 - \zeta)\} +$$

$$+ \frac{H^2\ell}{EI_o}\{\int_\eta^\zeta [T(\xi) - T_\eta - Hq_u(\xi - \eta)](\xi - \eta)d\xi + C_3(1 - \zeta)(\frac{1+\zeta}{2} - \eta)\} \quad (3.15)$$

where:

$$C_3 = T_\zeta - T_\eta - Hq_u(\zeta - \eta) \quad (3.16)$$

The difference, $\delta'(\xi) - \delta'''(\xi)$, actually expresses the elastic deflection of the system (Eq. (2.17)). Therefore, the deflection can be written in the form:

$$\delta(\xi) = \delta_e(\xi) + \delta'''(\xi) \quad (3.17)$$

Substituting for $T(\xi)$, T_η, and T_ζ in Eq. (3.15) and integrating results in:

$$\delta(\xi) = \delta_e(\xi) + \frac{H^2\ell}{EI_o}(D_1 - D_2 - D_3 - D_4 + D_5) \quad (3.18)$$

where:

$$D_1 = \frac{2\gamma W}{\alpha^4}\{\frac{C}{\alpha}[\zeta\cosh\alpha\zeta - \eta\cosh\alpha\eta - \frac{1}{\alpha}(\sinh\alpha\zeta - \sinh\alpha\eta)] -$$

$$- \frac{1}{\alpha}[\zeta\sinh\alpha\zeta - \eta\sinh\alpha\eta - \frac{1}{\alpha}(\cosh\alpha\zeta - \cosh\alpha\eta)] -$$

$$- \frac{1}{3}(\zeta^3 - \eta^3) + \frac{1}{2}(\zeta^2 - \eta^2) - \frac{\alpha^2}{2}[\frac{1}{15}(\zeta^5 - \eta^5) - \quad (3.19a)$$

$$- \frac{1}{4}(\zeta^4 - \eta^4) - \frac{\rho}{3}(\zeta^3 - \eta^3)]\}$$

$$D_2 = \frac{2\gamma W}{\alpha^4}\xi\{\frac{C}{\alpha}(\cosh\alpha\zeta - \cosh\alpha\eta) - \frac{1}{\alpha}(\sinh\alpha\zeta - \sinh\alpha\eta) -$$

$$- \frac{1}{2}(\zeta^2 - \eta^2) + \zeta - \eta - \frac{\alpha^2}{2}[\frac{1}{12}(\zeta^4 - \eta^4) - \quad (3.19b)$$

$$- \frac{1}{3}(\zeta^3 - \eta^3) - \frac{\rho}{2}(\zeta^2 - \eta^2)]\}$$

$$D_3 = T_\eta[\frac{1}{2}(\zeta^2 - \eta^2) - \xi(\zeta - \eta)] \quad (3.19c)$$

$$D_4 = Hq_u[\frac{1}{3}(\zeta^3 - \eta^3) - \frac{1}{2}(\eta + \xi)(\zeta^2 - \eta^2) + \quad (3.19d)$$

$$+ \eta\xi(\zeta - \eta)]$$

$$D_5 = [T_\zeta - T_\eta - Hq_u(\zeta - \eta)](1 - \zeta)(\frac{1 + \zeta}{2} - \xi) \quad (3.19e)$$

3.3.2 Middle Zone -- ($\eta \leq \xi \leq \zeta$)

In this zone the coupling beams have plastic hinges. The axial force can be expressed as:

$$T(\xi) = T_\eta + Hq_u(\xi - \eta) \quad (3.20)$$

with total bending moment $M(\xi)$ and moments $M_1(\xi)$ and $M_2(\xi)$,

acting on walls 1 and 2, respectively defined by Eqs. (3.1) and (3.2).

Applying Eq. (3.5), coupling beam end rotation is determined in this zone by:

$$\theta(\xi) = W \frac{H^2 \ell}{sEI_o} \left[\frac{1}{4} + \frac{\xi^4}{12} - \frac{\xi^3}{3} + \frac{\rho}{2}(1 - \xi^2)\right] -$$

$$- \frac{H\ell^2}{sEI_o} \{T_\eta(1 - \xi) + Hq_u[(\xi - \eta)(1 - \xi) + \tag{3.21}$$

$$+ \zeta - \xi - \zeta^2 + \frac{1}{2}(\zeta^2 + \xi^2)] + C_2 - T_\zeta(1 - \zeta)\}$$

where constant C_2 is defined by Eq. (3.10).

At any middle zone section the lateral deflection is obtained from Eq. (3.17), with:

$$\delta'''(\xi) = \frac{H^2 \ell}{EI_o} \{ \int_\xi^\zeta [T(\varepsilon) - T_\eta - Hq_u(\varepsilon - \eta)](\varepsilon - \xi)d\varepsilon + \tag{3.22}$$

$$+ [T_\zeta - T_\eta - Hq_u(\zeta - \eta)](1 - \zeta)(\frac{1 + \zeta}{2} - \xi)\}$$

Substituting into Eq. (3.22) the corresponding expressions for $T(\varepsilon)$, T_η and T_ζ, and integrating, Eqs. (3.22) and (3.17) yield:

$$\delta(\xi) = \delta_e(\xi) + \frac{H^2 \ell}{EI_o}(D_6 - D_7 - D_8 - D_9 + D_5) \tag{3.23}$$

where:

$$D_6 = \frac{2\gamma W}{\alpha^4}\{\frac{C}{\alpha}[\zeta\cosh\alpha\zeta - \xi\cosh\alpha\xi - \frac{1}{\alpha}(\sinh\alpha\zeta - \sinh\alpha\xi)] -$$

$$- \frac{1}{\alpha}[\zeta\sinh\alpha\zeta - \xi\sinh\alpha\xi - \frac{1}{\alpha}(\cosh\alpha\zeta - \cosh\alpha\xi)] -$$

$$- \frac{1}{3}(\zeta^3 - \xi^3) + \frac{1}{2}(\zeta^2 - \xi^2) - \frac{\alpha^2}{2}[\frac{1}{15}(\zeta^5 - \xi^5) - \quad (3.24a)$$

$$- \frac{1}{4}(\zeta^4 - \xi^4) - \frac{\rho}{3}(\zeta^3 - \xi^3)]\}$$

$$D_7 = \frac{2\gamma W}{\alpha^4}\xi\{\frac{C}{\alpha}(\cosh\alpha\zeta - \cosh\alpha\xi) - \frac{1}{\alpha}(\sinh\alpha\zeta - \sinh\alpha\xi) -$$

$$- \frac{1}{2}(\zeta^2 - \xi^2) + \xi - \frac{\alpha^2}{2}[\frac{1}{12}(\zeta^4 - \xi^4) - \quad (3.24b)$$

$$- \frac{1}{3}(\zeta^3 - \xi^3) - \frac{\rho}{2}(\zeta^2 - \xi^2)]\}$$

$$D_8 = T_\eta[\frac{1}{2}(\zeta^2 + \xi^2) - \xi\zeta] \quad (3.24c)$$

$$D_9 = Hq_u[\frac{1}{3}(\zeta^3 - \xi^2) - \frac{1}{2}(\eta - \xi)(\zeta^2 - \xi^2) + \quad (3.24d)$$

$$+ \eta\xi(\zeta - \xi)]$$

Constant D_5 is defined by Eq. (3.19e).

3.3.3 Lower Zone - $(\zeta \leq \xi \leq 1)$

In this zone the coupling beams behave elastically. The laminar shear distribution along the height is assumed to follow the same pattern as that found for elastic analysis.

Axial force function $T(\xi)$, for the load shown in Figure 1, is:

$$T(\xi) = T_\eta + Hq_u(\zeta - \eta) + T_\xi - T_\zeta \qquad (3.25)$$

where T_ξ = axial force defined for elastic behaviour and using the inelastic lateral load of Eq. (3.38) in place of W_e in Eq. (2.4). As before, bending moments $M(\xi)$, $M_1(\xi)$, and $M_2(\xi)$ are defined by Eqs. (3.1) and (3.2).

Knowing bending moment $M(\xi)$ and axial force $T(\xi)$, as well as wall rotational and extensional deformation, Eq. (3.5) gives:

$$\begin{aligned}\theta(\xi) = {} & W\frac{H^2\ell}{sEI_o}\left[\frac{1}{4} + \frac{\xi^4}{12} + \frac{\xi^3}{3} + \frac{\rho}{2}(1 - \xi^2)\right] - \\ & - \frac{H^2\ell}{sEI_o}\{T_\eta(1 - \xi) + Hq_u(\zeta - \eta)(1 - \xi) + \\ & + \frac{2\gamma W}{\alpha^4}\{\frac{C}{\alpha}(\cosh\alpha - \cosh\alpha\xi) - \frac{1}{\alpha}(\sinh\alpha - \sinh\alpha\xi) + \\ & + \frac{\alpha^2}{2}[\frac{1}{4} + \frac{\xi^4}{12} - \frac{\xi^3}{3} + \frac{\rho}{2}(1 - \xi^2)] + \\ & + \frac{1}{2}(1 + \xi^2 - 2\xi)\} - T_\zeta(1 - \xi)\}\end{aligned} \qquad (3.26)$$

Applying Eq. (3.17), with $\delta'''(\xi)$ in this zone given by:

$$-\delta'''(\xi) = \frac{H^2\ell}{EI_o}\{[T_\zeta - T_\eta - Hq_u(\zeta - \eta)](1 - \xi)(\frac{1-\xi}{2}) \qquad (3.27)$$

and using the expressions for T_ζ and T_η leads to the final form for lower zone deflection:

$$\delta(\xi) = \delta_e(\xi) + \frac{H^2 \ell}{EI_o} [T_\zeta - T_\eta - Hq_u(\zeta - \eta)](1-\xi)(\frac{1-\xi}{2}) \qquad (3.28)$$

3.3.4 Special Cases -- 1.

In the case of relatively stiff walls the plastification of coupling beams may extend to the top of the structure. Hence, only two zones remain; a plastic one in the upper part, and an elastic one in the lower. The laminar shear in the plastic zone is constant at q_u, and Eq. (2.7) represents the assumed elastic shear distribution in the lower zone.

Axial force at any section of the upper plastic zone is:

$$T(\xi) = Hq_u\xi \qquad (3.29)$$

while for the lower, or elastic, zone:

$$T(\xi) = Hq_u\zeta + T_\xi - T_\zeta \qquad (3.30)$$

where T_ξ is the axial force for elastic behaviour at ξ given by Eq. (2.4).

With axial force known, bending moments in the walls and coupling beams may be determined by the procedure explained previously.

Laminar rotation, as well as coupled wall deflection, may be found following previous procedures. The laminar rotation, in final form, for the upper zone is:

$$\theta(\xi) = W\frac{H^2\ell}{sEI_o}\left[\frac{1}{4} + \frac{\xi^4}{12} - \frac{\xi^3}{3} + \frac{\rho}{2}(1 - \xi^2)\right] -$$

$$- \frac{H\ell^2}{sEI_o}\left\{Hq_u\left[\xi(1 - \xi) + \zeta - \xi - \zeta^2 + \right.\right. \tag{3.31}$$

$$\left.\left. + \frac{1}{2}(\zeta^2 + \xi^2)\right] + C_2 - T_\zeta(1 - \zeta)\right\}$$

where constant C_2 is defined by Eq. (3.10).

The corresponding deflection is expressed by:

$$\delta(\xi) = \delta_e(\xi) + \frac{H^2\ell}{EI_o}(D_6 - D_7 - D_{10} + D_{11}) \tag{3.32}$$

where D_6 and D_7 are constants defined by Eqs. (3.24a) and (3.24b), respectively, and:

$$D_{10} = Hq_u\left[\frac{1}{3}(\zeta^3 - \xi^3) + \frac{1}{2}\xi(\zeta^2 - \xi^2)\right] \tag{3.33a}$$

$$D_{11} = [T_\zeta - Hq_u\zeta](1 - \zeta)\left(\frac{1 + \zeta}{2} - \xi\right) \tag{3.33b}$$

The lower zone laminar rotation and wall deflection are obtained from Eqs. (3.26) and (3.28) of Section 3.3.3 for $\eta = 0$. Thus:

$$\theta(\xi) = W\frac{H^2\ell}{sEI_o}\left[\frac{1}{4} + \frac{\xi^4}{12} - \frac{\xi^3}{3} + \frac{\rho}{2}(1 - \xi^2)\right] -$$

$$- \frac{H\ell^2}{sEI_o}\left\{Hq_u\zeta(1 - \xi) + \frac{2\gamma W}{\alpha^4}\left\{\frac{C}{\alpha}(\cosh\alpha - \cosh\alpha\xi) - \right.\right. \tag{3.34}$$

$$- \frac{1}{\alpha}(\sinh\alpha - \sinh\alpha\xi) + \frac{\alpha^2}{2}\left[\frac{1}{4} + \frac{\xi^4}{12} - \frac{\xi^3}{3} + \right.$$

$$\left.\left.\left. + \frac{\rho}{2}(1 - \xi^2)\right] + \frac{1}{2}(1 - \xi^2 - 2\xi) - T_\zeta(1 - \xi)\right\}\right.$$

and

$$\delta(\xi) = \delta_e(\xi) + \frac{H^2 \ell}{EI_o}[T_\zeta - Hq_u\zeta](1 - \xi)(\frac{1 - \xi}{2}) \qquad (3.35)$$

3.3.5 Special Case -- 2.

The equations of Sec. 3.3.4 for the case where laminar plastification has spread to the top of the structure assumed both walls to behave elastically.

In case of a plastic hinge occurring at the base of one of the walls, it is assumed that this wall will continue to participate as part of the system following its moment-axial force interaction relationship. This allows increase of the axial force in the wall until all laminae have yielded, or a hinge forms in the second wall, whichever occurs first.

This is a relatively gross approximation but the error involved (from comparing results with those obtained by other methods as done in Section 3.7) is not significant.

The equations derived in previous section are employed for calculation of moments and axial force at any section for this special case, as well as laminar rotation and wall deflection.

In the case of unsymmetrical walls it is not mandatory to have a plastic hinge at the base of the wall exposed to

bending and axial tension before a hinge occurs in the wall exposed to bending and axial compression. This will depend on the placement of reinforcement, as well as on the strength of the concrete.

Bending moment M_2 at the base of wall 2, which is still elastic after a plastic hinge occurs at the base of wall 1, is:

$$M_2 = M - M_{u_1} \tag{3.36}$$

where M is the moment at the base defined by Eq. (3.1) and M_{u_1} is the moment resisted by the plastic hinge at the base of wall 1.

3.4 Numerical Procedure

This section explains the numerical procedure used in the computation of the non-linear behaviour by the proposed method of analysis. Evaluation of the boundary coordinates, determination of external load and step-by-step calculation of load-displacement response are explained.

3.4.1 Evaluation of Boundary Coordinates

The boundary coordinates η and ζ define the plastic region and yield the shear distribution for non-linear action shown in Figure 2(b).

Each increment of the associated elastic load W_e (defined in Section 2.2) leads to change of the shear distribution in the coupling beams, considering pure elastic behaviour. The shear force for any value of ξ is defined by Eq. (2.7). Once first yield has occurred there will be, for every increase of W_e, two values of ξ for which $q(\xi) = q_u$. These values of ξ are the boundary coordinates η and ζ. Hence, η and ζ are evaluated from Eq. (2.7) for the conditions:

$$q_\eta = q_u \tag{3.37a}$$

$$q_\zeta = q_u \tag{3.37b}$$

The determination of η and ζ for the numerical work of this study was accomplished using an iterative bisection method [15].

3.4.2 Determination of External Load

The assumed inelastic shear distribution must be in equilibrium with the external loads. The external load W for the three zones and Special Case 2 of Section 3.3 (i.e., all cases except Special Case 1) is obtained from the condition that the laminar rotation at the boundary between the upper and the middle zones (defined by η) is equal to yield laminar rotation θ_y. After substitution of θ_y in Eq. (3.8) and solving for W, Eq. (3.38) is obtained.

$$W = \frac{F}{G} \tag{3.38a}$$

with:

$$F = H^2\left[\frac{\ell^2}{I_o} + \frac{1}{A_1} + \frac{1}{A_2}\right]\left[(\zeta - \eta) - \frac{1}{2}(\zeta^2 - \eta^2)\right]q_u + sE\theta_y \qquad (3.38b)$$

$$G = \frac{H^2\ell}{12\,I_o}\left[3 + \eta^4 - 4\eta^3 + 6\rho(1 - \eta^2)\right] -$$

$$- H\left[\frac{\ell^2}{I_o} + \frac{1}{A_1} + \frac{1}{A_2}\right]\left\{\bar{T}_\eta(1 - \eta) + \int_\zeta^1 \bar{T}(\xi)d\xi - \right. \qquad (3.38c)$$

$$\left. - \bar{T}_\zeta(1 - \zeta)\right]$$

and

$$\bar{T}_\eta = \frac{T_\eta}{W}$$

$$\bar{T}_\zeta = \frac{T_\zeta}{W}$$

$$\bar{T}(\xi) = \frac{T(\xi)}{W}$$

Here, W represents the sum of the distributed portion of the total load for the non-linear state of the structure defined by coordinates η and ζ.

The total external lateral load, expressed by base shear V for the non-linear state specified by boundary coordinates η and ζ, has the final form:

$$V = W(1 + \rho) \qquad (3.38d)$$

3.4.3 Step-by-Step Calculation of Load Displacement -- Response

It was found convenient to calculate the load-displacement history of the non-linear structure by proceeding in increments of the associated elastic load W_e, for fixed value of p. The computation of response data, to be presented in the following parts of this report, involved the above non-linear analysis applied in the following steps:

1. Determine the associated elastic load W_e by proceeding in increments ΔW_e.

2. Evaluate plastic boundary coordinates η and ζ from Eq. (2.7) for the conditions expressed by Eqs. (3.36a) and (3.36b).

3. Obtain the true external load W corresponding to the assumed shear distribution for non-linear behaviour using Eq. (3.38).

4. Calculate non-linear displacement and force response for walls and beams using formulations developed in Section 3.3.

5. Proceed with next increment of W_e. For Special Case 1 of Section 3.3.4, axial force $T(\xi)$ and coupling effect $\ell T(\xi)$ remain constant after yielding of the topmost lamina. Hence, walls act as simple cantilevers for addition in load and the loading process consists of increments of W.

Suitable value of load increment was selected from an examination of the rate of convergence of response data with variation in ΔW_e.

3.5 Definition of Ductility Factors

The emphasis on plastic action as the key to optimal seismic performance leads to the need of a concrete structure (by careful detailing and proportioning of the components) to fail forming a ductile failure mechanism. Therefore, it is important to treat the ductility requirements, particularly in the coupling beams, as a critical factor for the ultimate strength of a shear wall structure. The elasto-plastic investigation reported here attempts to expose the ductility demand of the coupling beams, as well as of the overall shear wall system.

The total laminar rotation, θ, for different loading stages, can be obtained from previously derived equations, and the rotational ductility factor at the support of the laminae can be expressed as:

$$\mu_b = \frac{\theta_{max}}{\theta_y} \tag{3.39a}$$

or, alternatively, in terms of the plastic laminar rotation θ_p:

$$\mu_b = \frac{\theta_p - \theta_y}{\theta_y} \tag{3.39b}$$

where μ_b represents ductility factor for coupling beams, θ_{max} = maximum laminar rotation at overall collapse, and θ_y = yield rotation of coupling beams.

Similarly, the ductility factor for the structure as a whole, obtained from the load-deflection relationship once known, is defined as:

$$\mu_s = \frac{\delta_{TOP}}{\delta_{y_{TOP}}} \tag{3.40}$$

where μ_s will be referred to as the system ductility factor, δ_{TOP} = deflection at top of the structure at ultimate load W_u corresponding to collapse, and δ_y = top deflection for load W_y, the load at first yield.

3.6 Illustrative Example of Non-Linear Analysis

The elasto-plastic behaviour of a coupled shear wall structure may be easily followed through stages of incremental loading. A numerical example, employing the proposed method, is presented in this section.

Each stage of behaviour with corresponding load intensity is examined in detail. The structure consists of the "shear core" of a 20-story building and is subjected to lateral load shown in Figure 1 with constant value of ρ = 13 percent. A summary of the properties of this structure is contained in Table I. Figure 6 as well as Table II shows elevation and cross-section dimensions.

The computer program utilized in this investigation is composed of 21 sub-routines and function sub-programs. Computations were carried out on the CDC 6400 at Concordia University Computer Centre. Throughout the investigation, effort was concentrated on developing an operating program. Consequently, no extensive effort was devoted to optimize numerical computations. For this reason a listing of the program is not given.

Considering different load stages the analysis, with results depicted in Figure 7, proceeds as follows:

Stage 1: The load characterizing this stage corresponds to the equivalent static design code loading. Under this load condition the structure responds elastically. The usual assumptions of structure theory concerning elasticity are assumed to be valid.

In the presence of low intensity gravity loading the lateral load corresponding to this stage may be large enough to cause cracking. The effects of cracking have been observed [16,17] and are introduced by a reduction in stiffness of coupled shear wall members by: (a) 70 percent loss of laminar stiffness as a consequence of diagonal and flexural cracking, and (b) 30 percent of the axial and 50 percent of the flexural stiffness of wall 1 is lost because of axial tension and bending moment cracks.

The distribution of the laminar rotation for this load stage is proportional to the laminar shear q. The required laminar ductility (i.e., $\mu_b = \theta/\theta_y$) along the height of the structure, corresponding to this load stage, is shown in Figure 7. The Newton-Raphson method was used to calculate the position of the critically situated lamina at ξ_o. For this structure, $\xi_o = 0.73$. The load which brings the lamina at ξ_o to its elastic limit is the yield load W_y, which can be obtained using Eq. (2.7) with $q_{\xi_o} = q_u$. Thus:

$$q_u = \frac{2\gamma W_y}{H\alpha^4}\left[C\alpha\cosh\alpha\xi_o - \alpha\sinh\alpha\xi_o - 1 - \right.$$
$$\left. - \frac{\alpha^2}{2}(\xi_o^2 - 2\xi_o - \rho)\right] \qquad (3.41)$$

The yield load and corresponding top deflection, for this example, are: $W_y = 617$ kips ($W_y/W_u = 0.6$) and $\delta_{y_{TOP}} = 4.56$ in. ($\simeq H/460$), as seen in Figure 6.

The critically situated lamina rotation, from Eq. (2.12) for $W = W_y$ and $\xi = \xi_o$, provides the yield laminar rotation θ_y. This laminar rotation, just prior to the onset of yielding corresponds to a ductility factor $\mu_b = 1$.

Stage 2: Further load increase will cause other coupling beams to enter the plastic range. The boundary coordinates η and ζ, defining the plastic region, are obtained using Eqs. (2.7) and (3.36). The total triangular load W, is obtained from Eq. (3.38).

This stage of behaviour terminates at load which brings the topmost lamina to its elastic limit. It is possible, however, that no plastic laminar rotation can occur in the upper stories of the structure. This will be a case when the walls are relatively slender with respect to the coupling beams. Hence, the load which will cause one of the walls to attain its elastic limit before the topmost lamina yields will terminate this load stage. This occurred in the present 20-story shear core, with 20 percent of all laminae unyielded when wall 1 attained its elastic limit. The termination of this stage is specified in Figure 6 with: W = 900 kips (W/W_u = 0.87) and δ_{TOP} = 8.9 in. (≈ H/236).

It is significant to note that Paulay's assumption that all laminae yield before hinging of wall 1 was not valid for this structure.

Stage 3: This stage describes the behaviour from yielding of wall 1 up to formation of plastic hinges at the ends of the topmost coupling beam. It is to be noted that the possibility exists of forming a plastic hinge at the base of wall 2 before the topmost lamina yields. If this happens the ultimate state (or effective overall collapse) of the structure is assumed to have been reached even though a complete collapse mechanism has not formed.

For the 20-story shear core analysed here the plastification of all laminae is achieved before wall 2 attains its elastic limit.

The load which defines the end of this stage is W = 992 kips ($W/W_u = 0.96$).

Assuming that, after a plastic hinge is formed at the base of wall 1, the yielded section can continue to carry additional axial force, laminar rotation and the wall deflection are defined by the same equations used in the previous stage. The validity of this assumption will be discussed in the next chapter.

Figure 6 shows the distribution of rotational ductility μ_b as well as wall top deflection at the end of this stage. The top deflection is $\delta_{TOP} = 10.86$ in. ($\approx H/193$).

Stage 4: This stage is characterized by plastic hinges formed at the ends of all connecting laminae and at the base of one of the walls (in this case, wall 1).

Any additional load will be taken by wall 2 acting as a simple cantilever while the wall 1 behaves as an ineffective member.

The load responsible for wall 2 yielding is W = 1032 kips ($W/W_u = 1.0$), with concentrated force at the top of the structure of 134 kips. This load, together with deflection

of δ_{TOP} = 13.6 in. (≈ H/150) defines overall collapse, as shown on Figure 6.

The presence of a plastic hinge at the base of wall 2 defines a complete collapse mechanism with wall 1 and all laminae yielded. The corresponding overall ductility factor μ_s = 3.0 characterizes the attainment of the ultimate load in this case. Figure 7 indicates, however, that the critically situated coupling beam, at about midheight of the structure, undergoes much larger plastic action, corresponding to a ductility factor of 9.75. For earthquake-resistant structures an overall ductility factor of at least 4 is considered to be essential. In the example structure this would correspond with 18.5 in. deflection of the top, and the critically situated coupling beam would need to possess a ductility capacity of more than 20.

3.7 Comparison with the Results from Other Methods

For the purpose of examining the approximations of the analysis proposed in this study comparisons of results with numerical examples provided by Glück [11] and Paulay [10] were made and these are discussed in this section.

The example of an 18-story shear core, reported by Glück [11] is used as the first comparison with the method of this study. Top deflection vs. lateral load (upper triangular pattern only) diagram as obtained in this study is shown in Figure 8. Also shown are solutions obtained by Glück's method up to

incipient yielding of wall 1 where Glück's method terminates. The agreement of the results is very good. Numerical values of this comparison, for wall axial force as well as beam ductility factor, are available in Table III. Overall failure of this structure was obtained by the present analysis and found to consist of a complete collapse mechanism with hinges in both walls and yielding of all connecting elements.

Since Glück's analysis defines failure as limitation on the ductility factor of the connecting laminae, with vertical walls completely elastic, results cannot be compared after wall one yields.

To demonstrate the accuracy of the analysis developed in this study for stages of behaviour when all laminae yield and a plastic hinge is formed at the base of one of the walls, a comparison was made with Paulay's elasto-plastic analysis [10]. The compared results are shown in Figure 9, where it can be seen that the difference between them is minimal.

Table IV contains numerical values for other response parameters, considered in this comparison, which show equally good agreement.

Thus, it may be concluded that the method of analysis of this study agrees closely with existing methods over ranges of behaviour where the latter are applicable. Unfortunately, inadequate experimental data on the elasto-plastic behaviour of coupled shear walls are available. Hence, the applicability and the accuracy of the proposed analysis cannot be verified by experimental behaviour.

CHAPTER IV

MOMENT-AXIAL FORCE INTERACTION IN WALLS

4.1 Introduction

The interrelationship between the effects of axial load and applied moment on a reinforced concrete cross-section is best shown by means of interaction diagrams. These diagrams are graphical depictions of material failure envelopes for reinforced concrete sections under various combinations of axial load and bending moment.

The walls of a coupled shear wall structure resisting seismic forces behave as beam-column elements subjected to bending moments from lateral loads and axial tension or compression resulting from the shear force in the coupling system. The magnitude of the axial force generated in the walls from efficient shear transfer between them can be large. Because axial force on shear walls increases with increasing load, ultimate moment capacity is simultaneously affected.

The importance of analyzing the interaction between applied, as well as resisting capacity, axial load and bending moment for the critical sections of the walls is therefore evident.

The investigation (or design) of square and rectangular sections subjected to axial compression in combination with bending moment has received considerable attention. Several

methods of analysis are available [18] and much experimental data has been reported. However, little attention has been given to the behaviour of rectangular or square sections subjected to axial tension combined with bending moment. Similarly "T" sections subjected to bending and axial compression have not been investigated to a meaningful extent.

The combination of axial force and bending moment is characteristic for the walls of a coupled shear wall structure, which carries low intensity gravity load. Common examples are "shear cores" of tall buildings which accommodate elevator shafts, stairwells and service ducts having "T", "U" or "I" cross sections.

Therefore, attention should be given in the analysis of the walls of a coupled shear wall structure to the interaction of axial compression in combination with bending moment, as well as axial tension and bending moment, for various shapes of cross section.

In this chapter ultimate strength analysis is examined for rectangular sections exposed to bending and axial tension and also "T" sections under bending moment and axial compression.

4.2 Interaction Diagrams

Combined bending and tension for rectangular sections as well as bending and compression for "T" sections will be

discussed in this section considering cases of small and large eccentricity of the axial force.

4.2.1 Combined Bending and Tension -- Rectangular Section

In general, the combination of bending and large axial tensile force in reinforced concrete is an undesirable situation. The problem will be treated from the viewpoint of ultimate strength of a section by satisfying force and rotational equilibrium conditions.

When combined axial tension and bending act on a section, depending on eccentricity e_o (expressed as the ratio of M to T), two cases arise:

1. Small eccentricity -- tension over the entire section such that the tensile stress in the steel reaches the yield stress, and

2. Large eccentricity -- tension over most of the section such that the tension steel yields before the compressive strain reaches 0.003 in the concrete.

In the first case, where eccentricity is small and where the tensile force is applied between the centroids of the primarily tension and compression steel, A_s and A'_s, respectively (see Figure C1(a)), the concrete will crack shortly after loading begins. Therefore, by distributing it according to the principle of a lever; i.e., in inverse proportion to distances from force T, failure will set in

when ultimate stresses are achieved in the steel. The derivation of the equations which govern the distribution of axial force T between A_s and A'_s is presented in Section C2.1 of Appendix C.

The second case, the case of large eccentricity, occurs when the tensile force acts beyond the centroids of A_s and A'_s (see Figure C2(a)). Part of the section will be in compression and part will be in tension. This is a condition similar to large eccentricity compression. Failure will occur due to yielding of the tension steel A_s, or due to crushing of the concrete. The analysis of this case, shown in Figure C2(a), is formulated in Section C2.2 of Appendix C.

The derivation of the ultimate capacity is accomplished by direct application of statics, using coefficients for rectangular sections, and assuming a rectangular compressive stress block.

Figure 10 illustrates results for a rectangular section subjected to combined bending and axial tension. This interaction diagram applies to the section of the base of wall 1 (Figure 6) of shear core of the 20-story building examined in Section 3.6.

4.2.2 Combined Bending and Compression -- "I" Section

Similarly, when combined axial compression and bending moment act, ultimate strength of a section also involves two cases:

1. Small eccentricity -- compression over most or all of the section such that the compressive strain in the concrete reaches 0.003 before tension steel yields, known as the "compression control" condition, and

2. Large eccentricity -- tension in a large portion of the section such that the tension steel has yielded when the compressive strain in the concrete reaches 0.003, known as the "tension control" condition.

The analysis of a "T" section, where ultimate strength lies at various points on the interaction diagram, is treated in detail in Section C1 of Appendix C.

The critical section, at the base of wall 2, was examined for combined bending moment and axial compression. The resulting interaction diagram is shown in Figure 11. The properties of this section are documented in Figure 6 and Tables I and II.

4.3 Effect of Moment-Axial Force Interaction on Coupled Shear Wall Behaviour

The effect of the interaction between axial load and bending moment on the beheaviour of a coupled shear wall structure is examined for the 20-story structure described in Section 3.6.

Four possible assumptions for wall ultimate capacity have been investigated: -

1. Ineffective Cantilever (Case 1) — After a plastic hinge is formed at the base of wall 1, according to the moment-axial tension capacity of Figure 10, the section cannot resist additional bending moment nor increase in axial force. In this case wall 1 becomes an ineffective cantilever and the additional applied load is resisted by wall 2 acting alone. The growth, with increasing external load, of moment and axial force in walls 1 and 2 is shown in Figures 12 and 15 (Case 1). The tensile force and bending moment for the critical section of wall 1 remain constant after yielding. Further load increase will cause additional bending moment at every section of wall two, while the axial compression force remains constant because of the termination of the coupling action between walls. The collapse mechanism is formed when the base section of wall 2 reaches its ultimate state for bending moment capacity in the presence of axial compression force P_u (Figure 12 and Figure 15(b), Case (1)).

2. Complete Interaction (Case 2) -- Before a plastic hinge is formed at the base of wall 1, the behaviour of the coupled shear wall system is the same as for the previous case. After wall 1 forms a hinge, according to the interaction diagram of Figure 10, coupling action between the walls is assumed to continue. Therefore, additional load will increase the axial force in the walls. The relation between bending moment and the axial force

capacity after formation of a hinge in wall 1 follows the moment-axial tension strength diagram as shown in Figure 13.

The history, up to overall collapse, of axial compression at the critical section of wall 2 is shown in Figure 14. The overall collapse mechanism is formed when the loading path on the base section of wall 2 reaches the failure envelope for this section.

3. Partial Interaction (Case 3) -- This is the case when, after yielding of wall 1, coupling action between the walls is not terminated but where it is assumed that the axial tensile force may continue to increase while the bending moment capacity at the base of wall 1 remains constant (at M_u = 115,000 in.-kips, from Figure 10). The bending moment at the base of wall 2, after every load increase, is:

$$M_2 = M - M_{u_1}$$

where M_2 is the bending moment at the base of wall 2, M is the total base moment on both walls, and M_{u_1} is the plastic hinge moment at the base of wall 1.

4. No Interaction (Case 4) -- After the moment-axial force ultimate capacity is reached at the base of wall 1 hinge action is ignored and this wall is assumed to continue to behave elastically until yield in pure

bending or pure tension occurs. Collapse occurs when wall 2 attains its moment-axial force capacity according to Figure 11. Case 4 of Figure 15 shows the moment-axial force loading history for walls 1 and 2 for this case.

The moment-axial force loading history for all four cases is summarized in Figure 15. For all cases collapse occurs when wall 2 attains its ultimate capacity. The effect of wall 1 behaviour on wall 2 loading history can be examined in Figure 15(b). Approximately the same ultimate bending moment at failure is characteristic for all cases, while the maximum variation in ultimate axial compression force is approximately 10 percent (between Cases 1 and 4).

The ultimate load capacity of the system and appropriate top deflection diagrams are shown in Figure 16. A maximum difference in W_u of 15 percent, between Cases 1 and 4, is found. The ductility required of the system to reach the ultimate load state can be obtained from this diagram. The corresponding system ductility factors are: (1) Case 1, $\mu_s = 3.3$; (2) Case 2, $\mu_s = 2$; (3) Case 3, $\mu_s = 2.2$; and (4) Case 4, $\mu_s = 2.4$. Therefore, the maximum difference in the system ductility factor is found between Cases 1 and 2:

The corresponding beam rotational ductility factors μ_b are 11.7, 5.6, 6.8 and 8.5 for Cases 1 through 4, respectively. Thus, the minimum beam rotational ductility requirement is obtained for Case 2, where wall one participates in the overall behaviour by following its moment-axial force interaction relationship.

Paulay's method [10] is based on a collapse mechanism similar to that of Case 1. As the data above show, both beam as well as system ductility factors are considerably overestimated for this structure by his method.

In case of coupled shear wall structures some moment-axial force interaction for the critical sections of the walls takes place. The probable behaviour will fall between Cases 1 and 2. For this reason, in the investigations reported in this study interaction is considered according to Case 2; namely, complete moment-axial force interaction in both walls.

CHAPTER V

PARAMETRIC INVESTIGATION OF NON-LINEAR BEHAVIOUR

5.1 Introduction

Employing the elasto-plastic analysis discussed in Chapter III, the lateral load response behaviour of a series of coupled shear wall structures is presented in this chapter. First, parameters related to the geometric stiffness properties of the coupled system are identified and the influence of certain building dimensions on typical values are examined. Non-linear behaviour is studied for variations of these stiffness parameters, as well as parameters related to strength and loading. In particular, ductility requirements at overall collapse, in terms of coupling beam rotational ductility factor μ_b and system displacement ductility factor μ_s, are examined in a parametric investigation where principal parameters are:

1. Coupling shear strength q_u;
2. System stiffness parameters α, γ, ψ and Z (defined in the following section); and
3. Loading condition as defined by ρ.

The series of structures analyzed was generated by variation of a particular parameter using the basic 20-story prototype structure described in Section 3.6.

5.2 Physical Interpretation of Stiffness Parameters

The parameter α, defined by Eq. 2.2, can be written alternatively as:

$$\alpha = \sqrt{\lambda}\left\{\left(\frac{144}{hs^3}\right)\left(\frac{I_b}{t}\right)\left(\frac{\ell^2}{d_1^3 + d_2^3}\right)\right\}^{1/2} H \qquad (5.1)$$

where t is the thickness when rectangular cross-sections of all members are considered, other terms were defined previously (Figure 6), and:

$$\lambda = 1 + \frac{A_0 I_0}{A_1 A_2 \ell^2} \qquad (5.2)$$

in which $A_0 = (A_1 + A_2)$, the sum of cross-section areas of walls 1 and 2.

Parameter λ may be rewritten in the form:

$$\lambda = 1 + \frac{1}{12}\left(\frac{d_1 + d_2}{d_1 d_2}\right)\left(\frac{d_1^3 + d_2^3}{\ell^2}\right) \qquad (5.3)$$

By considering typical dimensions to be encountered for the 20-story prototype structure the range of variation of parameters α and λ may be obtained.

As Eq. (5.3) indicates, parameter λ is a function of the wall cross-sectional dimensions only. The clear span of the coupling beams in this 20-story shear core was assumed constant at 6 ft. The story height h = 8.75 ft. is fairly typical for modern apartment buildings. With these values for s and h, parameters λ and α depend only on variables d_1, d_2, I_b and t, since the wall centroidal distance ℓ is specified by:

$$\ell = \frac{1}{2}(2s + d_1 + d_2) \qquad (5.4)$$

for walls which are rectangular in cross-section. Similarly, the height of the structure H may also be treated as a known parameter. The width of buildings considering a possible height range of 100 to 300 ft. will generally lie within the range 46 to 70 ft. Thus, $(d_1 + d_2)$ will lie between 40 and 64 ft. for walls extending through the entire width of the building. On the other hand, in the case of shear cores of tall buildings which accommodate elevator shafts, stair-wells and service ducts, $(d_1 + d_2)$ may range from 18 to 38 ft.

For simplicity, walls may be assumed to have equal widths, i.e., $d_1 = d_2$. This leads to values of λ for the two possible extreme values for $(d_1 + d_2)$, i.e., 18 and 64 ft., of 1.12 and 1.24, a maximum variation of 10 percent. As will be shown later, this variation in λ may have a considerable influence on the non-linear response behaviour of the coupled shear wall system.

Finally, with fixed values of s and h this range for λ leads to expected values for stiffness parameter α given by:

$$\alpha = (0.115 \text{ to } 0.046)\left(\frac{I_b}{t}\right)^{1/2} H \qquad (5.5)$$

In buildings with 6 to 8 in.-floor slabs and panel widths of, say, 20 to 24 ft., the value of I_b may be expected to

range from 0.21 to 0.59 ft^4. On the other hand, where wall coupling is due to spandrel beams 18 to 36 in. deep and usually 12 in. wide, the value of I_b may vary from 0.28 to 2.25 ft^4. With shear wall thickness t from 12 to 24 in., the term $(I_b/t)^{1/2}$ varies between 0.32 and 1.5, with I_b and t expressed in ft.

The preceding discussion of the expected variation of values for α is summarized in Figure 17. The values of α expected to occur in practice for varying connecting beam moment of inertia I_b, wall thickness t, building height H, and wall widths $d_1 = d_2$, are thus expected to lie between 2 and 50, approximately. Figure 17 also indicates that increase of height H for constant width of walls is accompanied by an increase in the value of α. Similarly, as the connecting beam moment of inertia increases, the value of α increases. This observation indicates that α is a geometric stiffness parameter representing the ratio of coupling beam to wall cross-sectional relative stiffness.

The parameter γ of Eq. (2.3) can also be rewritten for walls with rectangular cross-sections as:

$$\gamma = \left[\frac{144\ell}{hs^3(d_1^3 + d_2^3)}\right]\left(\frac{I_b}{t}\right) H^3 \qquad (5.6a)$$

For the variations in typical building dimensions discussed above, the expected values of γ for given overall height H,

---

† The values of the parameters α, γ, ψ and Z for the prototype structure are 12.3, 1094.6, 7.23 and 6.06×10^{-3}

coupling beam moment of inertia I_b, and wall thickness t are provided by Figure 18. For any arbitrarily chosen wall cross-sections parameter γ can be presented as:

$$\gamma = 12\left(\frac{I_b/s^3}{I_0/H^3}\right)\frac{\ell}{h} \tag{5.6b}$$

Considering that the terms I_b/s^3 and I_0/H^3 represent the relative stiffnesses of coupling beams and walls, respectively, it is obvious (from Eqs. (5.6a) and (5.6b)) that parameter γ also represents the system's ratio of beam to wall relative stiffness. Consequently, γ increases with increase of the relative stiffness of connecting beams in a manner similar to that of α.

To attempt to isolate the influence of wall width, thickness, and height on overall behaviour, a third stiffness parameter ψ may be introduced as:

$$\psi = \frac{\gamma}{\alpha^2} \tag{5.7}$$

Alternatively written, this becomes:

$$\psi = \frac{H}{\left[1 + \frac{1}{12}\left(\frac{d_1 + d_2}{d_1 d_2}\right)\left(\frac{d_1^3 + d_2^3}{\ell^2}\right)\right]\ell} \tag{5.8}$$

which may also be expressed as:

$$\psi = \frac{1}{\lambda}\left(\frac{H}{\ell}\right) \tag{5.9}$$

Employing the extreme values of λ obtained previously, Figure 19 shows the variation of ψ as a function of H/ℓ. It

is apparent that the value of ψ depends primarily on coupling aspect ratio H/ℓ. The influence of λ is seen to be negligible for practical consideration; thus, parameter ψ may be treated as representing the coupled system aspect ratio H/ℓ.

Finally, the ratio of beam to wall rotational stiffness may be expressed directly by parameter Z, defined by:

$$Z = \frac{(I_b/\ell)}{(I_o/h)} \qquad (5.10)$$

Coupled shear wall structures often have walls with "T" sections. As noted previously, this is the case when elevator shafts, stairwells, etc., need to be accommodated. The parameters discussed above apply equally to such walls as to rectangular ones. The size of flanges of "T" sections affect the stiffness of the overall system and the values of α, γ, ψ, and Z will correspond to those obtained for structures with stiff rectangular walls.

5.3 Results and Discussion

5.3.1 Parametric Scheme

The parametric investigation discussed in Section 5.1 was conducted according to the following variation of parameters:

1. Ultimate coupling shear capacity q_u (expressed in kips per inch of height) for the example structure was varied from q_u = 0.5 kips/in. which corresponds to the

shear capacity of coupling beams with tensile reinforcement $p = 0.125\ p_b$ to $q_u = 4.0$ kips/in. which corresponds to balanced tensile reinforcement $p = p_b$. The structural geometry and stiffness as well as the ultimate capacity of walls (Tables I and II) remain unchanged.

2. The value of geometric stiffness parameter α was varied from 9 to 14. This range corresponds to the geometry of frequently utilized coupled shear walls. Variation of α was accomplished for the prototype structure by modifying wall widths d_1 and d_2, which is automatically accompanied by a change in ℓ, the distance between wall centroidal lines. All other quantities remained unchanged from values listed in Tables I and II. The value $\alpha = 9$ corresponds to $d_1 = 18$ ft., $d_2 = 18$ ft., and $\ell = 28.1$ ft., while $\alpha = 14$ corresponds to $d_1 = 10$ ft., $d_2 = 10$ ft., and $\ell = 19.30$ ft. It is to be noted that smaller values of α are associated with relatively stiff walls and larger values relate to slender walls.

3. Variation in the loading condition consisted of varying the top point load ρW of Figure 1 over the range $\rho = 0$ to $\rho = 0.15$, with W representing the resultant of the distributed lateral load. The concentrated force ρW applied to the top of the structure is specified by seismic codes to include the effect of higher modes. The 1975 National Building Code of Canada [19] specifies values of ρ from 0 to a maximum of 0.15 of the

base shear, depending on the slenderness ratio of the lateral load resisting system. All data obtained for other parameter variations were obtained for $\rho = 0.13$†.

The above parametric scheme involving α and q_u result in four different types of structures which may be defined as follows:

1. Stiff walls (α = 9) combined with a strong coupling system (q_u = 4.0 kips/in.).
2. Stiff walls (α = 9) combined with weak coupling system (q_u = 0.5 kips/in.).
3. Slender walls (α = 14) combined with strong coupling system (q_u = 4.0 kips/in.).
4. Slender walls (α = 14) combined with weak coupling system (q_u = 0.5 kips/in.).

The data obtained from analysis of the non-linear behaviour of these four types of structures are discussed below.

5.3.2 Load-Displacement Behaviour

The response of a particular structure to horizontal loading can be characterized in terms of load-displacement diagrams. The effect of strength of the coupling beams expressed in terms of q_u on the load-displacement behaviour

† The value of $\rho = 0.13$ was selected to represent relatively slender structures where the base overturning moment is equal to 0.8 WH.

for the example structure (Section 3.6; Figure 6 and Tables I and II) is illustrated in detail in Figure 20(a).

The behaviour for q_u = 0.5 kips/in. and q_u = 4.0 kips/in. may be considered limiting cases. The value of q_u = 0.5 kips/in. corresponds to strength of the coupling beams reinforced slightly less than the minimum required for any flexural member†, and q_u = 4.0 kips/in. represents coupling beams reinforced to produce balanced condition as noted earlier. The value q_u = 2.5 kips/in. corresponds to reinforcement ratio $p = 0.5\ p_b$, the maximum permissible ratio for ductile design [19].

The following observations concerning the effect of coupling capacity q_u are indicated by the load-displacement behaviour shown in Figure 20(a):

(i) For the coupled shear wall with normal level of coupling action (q_u = 2.5 kips/in.) between the walls, the ultimate load (W_u = 1170 kips) may be up to 10 times greater than for corresponding uncoupled cantilever walls (q_u = 0; W_u = 112 kips).

(ii) The introduction of coupling action (i.e., $q_u > 0$) is accompanied by ductile system behaviour. However, as strength q_u is increased to values beyond the original design (i.e., q_u > 2.5 kips/in.) the behaviour

† $p_{min} = 200/f_y$ [19].

becomes increasingly less ductile. For example, the system ductility factor μ_s is 1.75 when q_u = 4.0 kips/in. and 9.9 when q_u = 0.5 kips/in. The value μ_s = 2.4 is obtained when q_u = 2.5 kips/in. (prototype design). The failure envelope, shown as the dashed line in Figure 20(b), indicates the variation in ductile behaviour with differing q_u.

(iii) Weak coupling beams (q_u = 0.5 kips/in.) lead to the formation of a ductile collapse mechanism where almost all of the coupling beams yield (98% for this example) and plastic hinges form at the base of the walls, while strong coupling beams (q_u = 4.0 kips/in.) lead to an incomplete collapse mechanism where a portion of the beams (13% at the top and 4% at the bottom) do not yield prior to formation of the wall hinges.

The effect of stiffness parameter α on the load displacement behaviour is shown in Figure 20(b). The data was obtained for coupling beams with $p = 0.5\ p_b$ (q_u = 2.5 kips/in.) and the following observations are indicated:

(i) A small value of α (9.0) implies relatively stiff walls and behaviour is characterized by small ultimate top deflection ($\delta_{u_{TOP}}$ = 4.0 in.) and small

ductility factor (μ_s = 1.39). This means brittle behaviour.

(ii) A large value of α (14) corresponds to slender walls and large deflection ($\delta_{u_{TOP}}$ = 23.0 in.) and ductility factor (μ_s = 3.57). First and last beam yielding is followed by a large displacement range, thus producing ductile overall behaviour. For the example with α = 14 first yield occurred at the critically situated beam (ξ_0 = 0.74) for load W_y = 620 kips ($\delta_{y_{TOP}}$ = 6.46 in.). This was followed by yielding first of wall 1 (W = 828 kips, δ_{TOP} = 10.67 in.), and then of the topmost beam (W = 1019 kips, δ_{TOP} = 16.94 in.) before a plastic hinge was formed at the base of wall 2 (W_u = 1069 kips).

(iii) The ultimate load W_u is not significantly affected by the change in α. A maximum difference of 11.7 percent (ΔW = 125 kips) was found, between the ultimate load (W_u = 1069 kips) for α = 14 and that for α = 10 (W_u = 1194 kips).

Based on the above observations, corresponding energy capacities of lateral collapse may be expected to follow similar trends. For a system with given distribution of structural strength, large values of α indicate ductile behaviour and, hence, good energy capacity.

5.3.3 Effect of Stiffness Parameters on Ductility Requirements

The variation of ductility demand with coupling beam strength for different values of α are shown in Figures 21 and 22. The following observations are noted:

(i) The classification of the structures into four different groups (Section 5.3.1) can be employed easily to examine the behaviour represented by these diagrams.

(ii) The curves for α = 9 to 14 incidate that increasing of strength q_u of the coupling beams reduces ductility requirements for given stiffness parameter α. This is particularly evident for stiff walls where values of α are small (9 and 10).

Here, collapse occurs when plastic hinges are formed at the bases of both walls while up to 45% of all coupling beams remain elastic (e.g., α = 9, q_u = 4.0 kips/in.; stiff walls combined with a strong coupling beams). For values of α = 12.3 and 14 and q_u = 4.0 kips/in. (slender walls combined with strong coupling beams) the percentage of beams still elastic when collapse occurs is 17% and 7%, respectively.

(iii) Weak coupling beams, where values of q_u are small, require large ductility capacities. This implies ductile failure behaviour provided beam ductility capacity is available to allow formation of the collapse mechanism. For example, it was found that for $\alpha = 14$ and $q_u = 0.5$ kips/in. (a structure with slender walls combined with weak beams) the beam ductility requirement is $\mu_b = 70$ and the system ductility factor $\mu_s = 13.6$. If the stiffness of walls is increased (so as to reduce the value of α to 9), the corresponding ductility factor decreases to more acceptable values of 4.6 and 4.6, respectively. The collapse mechanism for all cases of structures when q_u is small (0.5 to 1.0 kips/in.) occurs when ≈ 98% of all laminae have yielded before plastic hinges are formed at the bases of both walls.

(iv) Increasing $q_u > 2.5$ kips/in. (i.e., stronger than the prototype design) does not result in significant changes in μ_b and μ_s, unless walls are very slender (i.e., $\alpha = 14$). For example, a change in q_u from 2.5 kips/in. to 4.0 kips/in. for $\alpha = 9$ changes μ_b from 1.5 to 1.3 and μ_s from 1.29 to 1.28.

(v) The dashed line in Figure 22 incidates the limit for practical ductility capacity of the system, while

Figure 21 shows the coupling beam ductility associated with failure at $\mu_s = 4$. Hence, to utilize a system ductility capacity of 4 requires a beam ductile capacity μ_b from 12 to 17. This implies that in most cases coupling beam ductility μ_b will define the ultimate state.

Figure 23 shows the effect of variations of d_1, d_2 and ℓ expressed in terms of geometric stiffness parameter α on the ductility factors μ_b and μ_s at failure, plotted for different strengths q_u. Observations similar to those noted for Figures 21 and 22 are evident, since this is the same data replotted.

The influence of stiffness parameter ψ† on ductility requirements is shown in Figure 24, where μ_b and μ_s are replotted as functions of ψ. The data presented in Figures 24(a) and 24(b) show that the ductility demand depends on ψ in a manner similar to that of α (Figure 23), regardless of the fact that ψ depends on the stiffness of walls only. Small values of ψ (5.5 and 6.0) correspond to relatively stiff walls (i.e., $d_1 = d_2 = 18$ to 16 or expressed by α as 9 to 10) while larger ψ (7.5 and 8) represent relatively slender walls ($d_1 = d_2 = 12$ to 10, where $\alpha = 12.3$ to 14). By analyzing plotted data, the following observations are

† Parameters ψ and Z were not varied independently; instead, they were evaluated from values of d_1, d_2 and ℓ generated for variation of α.

noted:

(i) Increasing the coupling beam strength q_u leads to more brittle failure for any value of stiffness parameter ψ. This is more characteristic when the value of ψ is small (i.e., stiff walls, ψ = 5.5). This type of structure was characterized earlier as stiff walls combined with strong coupling beams.

(ii) Ductile failure will correspond to large values of ψ (above 7.5) in combination with weak coupling beams (q_u = 0.5 to 1.0). In this case the coupling beam ductility capacity has to be ensured to allow formation of a ductile failure mechanism.

(iii) Comparison of Figures 24(a) and 24(b) shows that the system ductility factor μ_s is considerably more sensitive to changes of ψ than is the beam ductility factor μ_b.

Figure 25 shows ductility factors μ_b and μ_s plotted as a function of stiffness parameter Z. The stiffness parameter Z expresses the ratio of beam rotational stiffness I_b/s to coupled wall story stiffness I_o/h where the change of the latter only leads to change in Z for the structures of this study. Small values of Z (i.e., 0.25 and 0.3) correspond to relatively stiff coupled systems (i.e., $d_1 = d_2$ = 16 to 18) while for slender walls corresponding values of Z are

larger (0.8 to 0.7) which correspond to wall widths of 10 to 12 feet. It is evident that variations of Z have similar effects on ductility factors μ_s and μ_b as previously described parameters α and ψ; namely, small values of Z (0.25 to 0.3) lead to brittle failure characteristic of stiff structures and large values of Z (0.7 to 0.8) lead to more ductile behaviour.

It is clear from the above discussion that parameters α, ψ and Z can be applied equally to represent the system stiffness characteristics in studying ductility demand.

In summary, the above observations and the data presented in Figures 21 through 25 allow the following general conclusions concerning the effect of the geometric stiffness parameters:

1. Shear walls that are flexible relative to the stiffness of connecting beams generally require large ductility capacities for both the beams (μ_b) as well as for the overall system (μ_s), (e.g., Figures 23, 24 and 25 for $\alpha = 14$, $\psi = 8$ and $Z = 1.4$).

2. An increase in the flexibility of walls results in a more rapid increase of ductility demand for weak beams than for strong beams (e.g., Figure 25 for $q_u = 1.0$ kips/in. and 4.0 kips/in.).

3. Flexible walls and weak beams usually exhibit a failure state involving yielding of ≈ 98% of all beams and plastic hinges at the base of both walls and require large ductility factors (e.g., Figure 23 for $\alpha = 14$, $q_u = 1.0$ kips/in., where $\mu_b = 38$ and $\mu_s = 8.15$).

4. Flexible walls in combination with strong beams exhibit a lateral failure state involving plastic hinges at the base of both walls while 5 to 15 percent of the beams at the top and 2 to 4 percent of those at the base behave elastically (e.g., Figure 23, for $\alpha = 14$ and $q_u = 4.0$ kips/in., where $\eta = 0.05$ and $\xi = 0.98$; and for $\alpha = 12.3$, $q_u = 4.0$ kips/in., where $\eta = 0.13$ and $\xi = 0.96$). The critically situated beam in the middle zone of the structure as well as the overall structure do not have large ductility requirements (e.g., Figure 23 for $\alpha = 14$ and $q_u = 4.0$ kips/in., where $\mu_s = 2.3$ and $\mu_b = 8.0$).

5. Stiff walls and weak beams usually exhibit a failure state involving yielding of ≈ 98 percent of all beams with plastic hinges at the base of both walls with not large ductility requirements (e.g., Figure 23 for $\alpha = 9$, $q_u = 1.0$ kips/in., where $\mu_b = 6.6$ and $\mu_s = 2.4$).

6. Stiff walls and strong beams usually exhibit a failure state involving plastic hinges at the base of both walls

while up to 45 percent of the coupling beams remain elastic (e.g., Figure 23, for $\alpha = 9$ and $q_u = 4.0$ kips/in.). It is evident that brittle failure occurs and the ductility requirements are very small (e.g., Figure 23, for $\alpha = 9$ and $q_u = 4.0$ kips/in., where $\mu_s \simeq 1.28$ and $\mu_b = 1.3$).

5.3.4 Effect of Loading Conditions

The requirements of many codes as well as the 1975 National Building Code of Canada [19] require a concentrated load at the top of the structure. Figure 26 shows the variation of the beam ductility factor μ_b and system ductility factor μ_s as functions of ρ, varied from 0 to 15 percent of the total base shear force for the example structure. The following observations are indicated:

(i) Top force reduces the calculated beam ductility factor at collapse by ≃ 3 percent and system ductility by ≃ 5 percent (i.e., Figure 26 for $\rho = 15\%$ the beam ductility factor $\mu_b = 4.7$ and the system ductility factor $\mu_s = 1.82$ and for $\rho = 0\%$ $\mu_b = 4.84$ and $\mu_s = 1.91$). Hence, more brittle (or less ductile) behaviour characterizes an increase of the top force.

(ii) Investigations where only triangular loading is assumed will produce conservative ductility requirements. This suggests that uniform loading will be more conservative still.

(iii) The collapse mechanism for both $\rho = 0\%$ and $\rho = 15\%$ includes plastic hinges in both walls and 98 percent of all lamina yielded with variation of the ultimate load of 3.7 percent.

CHAPTER VI

SUMMARY AND CONCLUSIONS

An elasto-plastic analysis has been presented for the behaviour of coupled shear wall structures under incremental lateral loading increasing monotonically up to overall collapse. For this method, the individual connecting beams were replaced by a continuum of laminae. The lateral loading consisted of a triangular distributed component together with a concentrated top force, a condition which approximates the pseudo-static forces of current seismic building codes.

Equations expressing the lateral deflections of the system and the rotations of the coupling beams were obtained, based on the following assumptions: (a) The shear distribution over the central height where beams are first yielded is expressed by the ultimate shear capacity q_u, while the shear distribution over the remainder of the height follows the same pattern as that obtained from elastic analysis; (b) A plastic hinge at the base of one of the walls may occur before the topmost beam becomes plastic. The wall with the plastic hinge at its base is considered to participate as part of the system following its moment-axial force interaction relationship; (c) One the topmost

beam reaches its ultimate capacity, the wall with the plastic hinge at its base is considered to be an ineffective cantilever; (d) Overall collapse is defined when the second wall hinge is formed, with total or partial yielding of the connecting continuum.

To examine the accuracy of the analysis developed in this study, comparisons with numerical examples provided by Glück [11] and Paulay [10] were made. Good agreement was obtained in both cases. The approximation in Paulay's method that 95 percent of all laminae at ultimate load have formed plastic hinges at their ends, was found satisfactory for structures with a relatively weak coupling system. This approximation may not be valid in cases when relatively stiff walls and coupling beams with large ultimate shear strength are combined. Glück's definition of failure, namely that of rotational failure of the coupling beams, was found to be the probable limit on overall capacity for structures where the coupled walls are relatively slender. On the other hand, when relatively stiff walls were combined with strong coupling beams failure was governed by the ultimate strength of the walls.

Four possible assumptions for the effect of moment-axial load interaction of the wall which yields first were investigated. In all cases where coupling beams provide adequate coupling of walls (which is the case usually to

be expected of reinforced concrete shear walls), wall 1 was found to yield first. Therefore, the influence of the post-elastic behaviour of wall 1 on the loading path of wall 2 was examined assuming that wall 1: (a) acts as an ineffective cantilever; (b) follows completely its moment-axial force interaction diagram; (c) follows a simplified moment-axial force interaction, where the moment has constant value while axial force increases; and (d) does not follow any interaction. Approximately the same ultimate bending moment at failure is characteristic of wall 2 for all four cases with a maximum variation of 10 percent in ultimate axial compression force in wall 2, and 15 percent in ultimate load. The minimum beam rotational ductility requirement as well as system ductility was obtained when wall 1 followed completely its moment-axial force interaction. The expected behaviour of a coupled shear wall structure falls between cases where wall 1 acts as an ineffective cantilever and where it follows completely its moment-axial force interaction diagram, after a plastic hinge is formed at its base.

The parametric study of the effect of coupling beam strength showed that the ultimate lateral load capacity of a coupled system may easily exceed the capacity of uncoupled walls by a factor of 10 or more. On the other hand, large ultimate capacity of coupling beams decreases the system ductility and produces non-ductile or brittle overall collapse. Weak

coupling beams lead to formation of a ductile collapse mechanism where almost all of the coupling beams yield, but, of course, also decreases the ultimate lateral load capacity. However, because the coupling beams have limited rotational capacity, the required ductilities may not be supplied to enable formation of ductile collapse mechanism. In some cases, to utilize a system ductility factor of say 4, required large beam ductility capacity of up to 17. This implies that coupling beam ductility will define the ultimate state in most cases.

The parametric study of the effect of the beam to wall stiffness ratio expressed by the stiffness parameter α showed that small values of α (relatively stiff walls) were characterized by reduced ultimate top deflection. However, the ultimate lateral load was found not significantly affected by changes in this stiffness parameter. Flexible walls (large value of α) combined with weak connecting beams require large beam ductility capacities. This suggests that, to avoid beam rotational failure, one should avoid designs which involve flexible wall in combination with weak connecting beams.

The parametric study of the effect of the lateral loading condition showed that the point load at the top required by many codes for tall structures reduces the computed beam

and system ductility requirements of coupled shear walls. Hence, investigations where only triangular or uniform loading is assumed will produce conservative estimates of ductility requirements.

The analyses performed for the parametric investigation summarized above have allowed the failure mechanism under incremental loading to be identified as a function of relative beam to wall properties of stiffness and strength. Depending upon the particular design, four basic types of behaviour were observed: (a) Flexible walls and weak beams usually exhibited a lateral failure process where 98 percent of all beams yielded with plastic hinges at the base of both walls; (b) Flexible walls and strong beams exhibited a lateral failure process involving plastic hinges at the base of both walls with 7 to 19 percent of all beams still elastic; (c) Stiff walls and weak beams involved yielding of up to 98 percent of all beams with plastic hinges at the base of the walls; and (d) Stiff walls and strong beams produced brittle failure where up to 45 percent of all beams remained elastic when plastic hinges had formed at the base of the walls.

Further studies are needed in both analytical and experimental areas to supplement present knowledge. An investigation of the effect of variation of the stiffness of both beams as well as walls with height should be considered. Additional

work by experimental testing is needed to determine reinforcing details which will assure optimum strength, stiffness, and ductility of coupled shear walls.

The extent of the yielding region needs to be investigated and more realistic definitions of ductility factors must be obtained. Also, the P-Δ effect has to be studied particularly for tall coupled shear walls structures.

Finally, it is of interest to attempt a simple function for the shear distribution in the elastic regions, such as a linear variation for example. This would greatly simplify the solution, which if shown to be sufficiently accurate, could allow easy evaluation of non-linear shear wall systems.

REFERENCES

[1] Coull, A. and Stafford Smith, B., The proceedings of a symposium on tall buildings with particular reference to shear wall structures. University of Southampton, April 1966, Pergamon Press, Oxford.

[2] Beck, H., "Contribution to the Analysis of Coupled Shear Walls", ACI Journal, Proceedings, V. 59, No. 8, August 1962, pp. 1055-1070.

[3] Rosman, R. "Approximate Analysis of Shear Walls Subject to Lateral Loads", ACI Journal, Proceedings, V. 61, No. 6, June 1964, pp. 717-733.

[4] MacLeod, I. A., "Lateral Stiffness of Shear Walls with Openings", Tall Building, Pergamon Press Limited, London, 1967, pp. 223-244.

[5] Candy, C. F., "Analysis of Shear Wall Frames by Computer", New Zealand Engineering (Wellington), V. 19, 1964, pp. 342-347.

[6] Girija Vallabhan, C. V., "Analysis of Shear Walls by Finite Element Method", Proceedings of the Symposium on Application of Finite Element Method in Civil Engineering, Vanderbilt University, Nashville, Tennessee, 1969.

[7] Chiyyarath, V., Girija Vallabhan, A., "Analysis of Shear Walls with Openings", Journal of the Structure Division, ASCE, Oct., 1969, No. ST10, pp. 2093-2102.

[8] MacLeod, I. A., "New Rectangular Finite Element for Shear Wall Analysis", Journal of the Structural Division, ASCE, Vol. 90, March, 1969, pp. 309-409.

[9] Winokur, A., and Glück, J., "Ultimate Strength Analysis of Coupled Shear Walls", ACI Journal, Proceedings, V. 65, No. 12, Dec., 1968, pp. 1029-1036.

[10] Paulay, T., "An Elasto-Plastic Analysis of Coupled Shear Walls", ACI Journal, Proceedings, V. 67, No. 11, Nov., 1970, pp. 915-922.

[11] Glück, J., "Elasto-Plastic Analysis of Coupled Shear Walls", Journal of the Structural Division, ASCE, Vol. 99, No. ST8, Aug. 1973, pp. 1743-1760.

[12] Elkholy, I. A. S., and Robinson, H., "An Inelastic Analysis of Coupled Shear Walls", Building Science, Vol. 9, Mar., 1974, pp. 1-7.

[13] Kumarapillai, K. Nayow and Coull, A., "Elastoplastic Analysis of Coupled Shear Walls", Journal of the Structural Division, ASCE, September 1976, No. ST9, pp. 1845-1860.

[14] Coull, A., and Choudhury, R. J., "Stresses and Deflections in Coupled Shear Walls", ACI Journal, Proceedings, V. 64, No. 2, Feb., 1967, pp. 65-72.

[15] Conte, S. D., and Carl de Boor, "Elementary Numerical Analysis", McGraw-Hill Boon Company, 1972.

[16] Paulay, T., "The Coupling of Reinforced Concrete Shear Walls", Proceedings, Fourth World Conference on Earthquake Engineering, Chile, 1969, B-2, pp. 75-90.

[17] Paulay, T., Discussion of "Analysis of Coupled Shear Walls", by A. Coull and J. R. Choudhury, ACI Journal, Proceedings, V. 65, No. 3, March, 1968.

[18] Chu-Kia Wang and Charles, G. Solman, "Reinforced Concrete Design", International Textbook Co., New York, N. Y., 1973.

[19] National Building Code of Canada 1975.

TABLE I - Section Properties for 20-Story Prototype Structure

	Walls				Beam
	A_1	A_2	I_1	I_2	I_b
Case	10^3in.^{2} (m^2)	10^3in.^{2} (m^2)	10^6in.^{4} (m^4)	10^6in.^{4} (m^4)	10^4in.^{4} ($10^{-2}m^4$)
(1)	(2)	(3)	(4)	(5)	(6)
Uncracked Sections	2.996 (1.935)	2.996 (1.935)	6.285 (2.616)	6.285 (2.616)	5.225 (2.170)
Beams and Wall 1 Cracked	2.097 (1.354)	2.996 (1.935)	3.142 (1.308)	6.285 (2.616)	1.567 (0.652)

Note: (1) Ultimate capacity of walls in pure bending, in in. - kips (m - kN):

$M_{u_1} = 4.85 \times 10^5$ (5.48×10^4)

$M_{u_2} = 1.89 \times 10^5$ (2.14×10^4)

(2) Ultimate capacity of walls for pure axial load in kips(kN)

$P_{u_1} = 5.78 \times 10^3$ (2.57×10^4)

$P_{u_2} = 15.44 \times 10^3$ (6.87×10^4)

TABLE II - Dimensions for 20-Story Prototype Structure

Dimension	Value	
Overall height, H, in ft (m)	175	(53.34)
Width of walls, $d_1 = d_2$, in ft (m)	12	(3.66)
Story height, h, in ft (m)	8.75	(2.67)
Connecting beam span, s, in ft (m)	6	(1.83)
Connecting beam depth, d_b, in ft (m)	3	(.91)
Wall flange width, b, in ft (m)	7	(2.14)
Thickness of walls, t, in in. (mm)	14	(356.)
Thickness of flanges, t_o, in in. (mm)	14	(356.)
Reinforcing steel in walls,		
A_{s_1} in in.^{2} (mm^2)	78	(50310.)
A_{s_2} in in.^{2} (mm^2)	30	(19350.)
Reinforcing steel in beams,		
A_s, in in.^{2} (mm^2)	6.8	(4386.)
$A_{s'}$, in in.^{2} (mm^2)	6.8	(4386.)

TABLE III - Comparison of Results with Gluck's Method

Analysis (1)	W kips (2)	$T_{(\xi=1)}$ kips (3)	δ_{TOP} in. (4)	μ_b (max) (5)	Notes (6)
Glück	887	4883	3.18	1.39	$q_u/q_{max} = 0.9$
Proposed		4827	3.23	1.47	
Glück	939	5074	3.46	1.92	
Proposed		5043	3.51	1.92	
Glück	997	5289	3.78	2.45	
Proposed		5268	3.85	2.52	
Glück	1025	5340	3.97	2.86	Wall 1
Proposed		5372	4.02	2.84	Yields
Glück	1140	n.a.	n.a.	n.a.	
Proposed		5753	4.80	4.33	
Glück	1228	n.a.	n.a.	n.a.	
Proposed		6022	5.46	5.63	
Glück	1330	n.a.	n.a.	n.a.	
Proposed		6292	6.26	7.19	
Glück	1398	n.a.	n.a.	n.a.	Wall 2
Proposed		6469	6.85	8.35	Yields

Note: [1] n.a. denotes not available from the corresponding method of analysis

[2] Comparisons in the table above are for case C of Ref. [11] and additional data are obtained by interpolation.

TABLE IV.- Comparison of Results with Paulay's Method

Analysis (1)	W kips (2)	δ_{TOP} in. (3)	$T_{(\xi=1)}$ kips (4)	Notes (5)
Paulay	697	3.30	4640	First Lamina
Proposed		3.22	4650	Yields
Paulay	750	n.a.	n.a.	
Proposed		3.68	4965	
Paulay	850	n.a.	n.a.	
Proposed		4.40	5469	
Paulay	963	n.a.	n.a.	
Proposed		5.30	5930	
Paulay	1076	6.5	6248	Topmost Lamina
Proposed		6.40	6314	Yields
Paulay	1203	9.40	6248	Wall 1
Proposed		9.18	6314	Yields
Paulay	1267	11.80	6248	Wall 2
Proposed		11.67	6314	Yields

Note: n.a. denotes not available from the corresponding method of analysis.

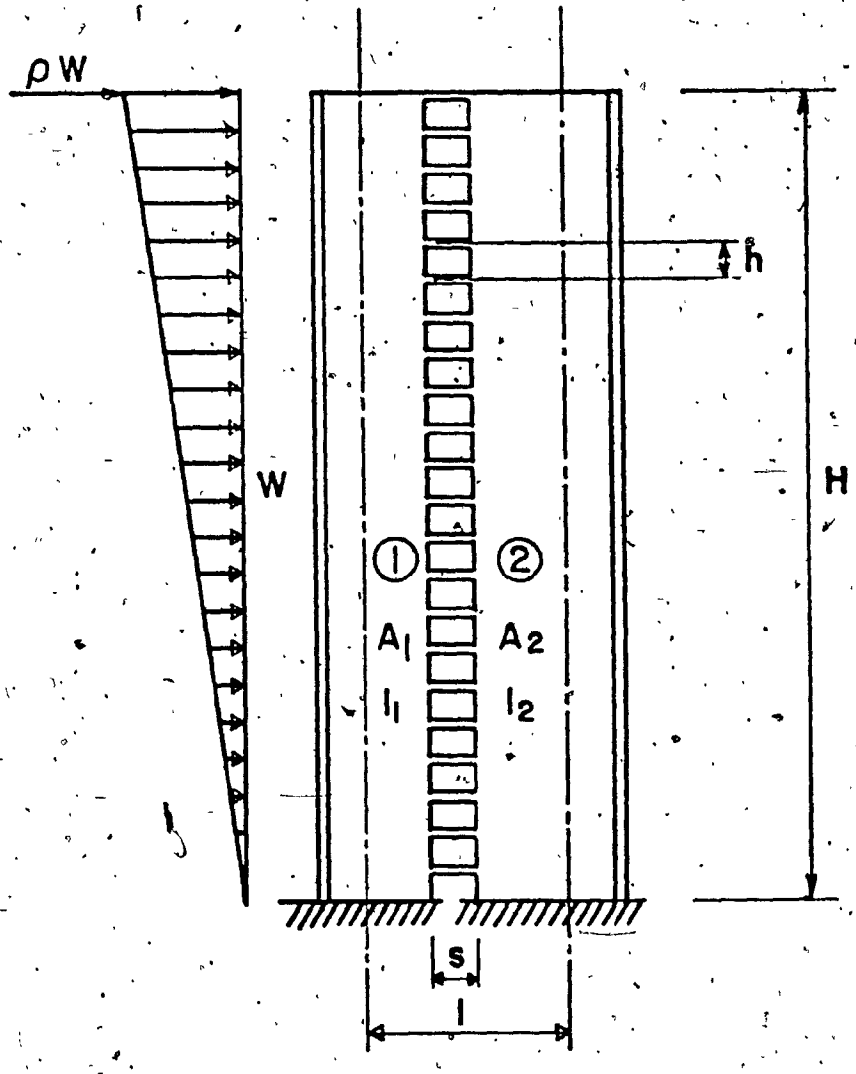

FIG. 1 - Coupled shear wall with lateral load pattern

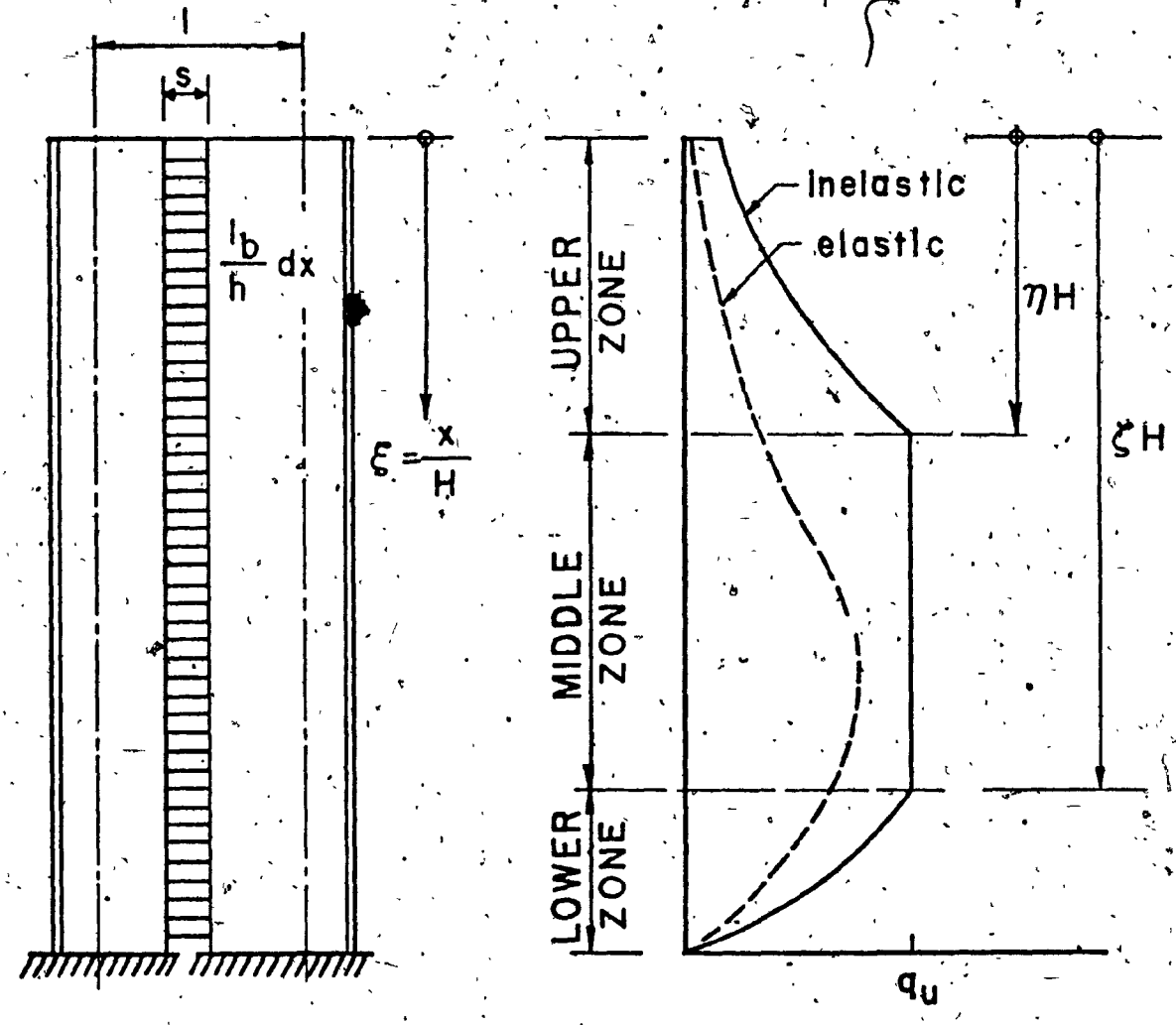

FIG. 2 - Coupled shear wall with: (a) coupling beams replaced by continuous system; (b) elasto-plastic shear distribution.

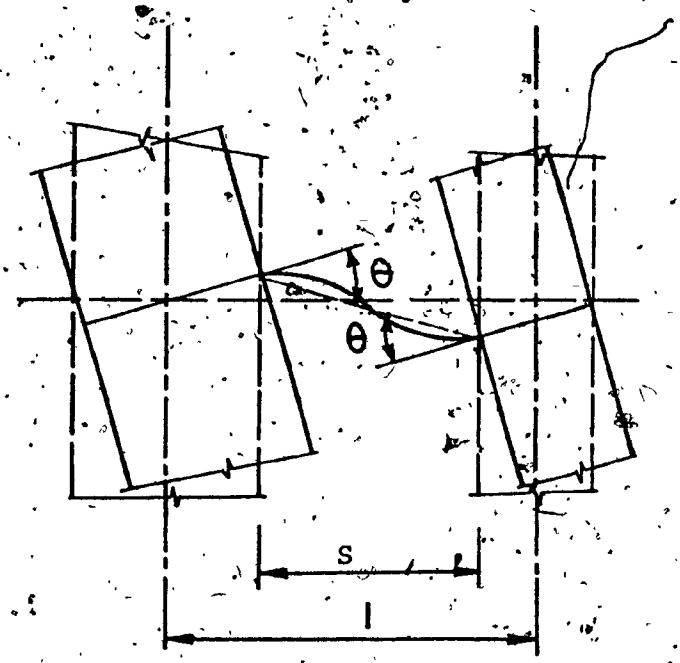

FIG. 3 - Connecting laminae deformation resulting from rotation and axial deformation of walls.

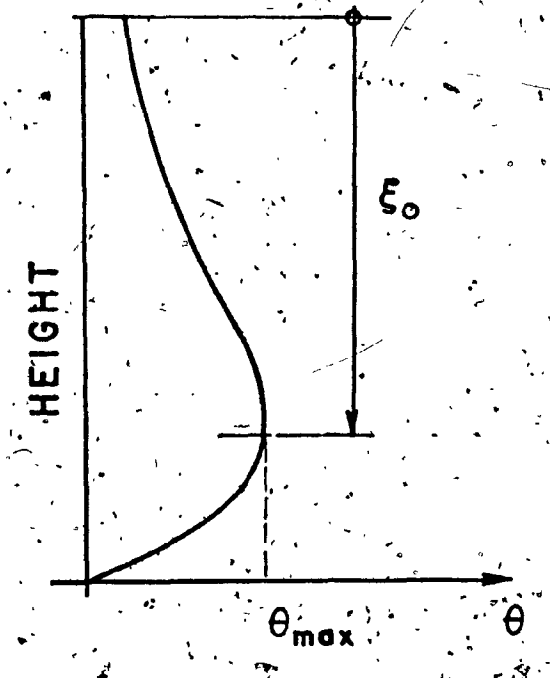

FIG. 4.- Distribution of laminar rotation.

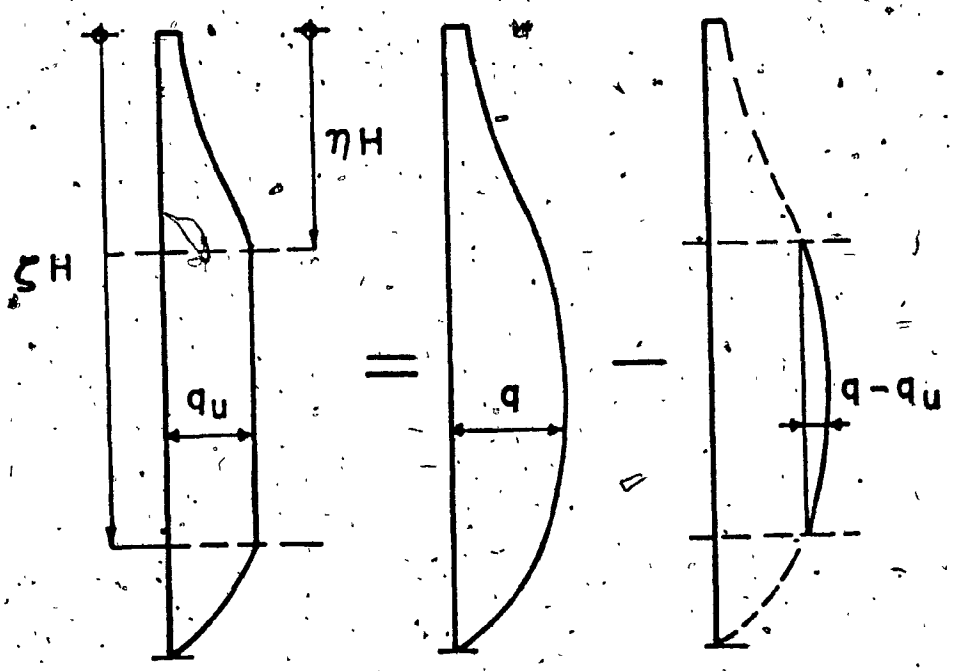

FIG. 5 - Scheme for shear distribution employed to obtain displacement for non-linear behaviour.

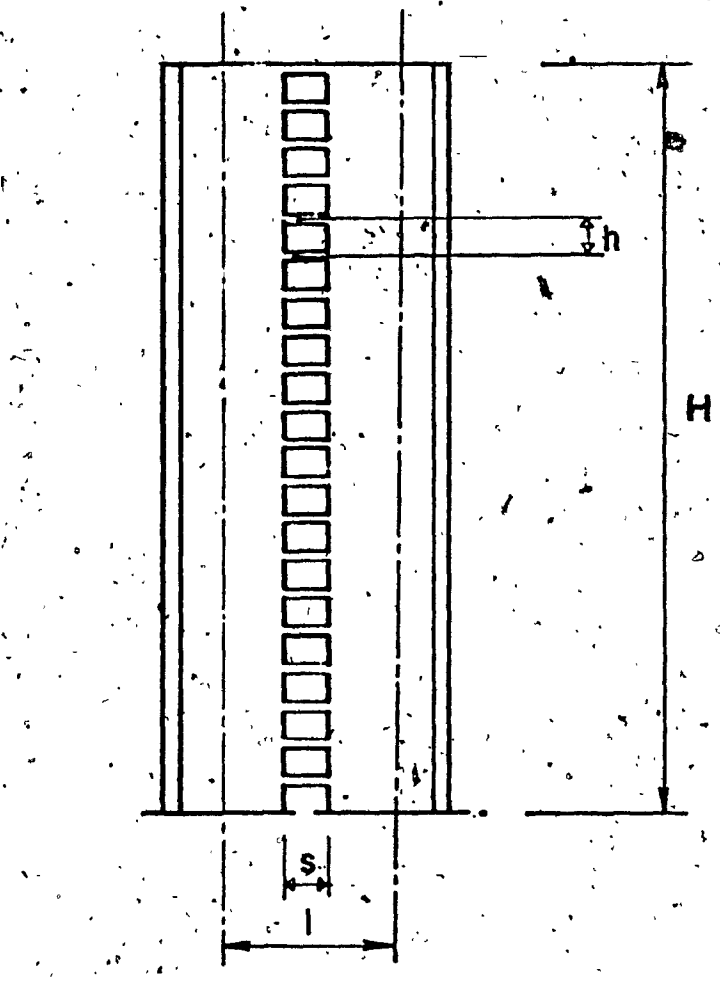

ELEVATION

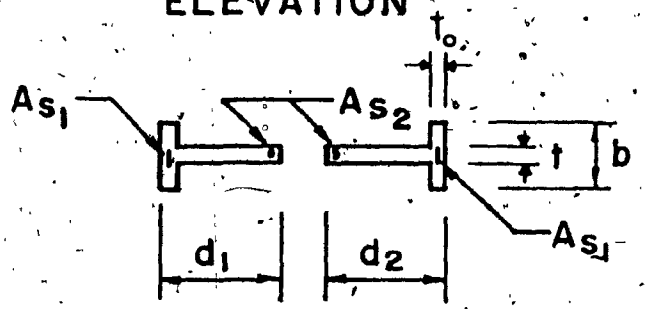

SECTION

FIG. 6 - Section details for prototype structure.

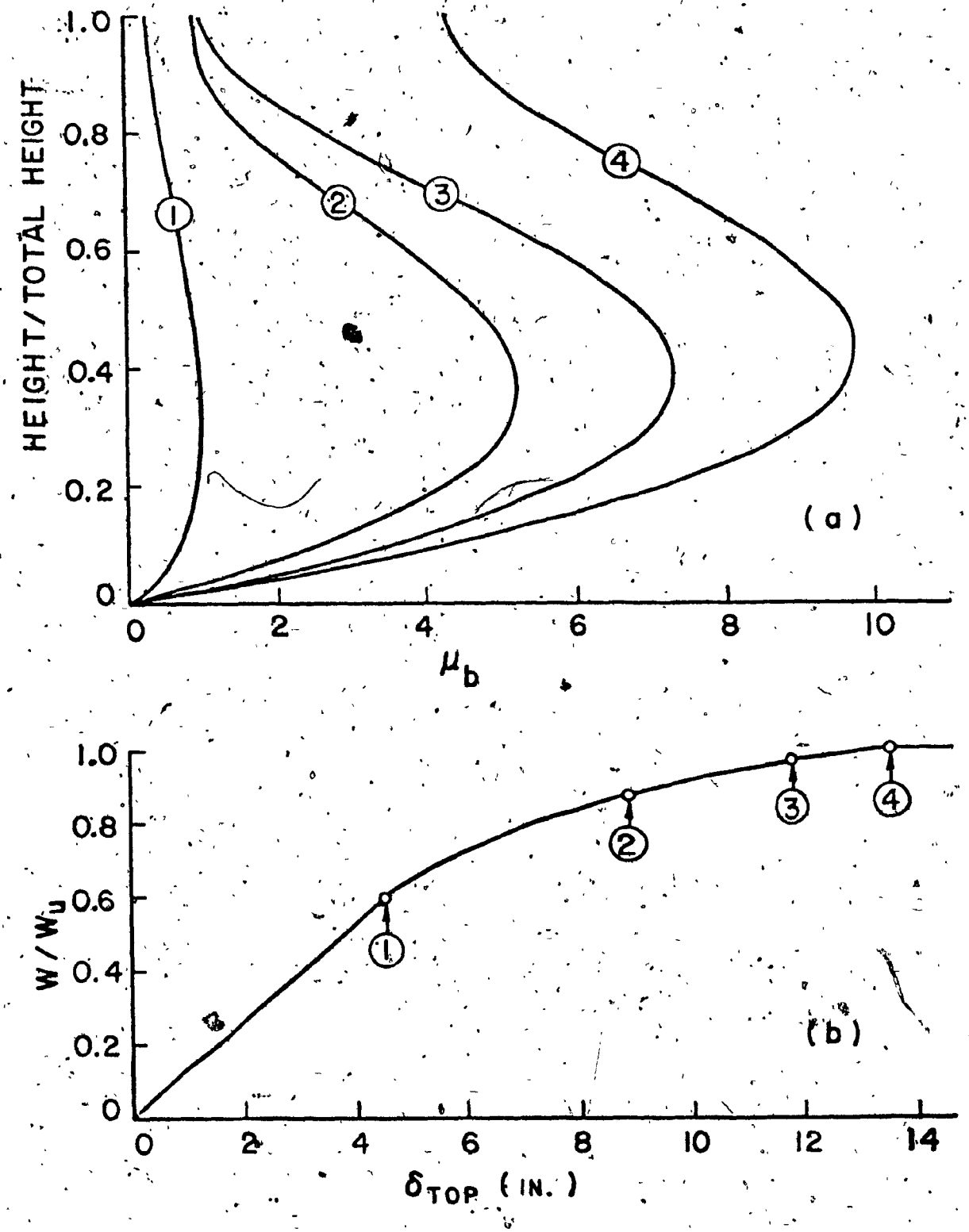

FIG. 7 - Illustrative example: (a) distribution of laminar ductility demand; (b) load displacement relation for the 20-story prototype structure.

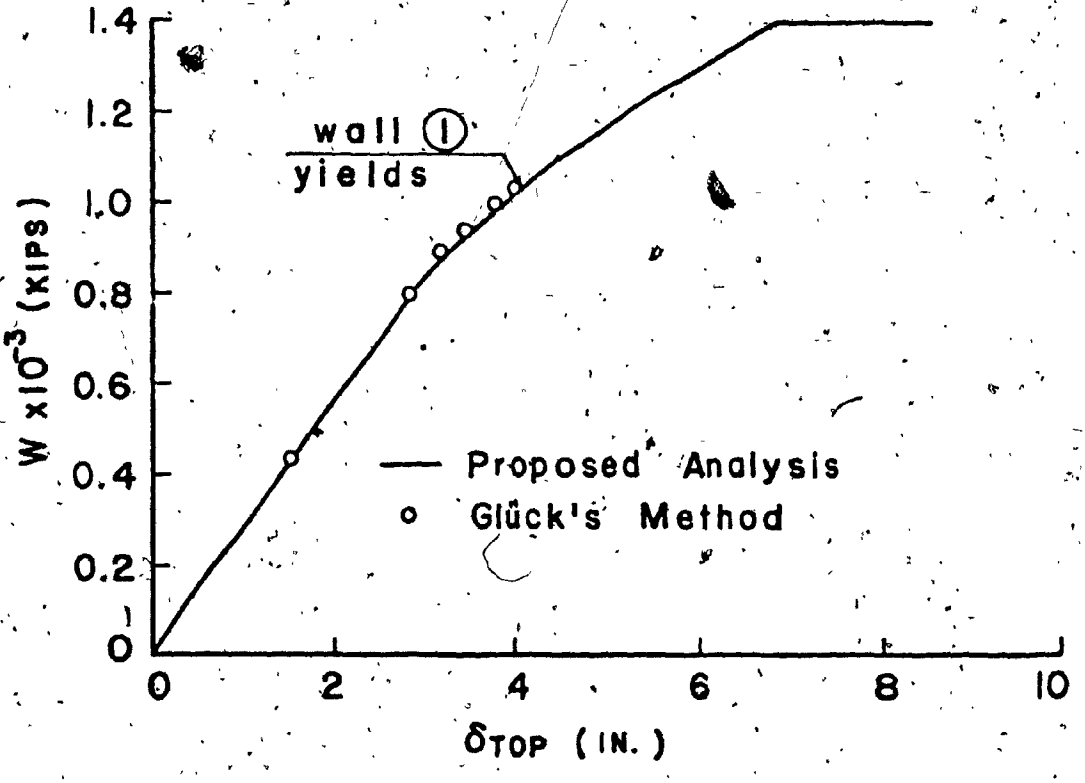

FIG. 8 - Comparison of proposed analysis with Glück's method for load-displacement of 18-story example structure from Ref. [11].

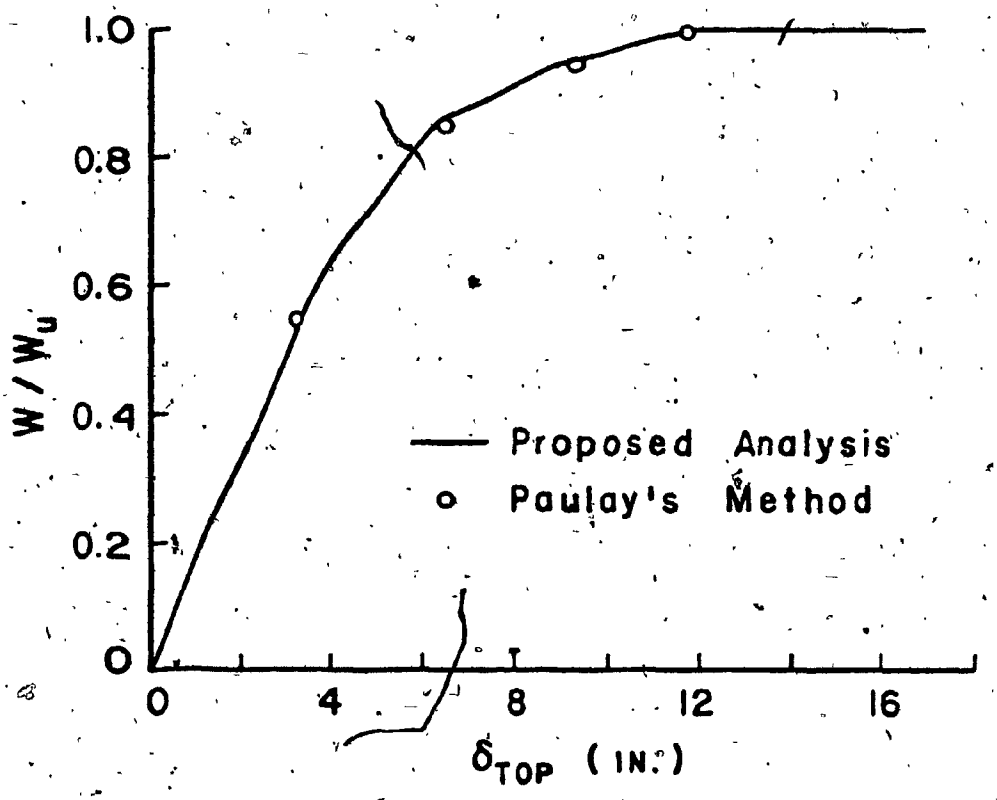

FIG. 9 - Comparison of proposed analysis with Paulay's method for load-displacement of the 18-story example structure from Ref. [10].

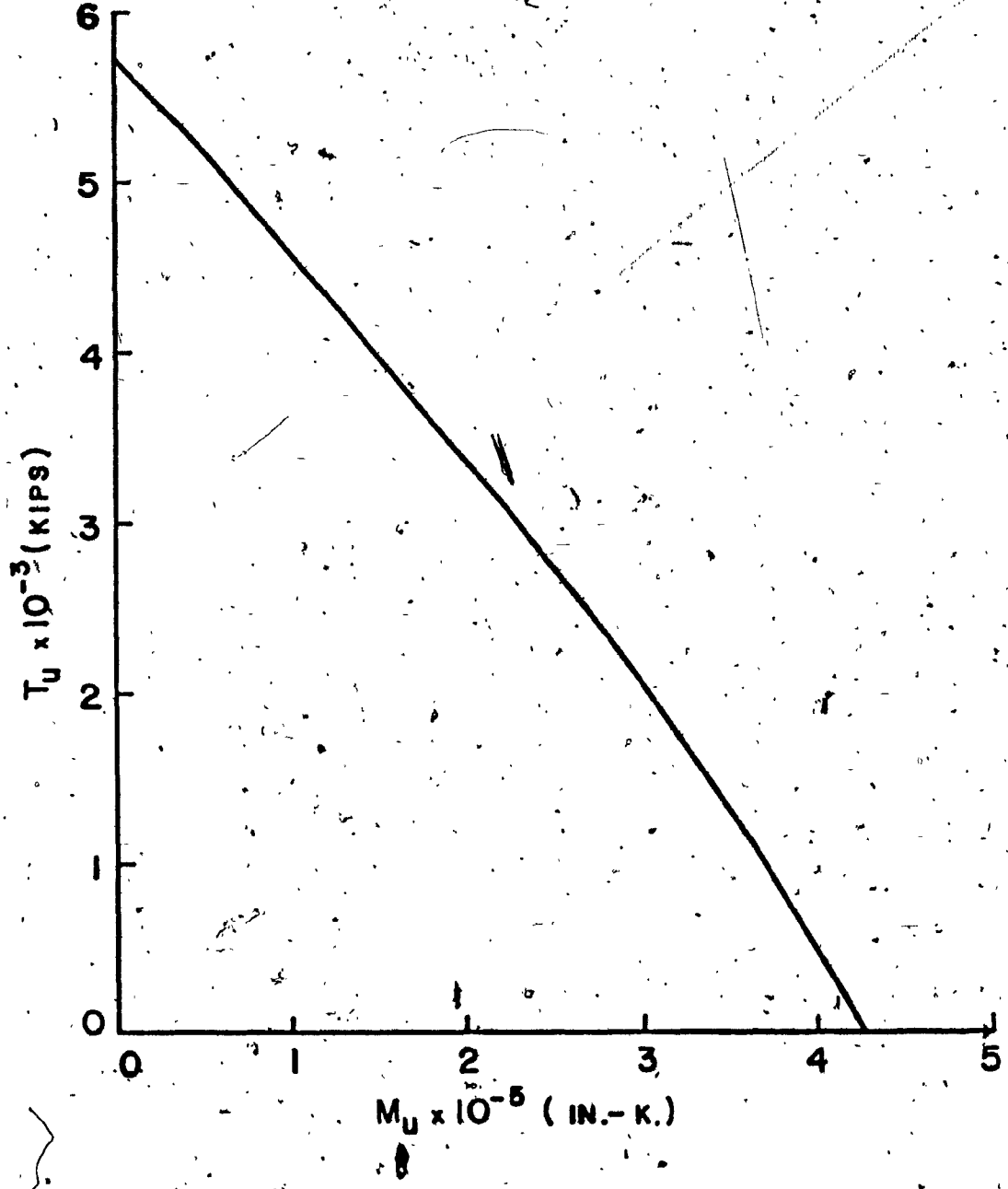

FIG. 10 - Moment-axial tension interaction diagram for wall 1 of the 20-story prototype structure.

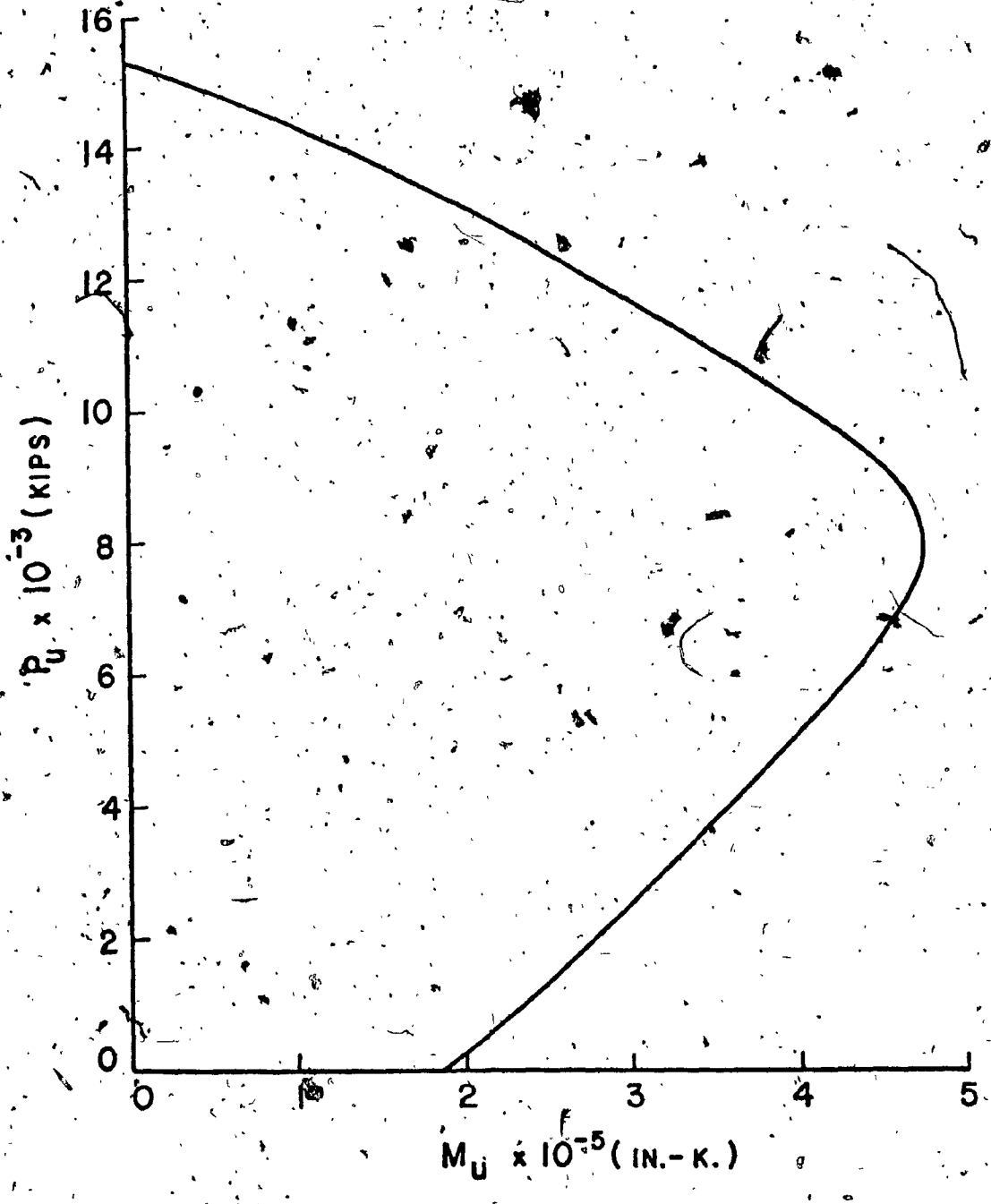

FIG. 11 - Moment-axial compression interaction diagram for wall 2 of the 20-story prototype structure.

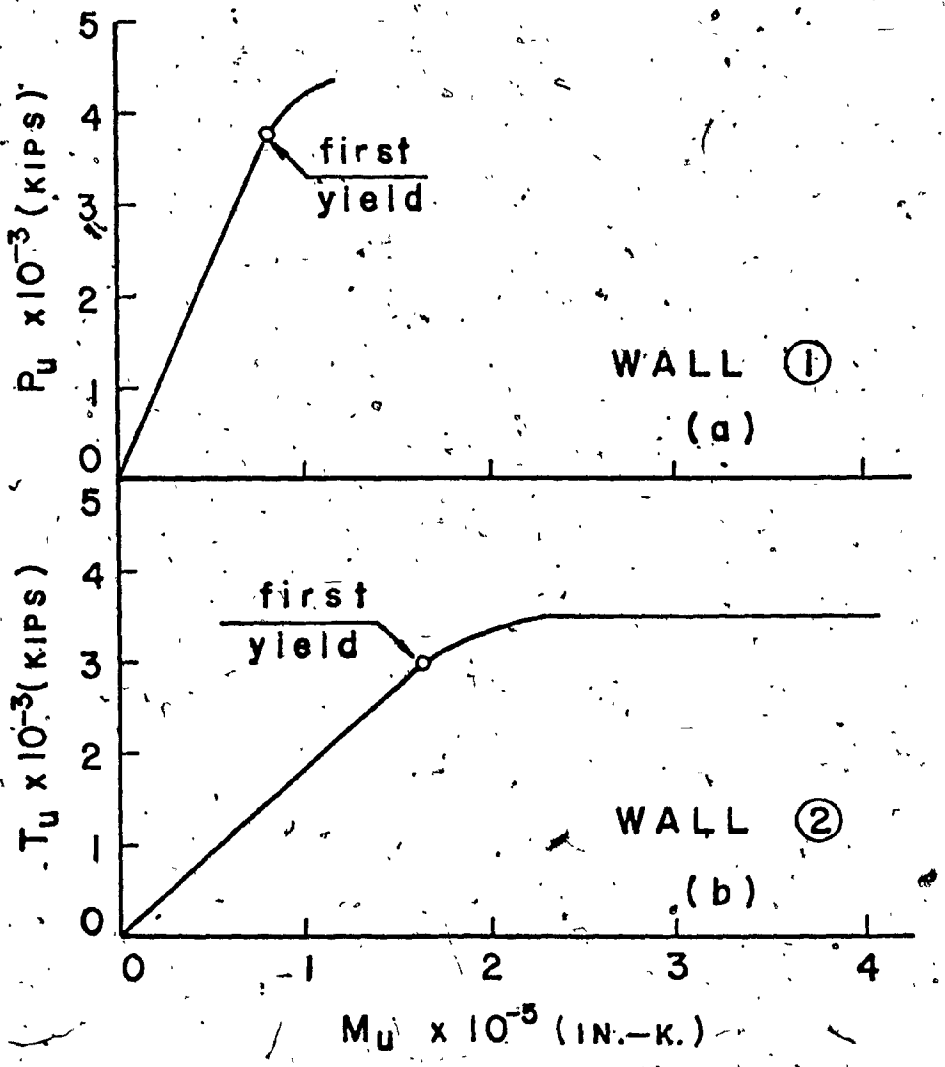

FIG. 12 - Moment-axial force loading paths when wall 1 acts as an ineffective cantilever after hinge formation.

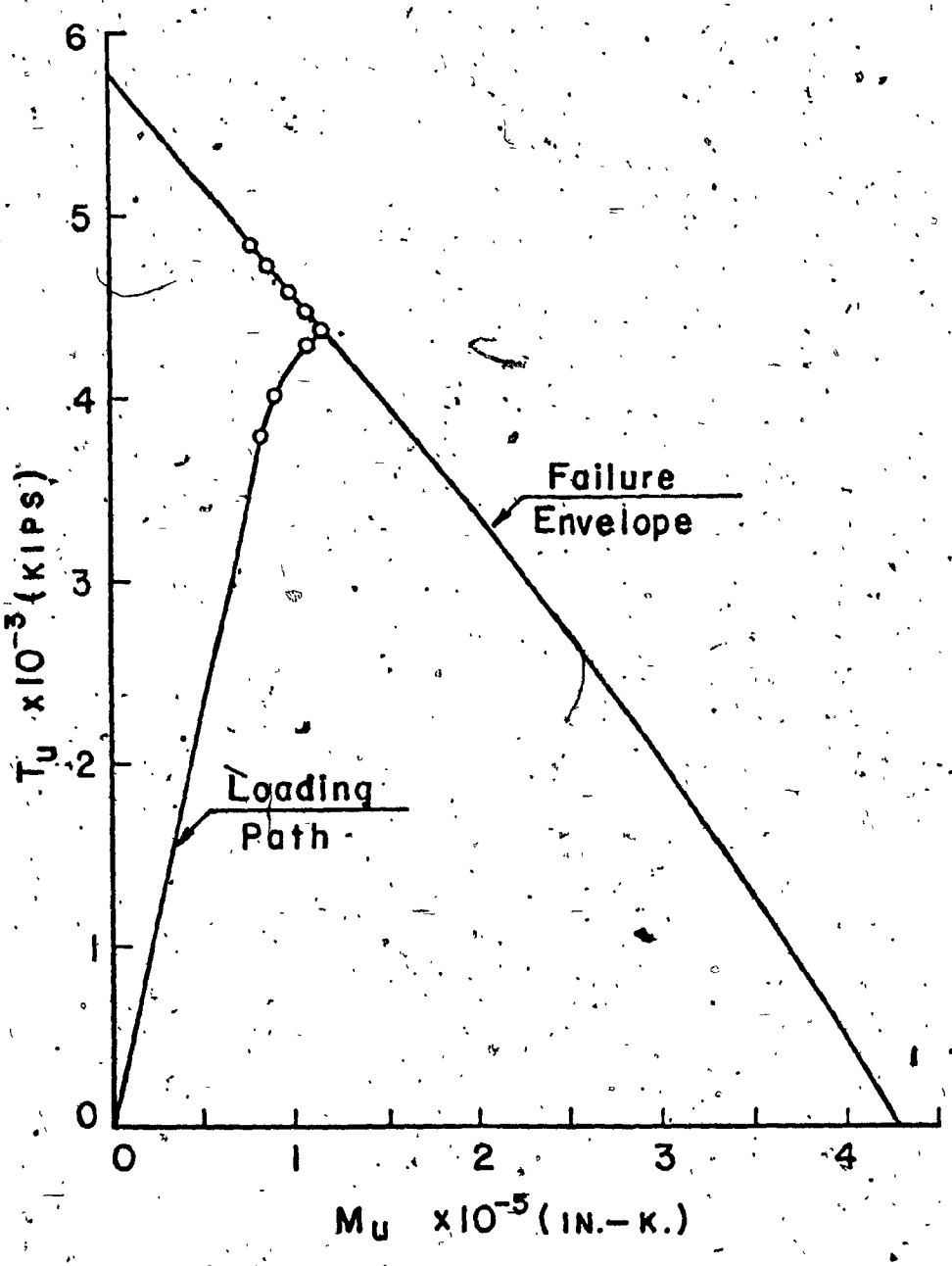

FIG. 13 - Moment-axial tension loading path of wall 1 when complete interaction is considered.

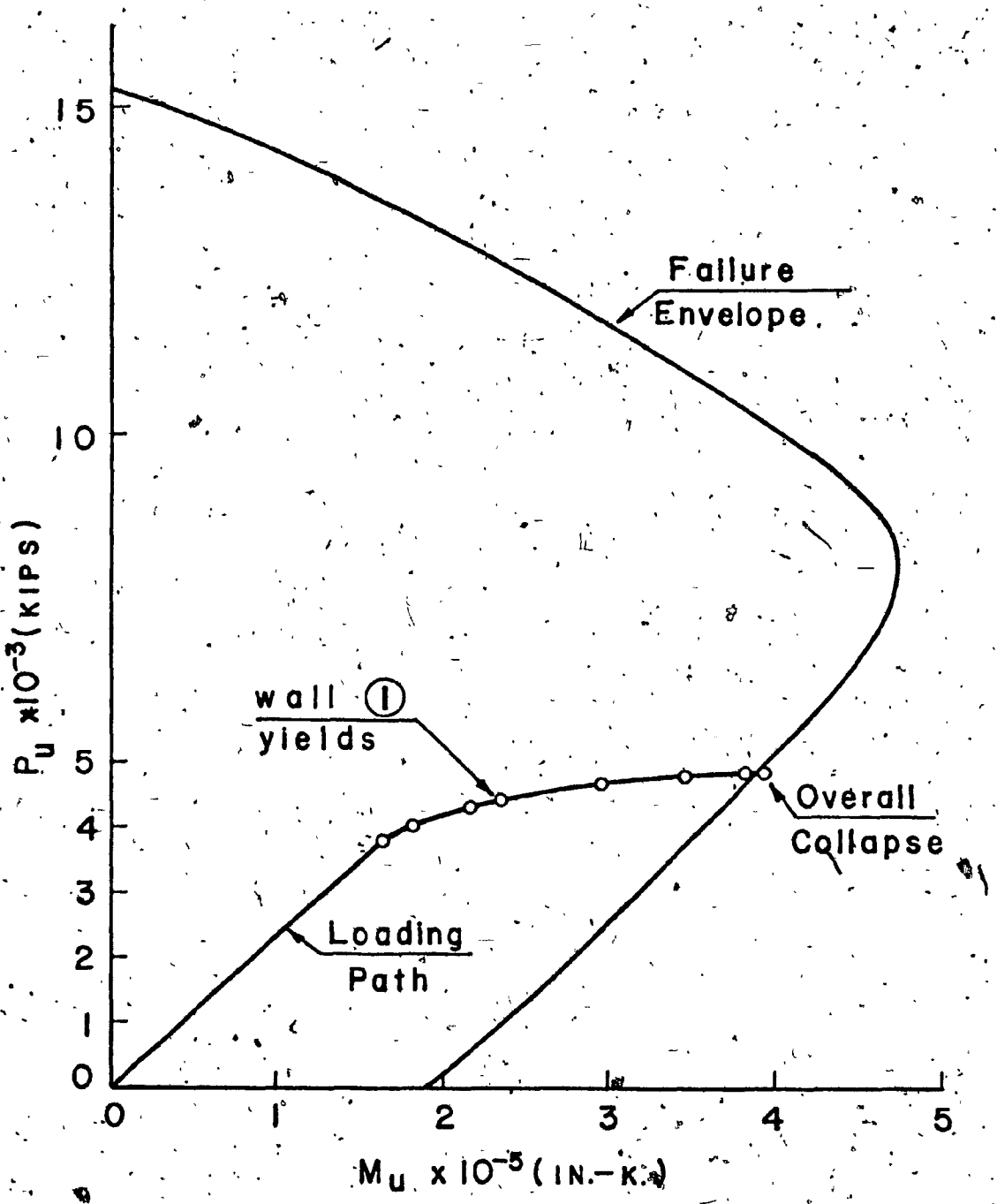

FIG. 14 - Moment-axial compression loading path of wall 2 when complete interaction is considered for wall 1.

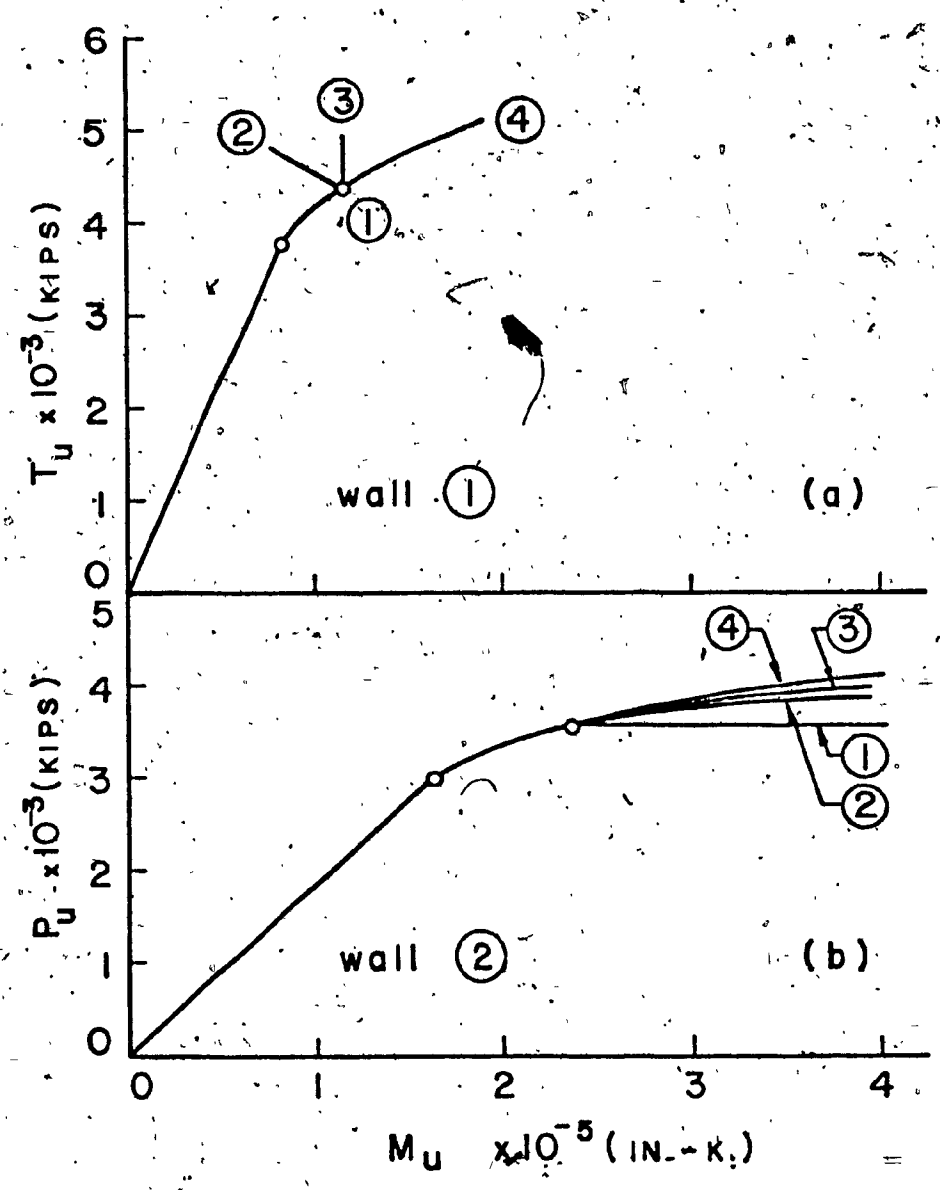

FIG. 15 - Effect of different assumptions for interaction on the loading paths of the walls.

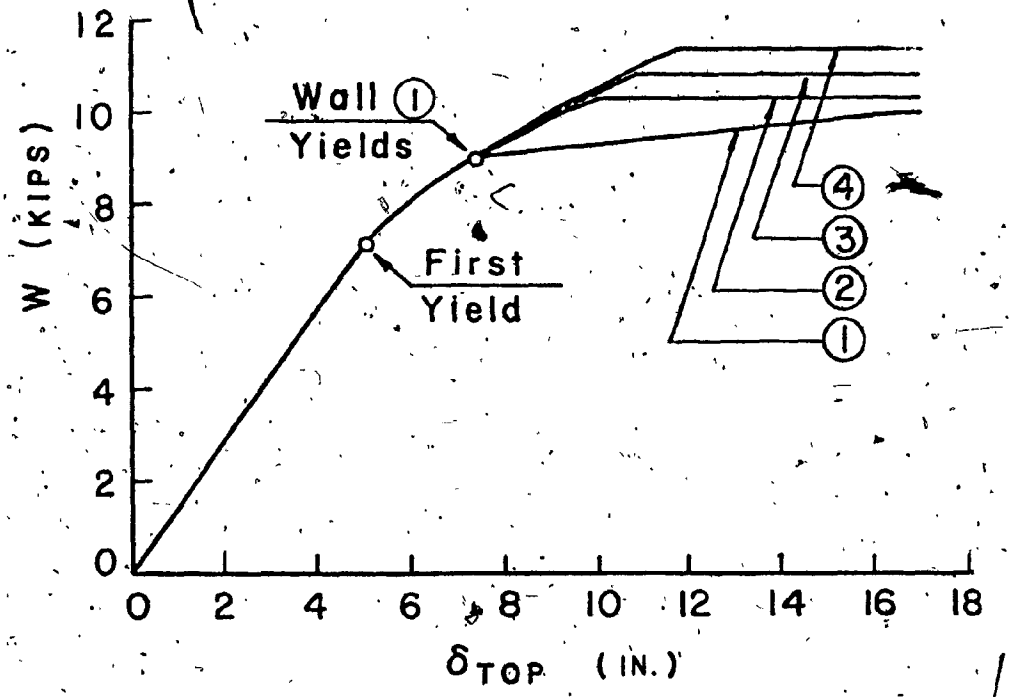

FIG. 16 - Effect of moment-axial force interaction on load-displacement behaviour.

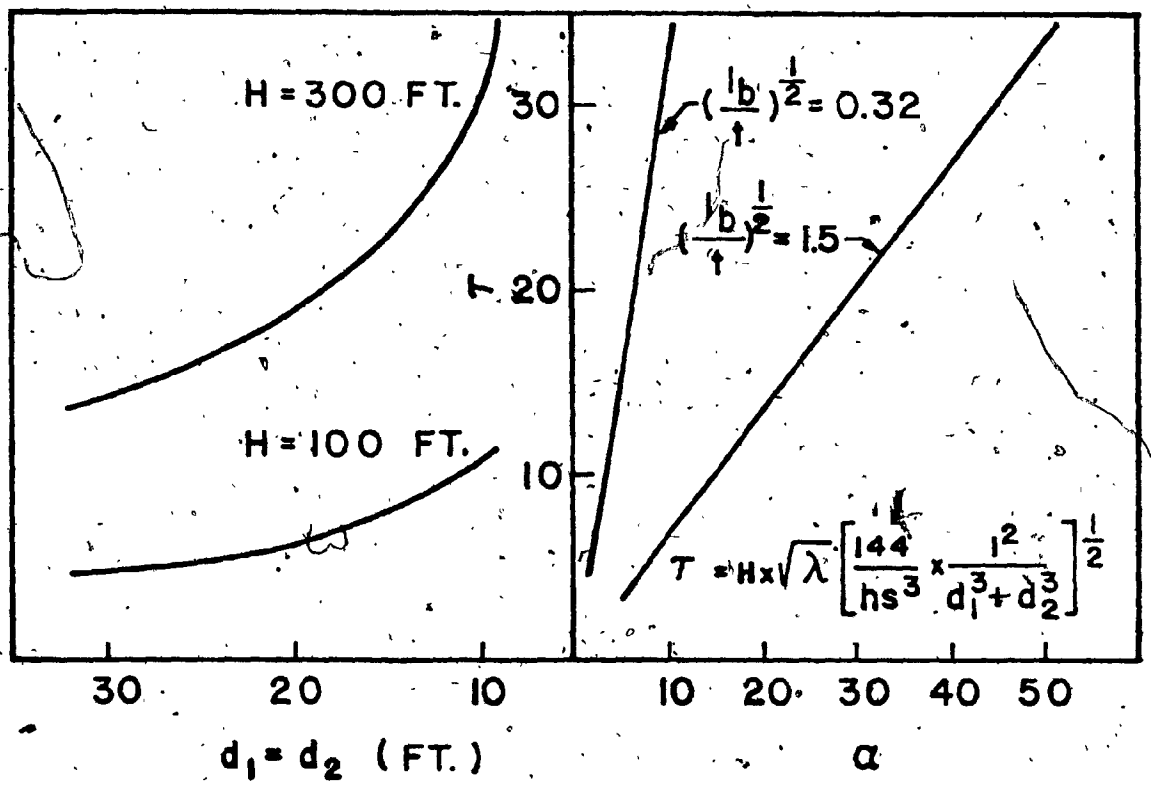

FIG. 17 - Variation of stiffness parameter α with typical building dimensions. (I_b/t is in FT.^{3}).

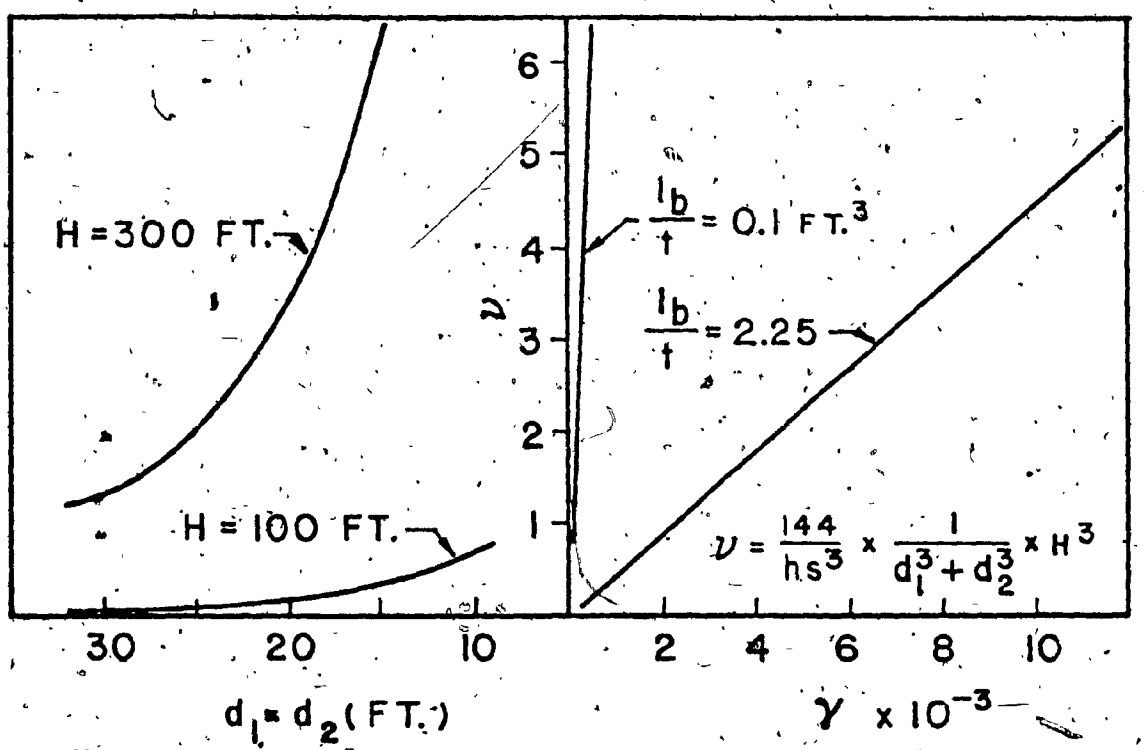

FIG. 18 - Variation of parameter γ with typical building dimensions.

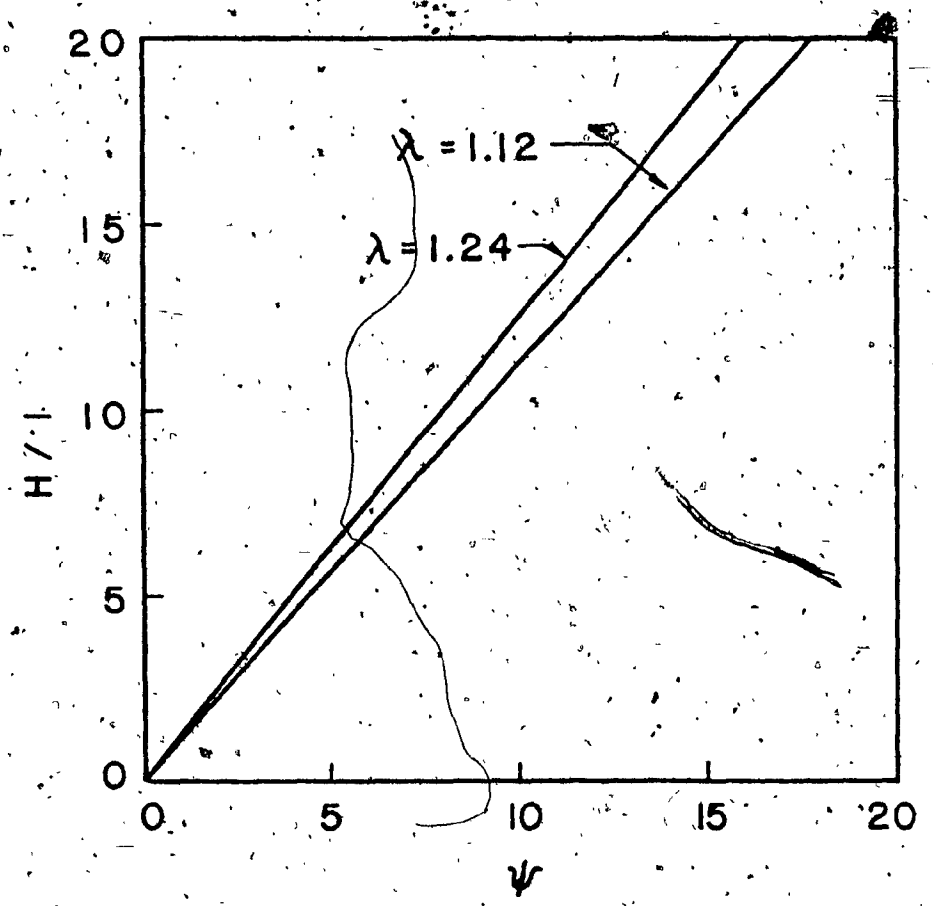

FIG. 19 - Variation of stiffness parameter ψ.

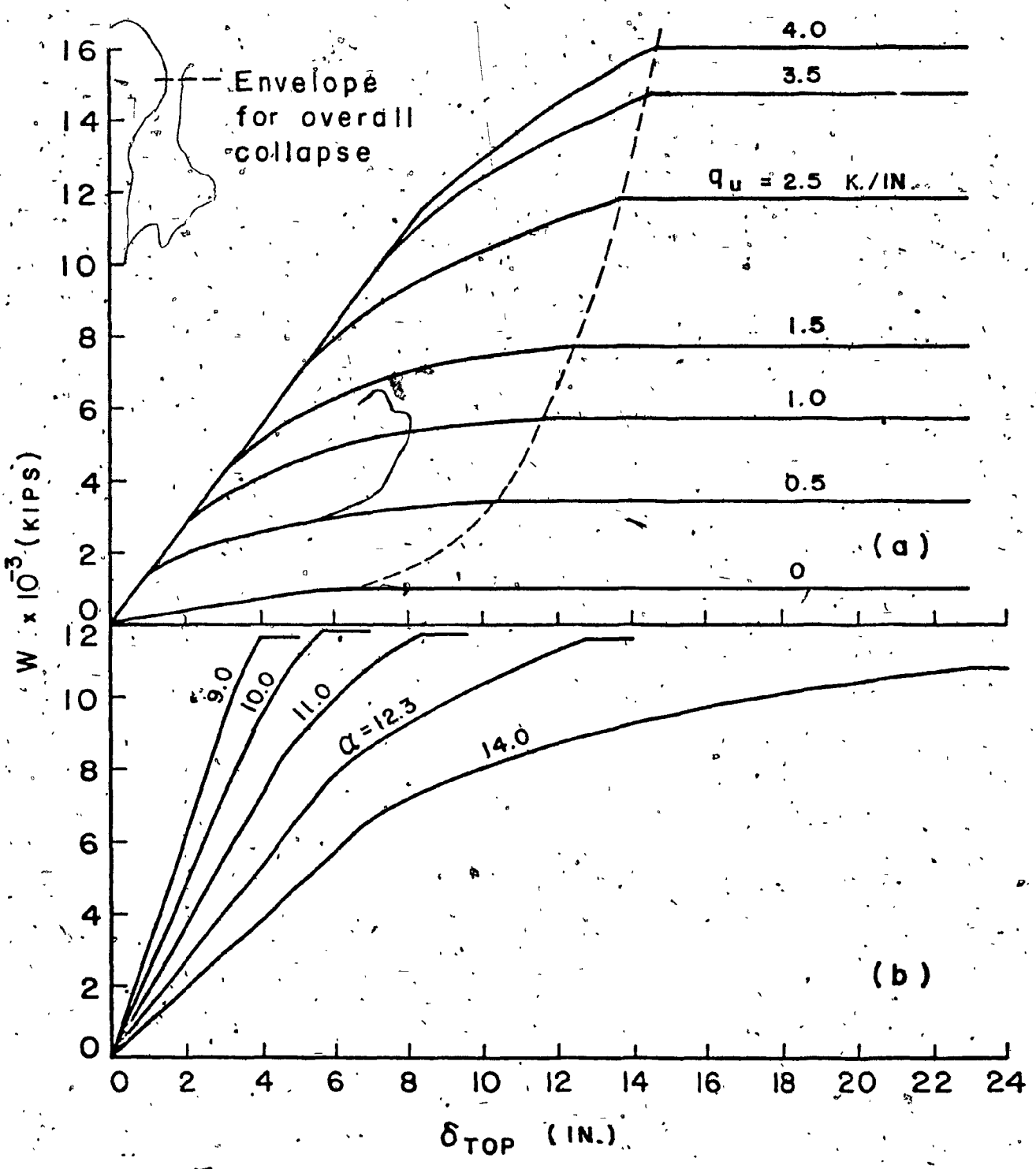

FIG. 20 - Effect on load-displacement relationship of:
(a) coupling beam shear capacity q_u (with α = 12.3)
(b) geometric stiffness parameter α (with q_u = 2.5 kips/in.).

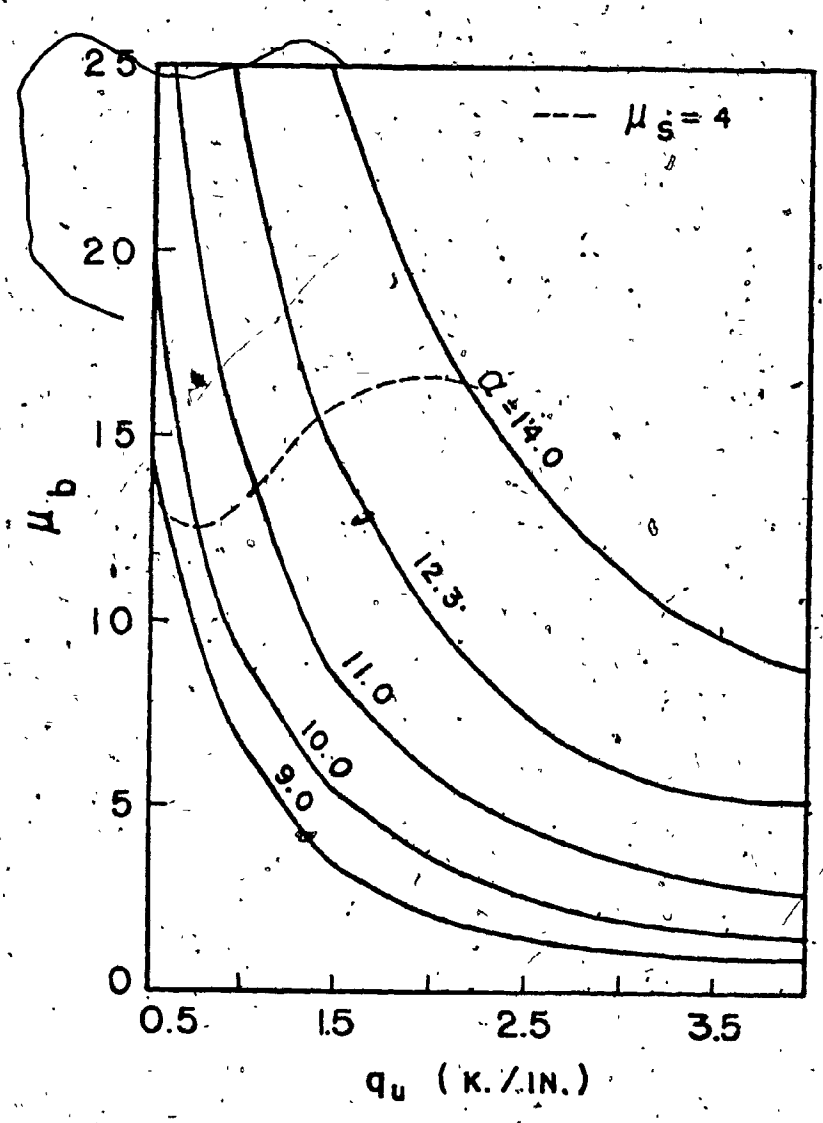

FIG. 21 - Effect of coupling shear capacity on beam rotational ductility requirement.

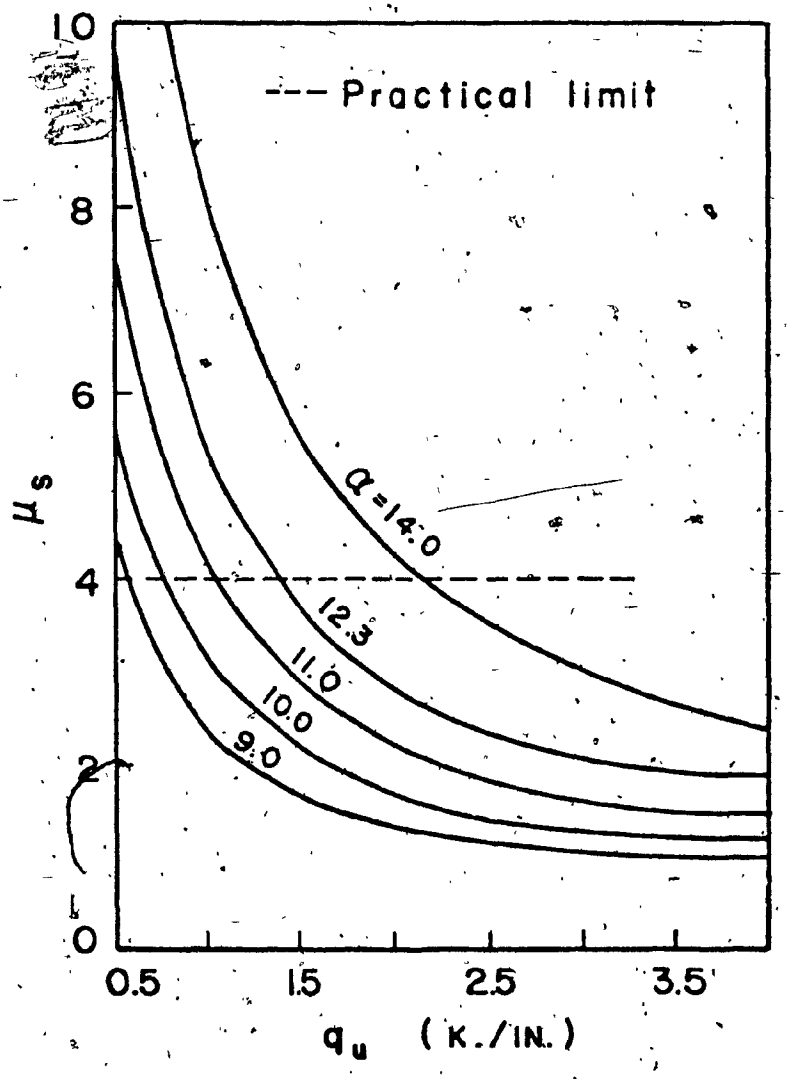

FIG. 22 - Effect of coupling shear capacity on system ductility requirement.

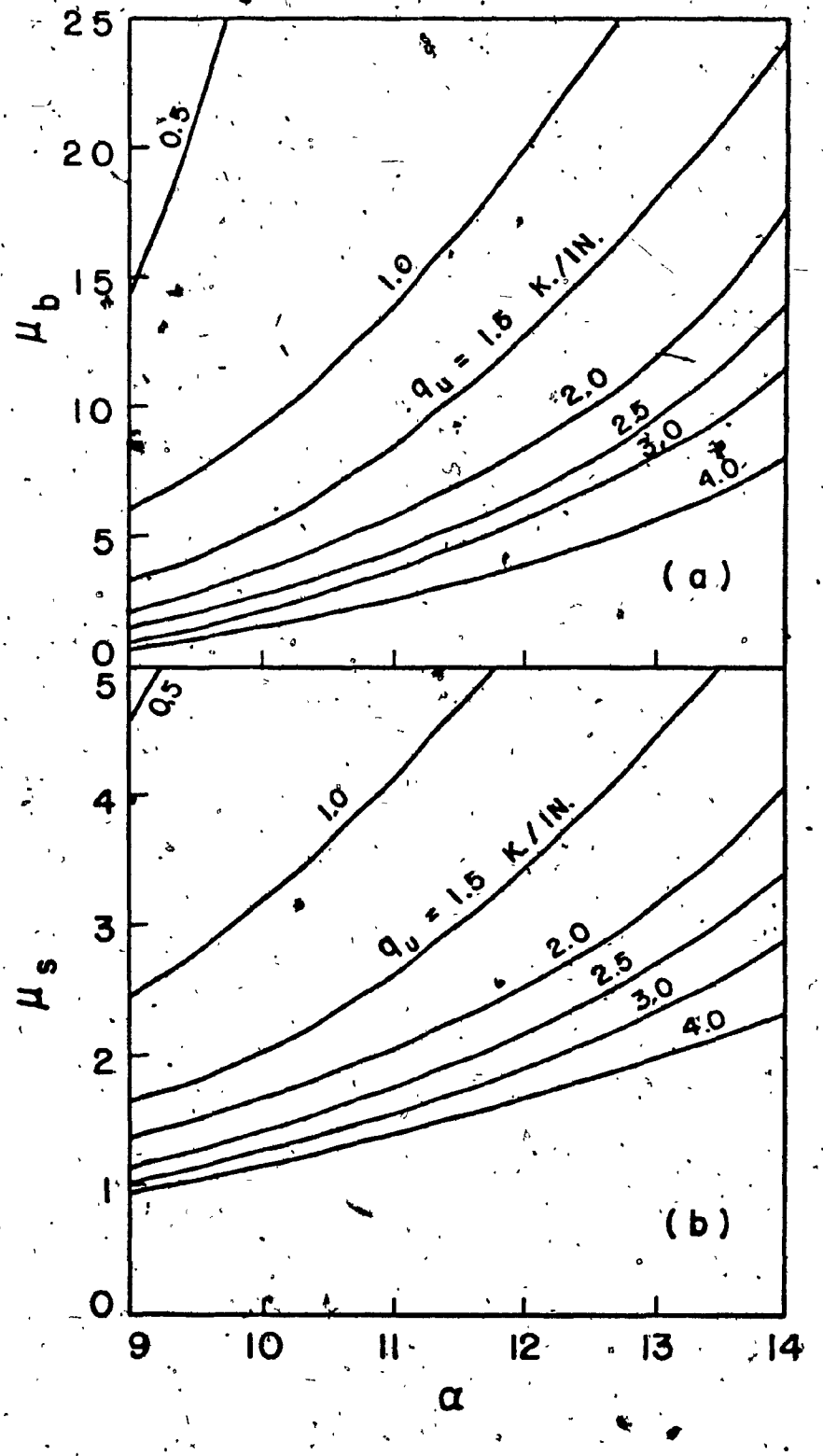

FIG. 23 – Effect of geometric stiffness parameter α on beam and system ductility requirements.

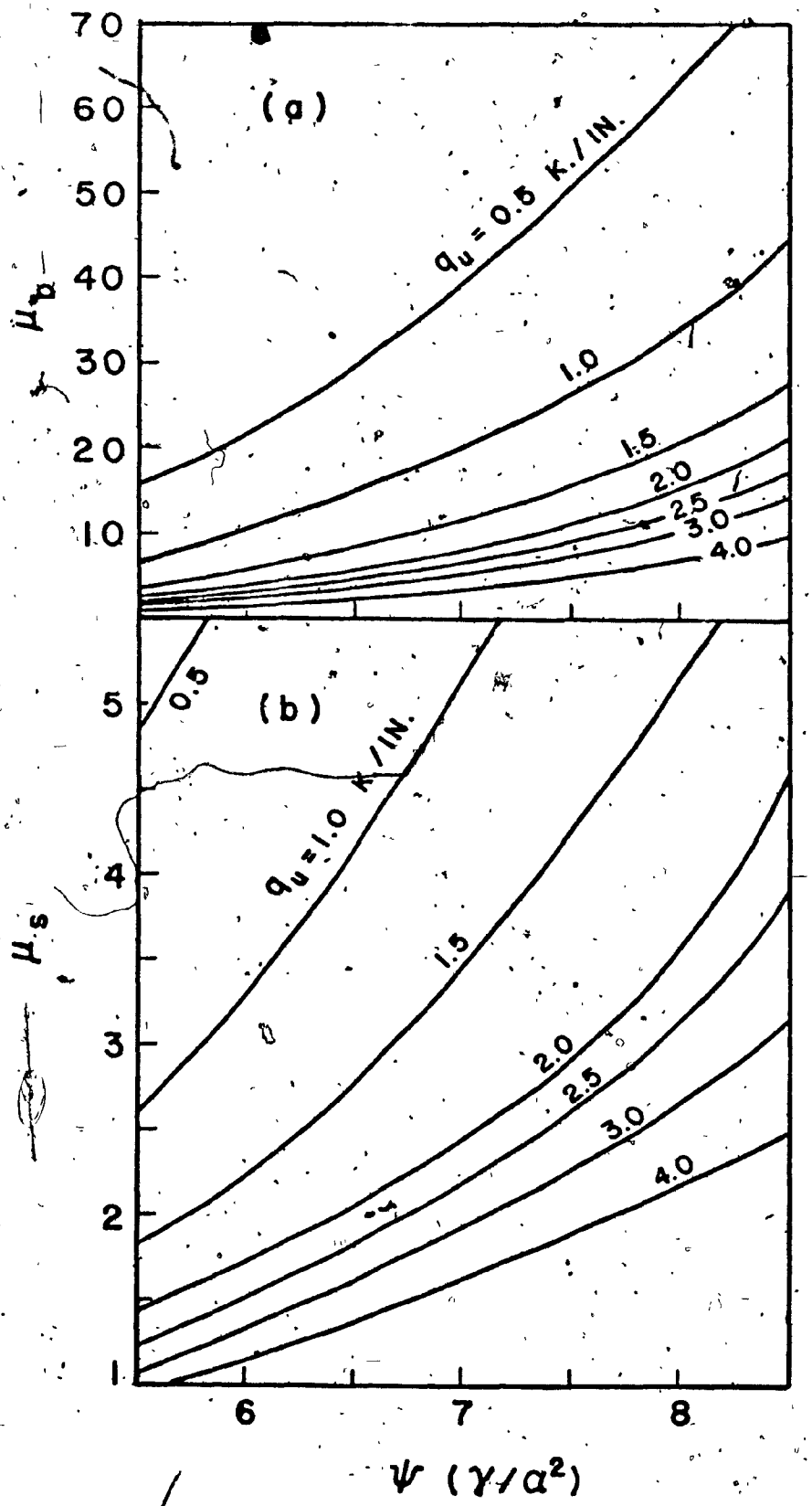

FIG. 24 - Ductility factors plotted as functions of q_u and ψ.

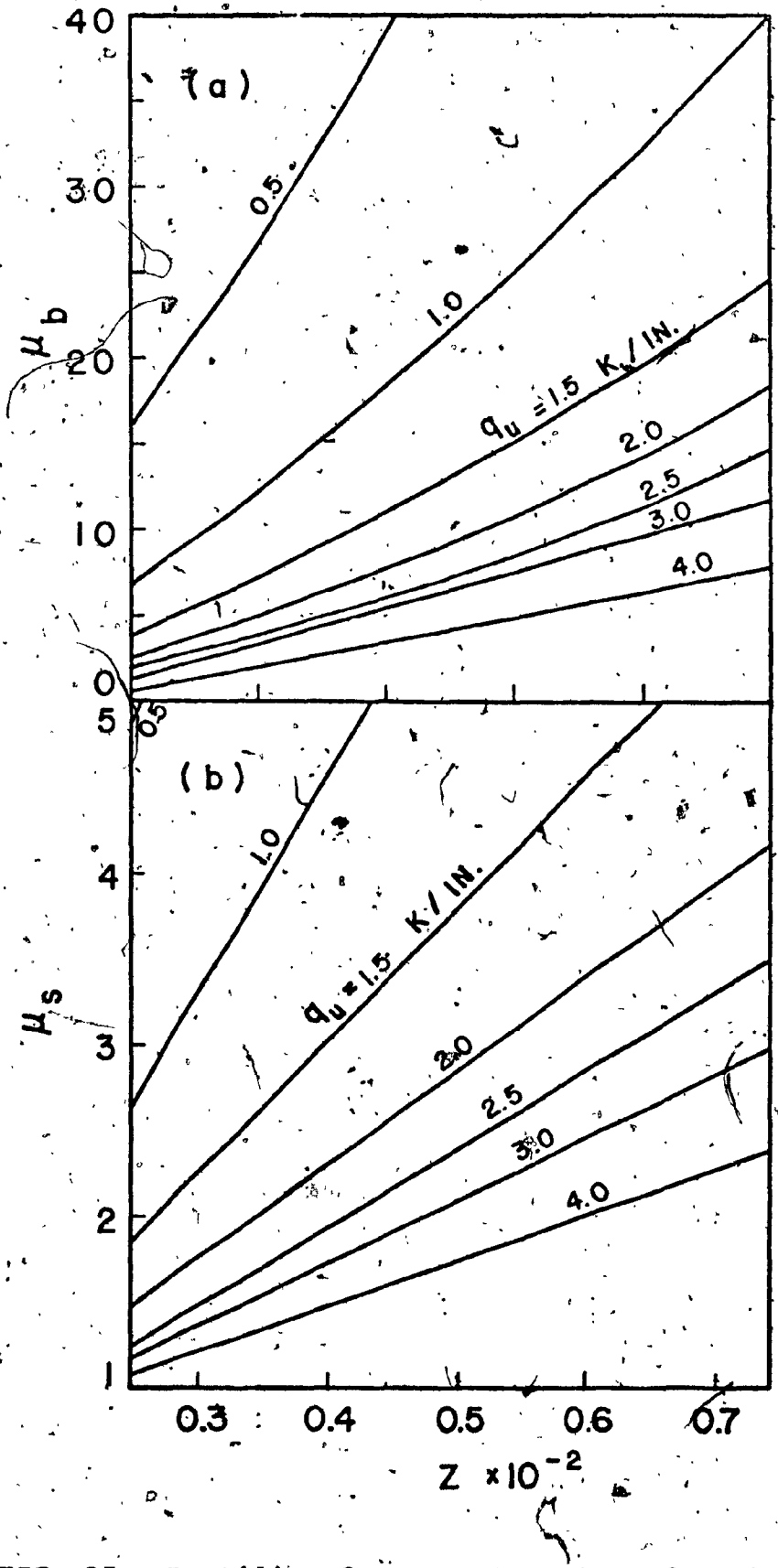

FIG. 25 - Ductility factors plotted as functions of q_u and Z.

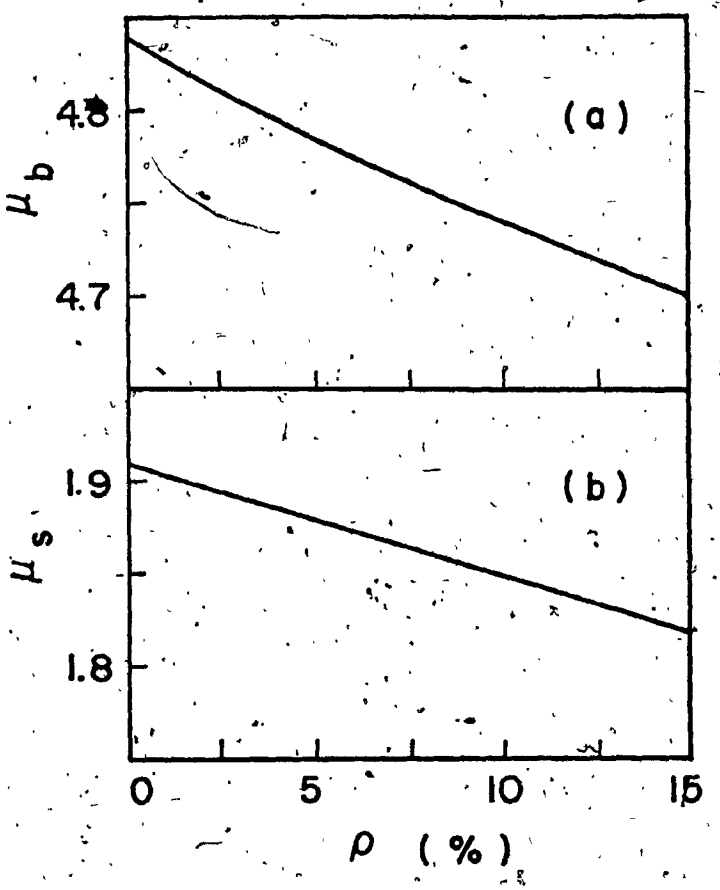

FIG. 26 - Effect of concentrated top force on ductility requirements.

APPENDIX A

DERIVATION OF THE DIFFERENTIAL EQUATION GOVERNING ELASTIC BEHAVIOUR

The beams (Figure 1) are replaced by laminae (Figure 2(a)) each of which has moment of inertia $\frac{I_b dx}{h}$. The upper beam has one-half the cross-section and one-half the moment of inertia of an interior connecting beam in order to have a continuous set of laminae over the full height. The points of contraflexure are assumed to be at the midspan of the connecting beams, which have rectangular cross-sections and are considered absolutely rigid in their longitudinal direction. Under an applied load the walls deflect and shear forces are induced in the laminae. By cutting the laminae through their points of contraflexure the gap shown in Figure A1 (Ref. [3]) can be found from the following elementary formulae from strength of materials:

(a) due to moment rotation of the walls:

$$\delta_p = \frac{\ell}{EI_o} \int_x^H M_o dx \qquad \text{(A1)}$$

where:

M_o is cantilever moment produced by external load, and

δ_p is displacement of the cut ends of the continuous lamina due to the bending moment produced by external load.

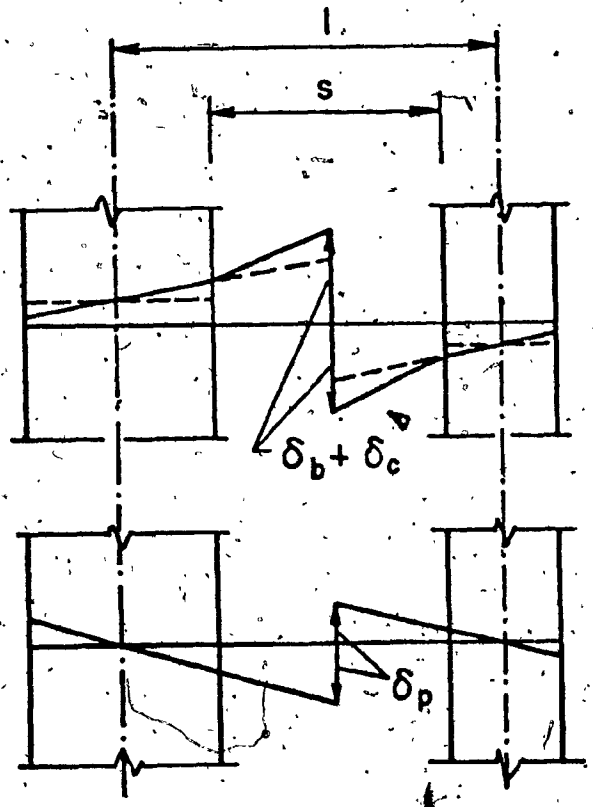

FIG. A1 - Displacements in compatibility condition for connecting lamina.

(b) due to bending of the laminae

$$\delta_b = \frac{h\, s^3}{12\, EI_b}\, q(x) + \frac{\ell^2}{EI_o} \int_x^h \left(\int_o^x q(\varepsilon)\, d\varepsilon \right) dx \qquad (A2)$$

where ε is dummy variable of integration .

(c) due to axial deformation of the walls:

$$\delta_c = \frac{1}{E}\left(\frac{1}{A_1} + \frac{1}{A_2}\right) \int_x^h \left(\int_o^x q(\varepsilon)\, d\varepsilon \right) dx \qquad (A3)$$

The compatibility condition requires:

$$\delta_b + \delta_c = \delta_p \qquad (A4)$$

or, using Eqs. (A1), (A2), and (A3),

$$\frac{hs^3}{12\, EI_b}\, q(x) + \frac{1}{E}\left(\frac{\ell^2}{I_o} + \frac{1}{A_1} + \frac{1}{A_2}\right) \int_x^H \left(\int_o^x q(\varepsilon)\, d\varepsilon \right) dx = \qquad (A5)$$

$$= \frac{\ell}{EI_o} \int_x^H M_o\, dx$$

Differentiating with respect to x gives:

$$\frac{hs^3}{12\, EI_b}\, \frac{dq(x)}{dx} - \frac{1}{E}\left(\frac{\ell^2}{I_o} + \frac{1}{A_1} + \frac{1}{A_2}\right) \int_o^x q(x)\, dx = \qquad (A6)$$

$$= -\frac{\ell}{EI_o}\, M_o$$

The axial force in the walls is given by:

$$T(x) = \int_o^x q(x)\, dx \qquad (A7)$$

By substitution $x = \xi H$ and introducing the following abbreviations into Eqs. (A6) and (A7):

$$\alpha^2 = \left(\frac{\ell^2}{I_o} + \frac{1}{A_1} + \frac{1}{A_2}\right) \frac{12\ IH^2}{hs^3} \tag{A8}$$

$$\gamma = \frac{12\ I_b \ell\ H^3}{hs^3\ I_o} \tag{A9}$$

yields the differential equation governing elastic behaviour:

$$\frac{d^2T(\xi)}{d\xi^2} - \alpha^2 T(\xi) = -\frac{\gamma}{H} M_o \tag{A10}$$

APPENDIX B

DERIVATION OF EQUATIONS GOVERNING NON-LINEAR BEHAVIOUR

B.1. MOMENT AND AXIAL FORCE ACTING AT DIFFERENT SECTIONS OF THE COUPLED SHEAR WALL

According to Figures 1, 2(a) and 2(b), the following equations for bending moments and axial forces in the walls for the three zones specified in Figure 2(b) can be derived.

The moment $M_o(x)$ due to lateral load shown in Figure 1 at any section at distance x from the top of the structure is:

$$M_o(x) = \rho W x + \frac{Wx^2}{H} - \frac{Wx^3}{3H^2} \qquad (B1)$$

Substituting $x = \xi H$ into Eq. (B1) and rearranging lead to:

$$M_o(\xi) = WH[\xi^2 - \frac{\xi^3}{3} + \rho\xi] \qquad (B2)$$

The distribution of the connecting shear force for elastic behaviour is obtained by solving the differential equation derived in Appendix A and is:

$$q(\xi) = \frac{2\gamma W_e}{H\alpha^4}\,[(C\alpha\cosh\alpha\xi - \alpha\sinh\alpha\xi - 1 - \frac{\alpha^2}{2}(\xi^2 - 2\xi - \rho))] \qquad (B3)$$

where:

$$C = \tanh\alpha + \frac{2 + \alpha^2(1 + \rho)}{2\alpha\cosh\alpha}$$

and the coefficients α and γ are defined in Appendix A.

The axial force in the walls for the three zones are derived separately, as follows:

1. Upper Zone $(0 \leq \xi \leq \eta)$

$$T(\xi) = \int_0^{\xi} q(\xi)d\xi$$

After integrating Eq. (B3) and arranging the results,

$$T(\xi) = \frac{2\gamma W}{\alpha^4}[C\sinh\alpha\xi - \cosh\alpha\xi - \xi + 1 - \frac{\alpha^2}{2}(\frac{\xi^3}{3} - \xi^2 - \rho\xi)] \quad \text{(B4)}$$

2. Middle Zone $(\eta \leq \xi \leq \zeta)$

$$T(\xi) = \int_0^{\eta} q(\xi)d\xi + Hq_u(\xi - \eta)$$

Indicating by T_η the force at $\xi = \eta$ and integrating:

$$T_\eta = \int_0^{\eta} q(\xi)d\xi$$

$$T_\eta = \frac{2\gamma W}{\alpha^4}[C\sinh\alpha\eta - \cosh\alpha\eta - \eta + 1 - \frac{\alpha^2}{2}(\frac{\eta^3}{2} - \eta^2 - \rho\eta)] \quad \text{(B5)}$$

and:

$$T(\xi) = T_\eta + Hq_u(\xi - \eta) \quad \text{(B6)}$$

3. Lower Zone ($\zeta \leq \xi \leq 1$)

$$T(\xi) = {}_0\int^{\eta} q(\xi)d\xi + Hq_u(\zeta - \eta) + {}_0\int^{\xi} q(\xi)d\xi - {}_0\int^{\zeta} q(\xi)d\xi$$

$$T_\xi = {}_0\int^{\xi} q(\xi)d\xi$$

$$T_\zeta = {}_0\int^{\zeta} q(\xi)d\xi$$

where T_ξ is defined by Eq. (B4) and:

$$T_\zeta = \frac{2\gamma W}{\alpha^4}[C\sinh\alpha\zeta - \cosh\alpha\zeta - \zeta + 1 - \frac{\alpha^2}{2}(\frac{\zeta^3}{3} - \zeta^2 - \rho\zeta)] \quad \text{(B7)}$$

Thus:

$$T(\xi) = T_\eta + Hq_u(\zeta - \eta) + T_\xi - T_\zeta \quad \text{(B8)}$$

A general relationship applicable to all three zones provides wall bending moment $M(\xi)$ acting on the cross-section of both walls:

$$M_a(\xi) = M_o(\xi) - \ell T(\xi) \quad \text{(B9)}$$

Substituting Eq. (B2) and corresponding values of $T(\xi)$ for the three zones (Eqs. (B4), (B6), and (B8)) into Eq. (B9), the expressions for the moments at any ξ can be easily found.

The two walls will assume moment according to their moments of inertia.

B.2 BEAM ROTATION EQUATIONS

Total laminar rotation $\theta(\xi)$ at any height is given by the difference between the bending moment rotation $\theta_b(\xi)$ and the rotation $\theta_t(\xi)$ due to wall axial deformations as:

$$\theta(\xi) = \theta_b(\xi) - \theta_t(\xi).$$

From strength of material this can be expressed as:

$$\theta(\xi) = \frac{\ell H}{s} \int_{\xi}^{1} \frac{M(\xi)}{EI_o} m(\xi) d\xi - \frac{H}{sE}\left(\frac{1}{A_1} + \frac{1}{A_2}\right) \int_{\xi}^{1} T(\xi) p(\xi) d\xi \tag{B10}$$

where $M(\xi)$ is expressed by Eq. (B9) and $m(\xi)$ and $p(\xi)$ are virtual moment and axial force at ξ respectively.

Substituting Eq. (B9) into Eq. (B10) and replacing of $m(\xi)$ and $p(\xi)$ by unity for any section give:

$$\theta(\xi) = \frac{\ell H}{s} \left\{ \int_{\xi}^{1} \frac{M_o(\xi)}{EI_o} d\xi - \frac{\ell}{EI_o} \int_{\xi}^{1} T(\xi) d\xi \right\} - \frac{H}{sE}\left(\frac{1}{A_1} + \frac{1}{A_2}\right) \int_{\xi}^{1} T(\xi) d\xi \tag{B11}$$

Integration of $T(\xi)$ from ξ to 1 for three zones:

1. Upper Zone

$$\int_{\xi}^{1} T(\xi)d\xi = \int_{\xi}^{\eta} T_{\xi}d\xi + T_{\eta}(1 - \eta) +$$

$$+ Hq_u[-\frac{1}{2}(\zeta^2 - \eta^2) + \zeta + \eta] + \qquad \text{(B12)}$$

$$+ \int_{\zeta}^{1} T_{\xi}d\xi - T_{\zeta}(1 - \zeta)\}$$

2. Middle Zone

$$\int_{\xi}^{1} T(\xi)d\xi = T_{\eta}(1 - \xi) + Hq_u[-\frac{1}{2}(\zeta^2 + \xi^2) +$$

$$+ \zeta - \eta + \xi\eta\ ] + \qquad \text{(B13)}$$

$$+ \int_{\zeta}^{1} T_{\xi}d\xi - T_{\zeta}(1 - \zeta)\}$$

3. Lower Zone

$$\int_{\xi}^{1} T(\xi)d\xi = T_{\eta}(1 - \xi) + Hq_u(\zeta - \eta)(1 - \xi) + \qquad \text{(B14)}$$

$$+ \int_{\xi}^{1} T_{\xi}d\xi - T_{\zeta}(1 - \xi)$$

The notations T_{ξ}, T_{η} and T_{ζ} in the above equations are: T_{ξ} is the value of the axial force at ξ for elastic wall behavious and is expressed by Eq. (B4), while T_{η} and T_{ζ} are values of T_{ξ} at the boundaries η and ζ respectively.

Integrating $M_o(\xi)$ from ξ to 1 and T_{ξ} from ξ to η and ζ to 1

and substituting into Eqs. (B12), (B13) and (B14), solutions of $\int T(\xi)d\xi$ for the three zones are obtained. After this the beam rotational equations are easily obtained from Eq. (B11) separately for the upper, middle and lower zones.

B.3 DISPLACEMENT EQUATIONS

The deflection $\delta(\xi)$ at any ξ is composed of $\delta'(\xi)$ = deflection due to the external load, $\delta''(\xi)$ = deflection due to shear $q(\xi)$ induced in the coupling beams, and $\delta'''(\xi)$ = deflection due to the component $q(\xi) - q_u$ after the approximation of the beam shear distribution of Figure 5.

Considering only the applied load (Figure 1) deflection $\delta'(\xi)$ is found:

$$\delta'(\xi) = H \int_{\xi}^{1} \frac{M_o(\varepsilon)}{EI_o} m(\varepsilon)\, d\varepsilon$$

where $M_o(\xi)$ is given by Eq. (B2), and the virtual moment $m(\xi) = \varepsilon - \xi$. Here ε is a dummy variable. Thus:

$$\delta'(\xi) = \frac{WH^3}{EI_o} \int_{\xi}^{1} \left(\varepsilon^2 - \frac{\varepsilon^3}{3} + \rho\varepsilon\right)(\varepsilon - \xi)d\varepsilon$$

and after integration:

$$\delta'(\xi) = \frac{WH^3}{60\, EI_o}[10\rho(2 - 3\xi + \xi^3) + 11 - 15\xi + 5\xi^4 - \xi^5] \qquad (B15)$$

Considering only shear distribution for elastic behaviour ($q(\xi)$ from Eq. (B3)), it follows that:

$$\delta''(\xi) = H \int_{\xi}^{1} \frac{T(\xi)\,\ell\,.\,m(\xi)}{EI_o} d\xi$$

Substituting for $T(\xi)$ from Eq. (B4) and $m(\xi)$ as given above leads to:

$$\delta''(\xi) = \frac{2W\gamma H^2 \ell}{\alpha^4\, EI_o} \int_{\xi}^{1} [C \sinh\alpha\varepsilon - \cosh\alpha\varepsilon +$$

$$+ \frac{\alpha^2}{2}(\rho\varepsilon + \varepsilon^2 - \frac{\varepsilon^3}{3}) + \varepsilon - \varepsilon](\varepsilon - \xi)d\varepsilon$$

Or, after integration:

$$\delta''(\xi) = \frac{2W\gamma H^2 \ell}{\alpha^4\, EI_o} \{\frac{1}{\alpha^2}[C \sinh\alpha\xi - \cosh\alpha\xi +$$

$$+ \cosh\alpha\,[1 + C\alpha(1 - \xi)] -$$

$$- \sinh\alpha[C + \alpha(1 - \xi)]\} + \frac{\alpha^2}{120}[10\rho(2 - 3\xi + \xi^3) +$$

$$+ 11 - 15\xi + 5\xi^4 - \xi^5] + \frac{(1 - \xi)^3}{6}$$

The difference between the expressions for $\delta'(\xi)$ and $\delta''(\xi)$ expresses the deflection for elastic behaviour of the walls, δ_e. Therefore for any section ξ the total deflection can be expressed as:

$$\delta(\xi) = \delta_e + \delta'''(\xi)$$

The expression for deflection $\delta'''(\xi)$ due to reduction $q(\xi) - q_u$ is obtained for the three zones from basic principles as:

1. Upper Zone

$$\delta'''(\xi) = (\xi - \eta)\frac{H^2\ell}{EI_o}\left\{\int_\eta^\zeta [T(\xi) - T_\eta - Hq_u(\xi - \eta)]d\xi + \right.$$

$$+ [T_\zeta - T_\eta - Hq_u(\zeta - \eta)](1 - \zeta)\} +$$

$$+ \frac{H^2\ell}{EI_o}\left\{\int_\eta^\zeta [T(\xi) - T_\eta - Hq_u(\xi - \eta)](\xi - \eta)d\xi + \right.$$

$$+ [T_\zeta - T_\eta - Hq_u(\zeta - \eta)](1 - \zeta)\left(\frac{1 + \zeta}{2} - \eta\right)\}$$

2. Middle Zone

$$\delta'''(\xi) = \frac{H^2\ell}{EI_o}\left\{\int_\xi^\zeta [T(\varepsilon) - T_\eta - Hq_u(\varepsilon - \eta)](\varepsilon - \xi)d\varepsilon + \right.$$

$$+ [T_\zeta - T_\eta - Hq_u(\zeta - \eta)](1 - \zeta)\left(\frac{1 + \zeta}{2} - \xi\right)\}$$

3. Lower Zone

$$\delta'''(\xi) = \frac{H^2\ell}{EI_o}\{[T_\zeta - T_\eta - Hq_u(\zeta - \eta)](1 - \xi)\frac{(1 - \xi)}{2}\}$$

The solutions of the integrals which appear in the above equations are listed below:

$$\int_{\xi}^{\zeta} T(\epsilon)(\epsilon - \xi)d\epsilon = \frac{2\gamma W}{\alpha^4}\{\frac{C}{\alpha}[(\zeta - \xi)\cosh\alpha\zeta -$$

$$- \frac{1}{\alpha}(\sinh\alpha\zeta - \sinh\alpha\xi)] - \frac{1}{\alpha}[(\zeta - \xi)\sinh\alpha\zeta -$$

$$- \frac{1}{\alpha}(\cosh\alpha\zeta - \sinh\alpha\xi)] - [\frac{1}{3}(\zeta^3 - \xi^3) -$$

$$- \frac{1}{2}(1 + \xi)(\zeta^2 - \xi^2) - \xi(\zeta - \xi)]$$

$$- \frac{\alpha^2}{2}[\frac{1}{15}(\zeta^5 - \xi^5) - \frac{1}{4}(1 - \frac{\xi}{3})(\zeta^4 - \xi^4) -$$

$$- \frac{1}{3}(\zeta - \xi)(\zeta^3 - \xi^3) + \frac{1}{2}\zeta\xi(\zeta^2 - \xi^2)]$$

$$\int_{\xi}^{\zeta} Tn(\epsilon - \xi)d\epsilon = Tn[\frac{1}{2}(\zeta^2 - \xi^2) - (\zeta - \xi)]$$

$$\int_{\xi}^{\zeta} H\zeta_u(\epsilon - \eta)(\epsilon - \xi)d\epsilon = H\zeta_u\{\frac{1}{3}(\zeta^3 - \xi^3) -$$

$$- \frac{1}{2}(\eta + \xi)(\zeta^2 - \xi^2) + \eta\xi(\zeta - \xi)\}$$

$$\int_{\xi}^{\zeta} T(\epsilon)d\xi = \frac{2\gamma W}{\alpha^4}\{\frac{C}{\alpha}(\cosh\alpha\zeta - \cosh\alpha\eta) -$$

$$- \frac{1}{\alpha}(\sinh\alpha\zeta - \sinh\alpha\eta) + \frac{1}{2}(\zeta^2 - \eta^2) + \zeta - \eta -$$

$$- \frac{\alpha^2}{2}[\frac{1}{2}(\zeta^4 - \eta^4) - \frac{1}{3}(\zeta^3 - \eta^3) - \frac{\zeta}{2}(\zeta^2 - \eta^2)]\}$$

APPENDIX C

MOMENT-AXIAL FORCE INTERACTION

Notation.

The following symbols, also shown in Figure C1 and C2, are used in this appendix:

a = depth of equivalent rectangular stress block;

A_s = area of tensile reinforcement;

A_s' = area of compressive reinforcement;

b = width of flange of T-wall;

C_c' = compression force in concrete (T-section's web);

C_c'' = compression force in concrete (T-section's flange);

C_s = compression force in compression steel;

d = effective depth of flexural members;

d' = distance from extreme fiber to compressive reinforcement;

d'' = distance from centroidal line of section to tensile reinforcement;

e = eccentricity measured from tensile steel axis in case of moment-axial tension and from centroidal line in case of moment-axial compression;

e_o = eccentricity measured from centroidal line in case of moment-axial tension;

e' = eccentricity measured from compression steel axis;

E_s = modulus of elasticity of steel;

f_c' = ultimate compressive strength of concrete;

f_s = stress in tensile reinforcement;

f_y = yield strength of reinforcement;

g = position of the centroidal line;

P_u = ultimate axial load in compression wall;

P_s = tension force in steel A_s;

P'_s = tension force in steel A'_s;

t = width of web in T-section wall;

t_o = flange thickness of T-section wall;

T = tension force in tension steel;

T_u = ultimate axial load in tension wall;

x = position of neutral axis

β = factor defines equivalent rectangular stress block;

ε_c = strain in concrete;

ε_s = strain in tension steel;

ε'_s = strain in compression steel.

C1 BENDING AND AXIAL COMPRESSION -- "T" SECTION

C1.1 Small Eccentricity -- "Compression Controls"

When the ultimate eccentric load P_u exceeds the balanced value of P_b or when eccentricity e is less than the balanced value e_b, the capacity of the section is controlled by compression in the concrete.

According to Figure C1(b), by considering the actual strain variation as the unknown and using the principles of statics, the ultimate eccentric load P_u may be obtained.

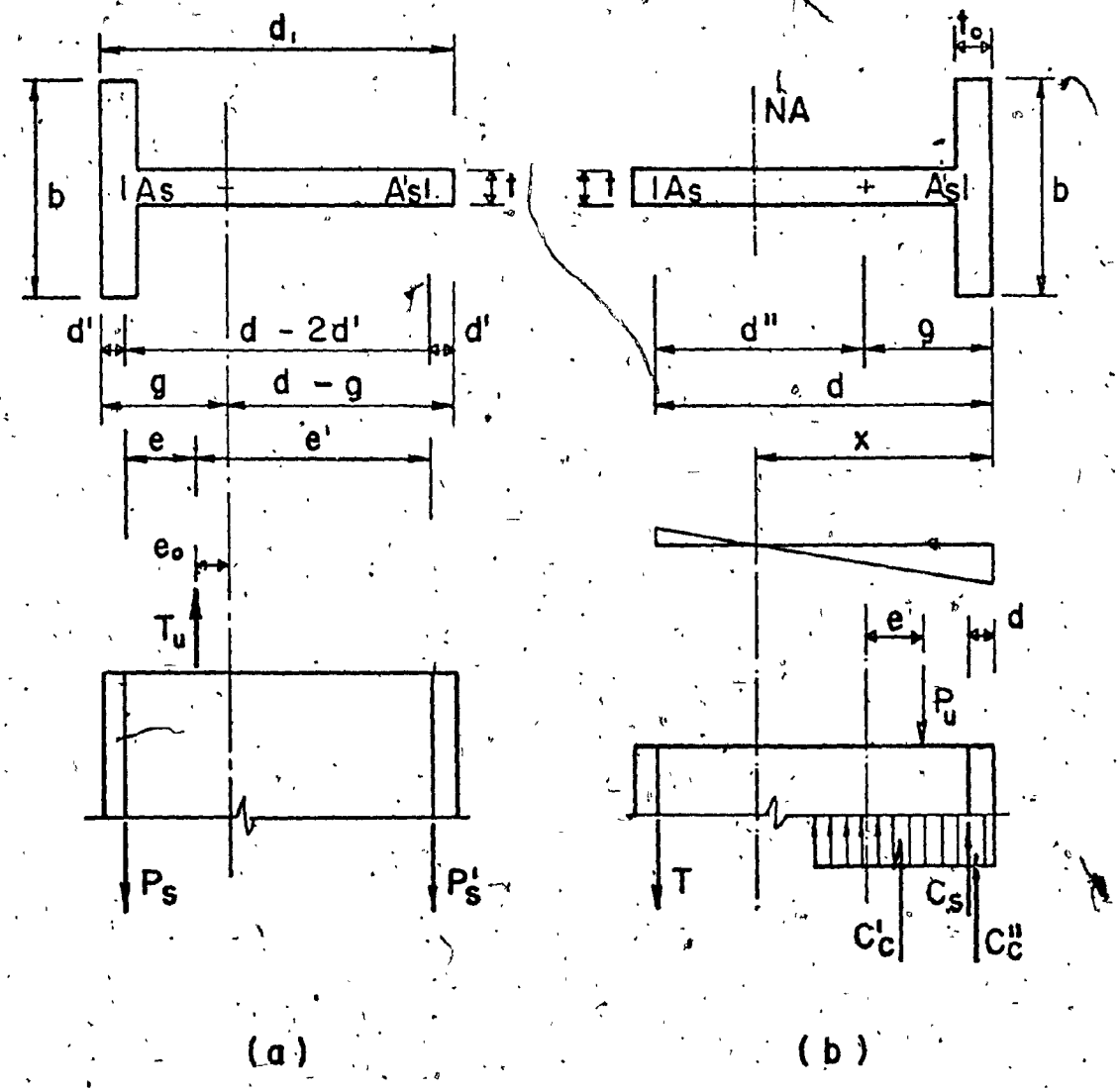

FIG. C1 - Moment-axial force interaction for small eccentricity: (a) tension in wall 1; (b) compression in wall 2.

Force equilibrium requires:

$$P_u = C_c' + C_c'' + C_s - T \tag{C1}$$

where the internal forces C_c', C_c'', C_s and T are expressed by:

$$C_c' = .85\, f_c'\, t(\beta x)$$

$$C_c'' = .85\, f_c'\, (b - t)t_o$$

$$C_s = A_s'(fy - .85\, f_c')$$

$$T = A_s\, f_s$$

$$\frac{\varepsilon_c}{x} = \frac{\varepsilon_s}{d - x}$$

$$f_s = \frac{E_s\, \varepsilon_c (d - x)}{x}$$

Rotational equilibrium of the forces is satisfied by taking moments about the applied force P_u:

$$C_s(g - e - d') + C_c''(g - e - \frac{t_o}{2}) - C_c'(\frac{a}{2} - g + e) + \tag{C2}$$

$$+ T(d'' + e) = 0$$

By substituting the values for C_c', C_c'', C_s and T and arranging the results, it is found that:

$$x^3 - F_1x^2 - F_2x - F_3 = 0 \tag{C3}$$

where:

$$F_1 = \frac{2(g - e)}{\beta}$$

$$F_2 = \frac{2[R - A_s E_s \varepsilon_c (d'' + e)]}{.85 f'_c t \beta^2}$$

$$F_3 = \frac{2A_s E_s \varepsilon_c (d'' + e)d}{.85 f'_c t \beta^2}$$

$$R = A'_s(f_y - .85f'_c)(g - e - d') +$$

$$+ .85f'_c(b - t)t_o(g - e - \frac{t_o}{2})$$

The above equation can be solved by using the known procedure for solving a cubic equation or else using one of the numerical methods when a computer is available. In this study the Newton-Raphson numerical procedure was used. All other quantities once x is known are readily found.

C1.2 Large Eccentricity -- "Tension Controls"

C1.2.1 Compression Steel Yields

This is the case when the ultimate capacity P_u is less than the balanced value P_b or the eccentricity e is greater than the balanced value e_b. The ultimate strain of the steel most distant from the neutral axis will be greater than the yield strain $\varepsilon_y = f_y/E_s$. According to Figure C2(b), forces C'_c C''_c C_s and T are:

$$C''_c = 0.85 f'_c (b - t)t_o$$

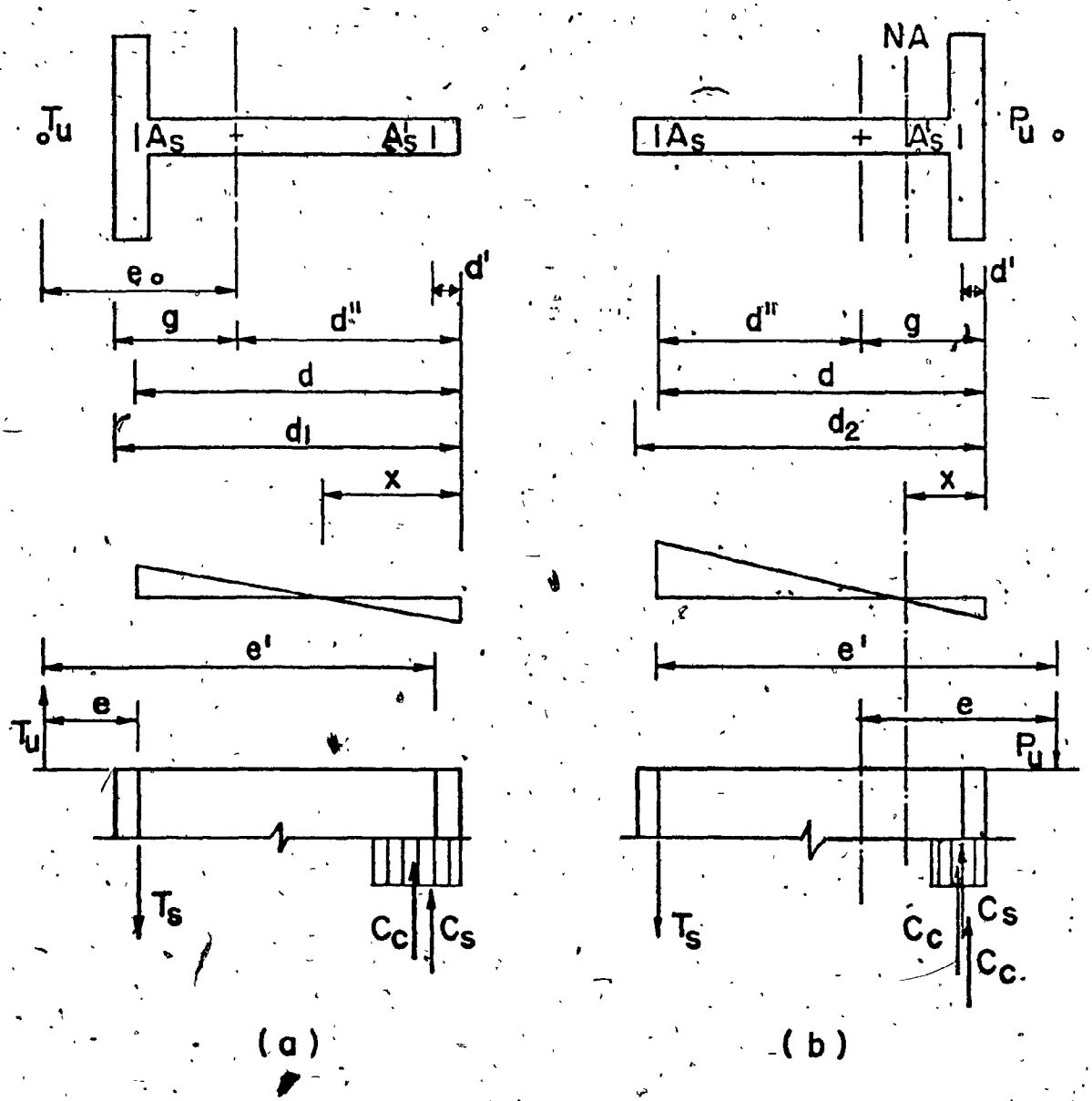

FIG. C2 - Moment-axial force interaction for large eccentricity: (a) tension in wall 1; (b) compression in wall 2.

$$T = A_s f_y$$

$$C_c' = 0.85\, f_c' (\beta x) t$$

$$C_s = A_s' (f_y - .85 f_c')$$

From force equilibrium:

$$P_u = (C_c' + C_c'') + C_s - T \qquad (C4)$$

From moment equilibrium with respect to the tension steel:

$$P_u e' = C_c''(d - \frac{t_o}{2}) + C_c'(d - \frac{\beta x}{2}) + C_s(d - d') \qquad (C5)$$

Substituting the values for C_c', C_c'', C_s and T into Eqs. (C4) and (C5), and solving for x, gives:

$$x^2 + F_1 x + F_2 = 0$$

where:

$$F_1 = \frac{2(e' - d)}{\beta}$$

$$F_2 = \frac{2 R_3}{0.85 f_c' \beta_1 t}$$

$$R_3 = R_1 e' - R_2$$

$$R_1 = 0.85 f_c' (b - t) t_o + A_s' (f_y - .85 f_c') - A_s f_y$$

$$R_2 = 0.85 f_c' (b - t) t_o (d - \frac{t_o}{2}) + A_s' (f_y - .85 f_c')(d - d')$$

The solution of the above quadratic equation is:

$$x = \frac{-F_1 + \sqrt{F_1^2 - 4F_2}}{2} \qquad (C6)$$

With x known all other quantities are defined.

C1.2.2 Compression Steel Does not Yield

In case when the eccentricity e is large and the neutral axes is in position $x < 2d'$ the compression reinforcement cannot yield before the extreme concrete fiber reaches its ultimate capacity defined by yield strain $\varepsilon_c = 0.003$.

By equating strains:

$$\frac{\varepsilon_c}{x} = \frac{\varepsilon'_s}{x - d'}$$

from which:

$$\varepsilon'_s = \frac{\varepsilon_c (x - d')}{x}$$

The stress in the compression steel is therefore:

$$f'_s = \frac{E_s \varepsilon_c (x - d')}{x}$$

The forces T, C'_c, C''_c and C_s are:

$$T = A_s f_y$$

$$C'_c = 0.85 f'_c (\beta x) t$$

$$C_c'' = 0.85\, f_c'\, (b - t)\, t_o$$

$$C_s = A_s'(f_s - 0.85\, f_c')$$

Force equilibrium requires:

$$P_u = C_c' + C_c'' + C_s - T \qquad (C7)$$

and taking the moment equilibrium about the tension steel gives:

$$P_u e' = C_c''(d - \frac{t_o}{2}) + C_c'(d - \frac{\beta x}{2}) + C_s(d - d') \qquad (C8)$$

The position of the neutral axis can be found by substituting the values for C_c', C_c'', C_s and T into the Eqs. (C7) and (C8).

After rearranging of the results the cubic equation for x is found:

$$x^3 - F_1 x^2 - F_2 x - F_3 = 0 \qquad (C9)$$

where:

$$F_1 = \frac{2(e' - d)}{\beta}$$

$$F_2 = \frac{2[R_2 + 87A_s'(e' - d + d')}{0.85\, f_c' t \beta^2}$$

$$F_3 = \frac{2A_s'\, 87(e' - d + d')d'}{0.85\, f_c' t \beta^2}$$

$$R_2 = R_1 e' - 0.85\, f'_c (b - t) t_o \left(d - \frac{t_o}{2}\right) +$$

$$+ 0.85\, f'_c A'_s (d - d')$$

$$R_1 = 0.85\, f'_c (b - t) t_o - 0.85\, f'_c A'_s - A_s f_y$$

It is obvious from the above that, in investigating the ultimate strength of a T-section in bending and axial compression, knowledge of the neutral axis location is of paramount importance.

If the neutral axis occurs at a distance t_o/β from the top surface of the flange and, on the basis of the assumption that a concrete stress intensity of $0.85\, f'_c$ is distributed over an equivalent compression zone of $\beta x b$, the T-section is to be investigated as a rectangular section.

The investigation of a rectangular section in bending and axial compression has received extensive attention in the literature to date [11] and will not be presented here.

C2 BENDING AND AXIAL TENSION-RECTANGULAR SECTION

C2.1 Small Eccentricity

From Figure C1(a), when $e_o \leq g - d'$, the following relations between the ultimate force P_u and the section properties can be derived:

$$e = g - e_o - d'$$

$$e' = d_1 - g - d' + e_o$$

where:

$$e_o = \frac{M}{T_u}$$

From moment equilibrium with respect to A_s and A'_s:

$$T_u e = P'_s (d - d') \qquad (C10)$$

$$T_u e' = P_s (d - d')$$

where:

$$P'_s = A'_s f_y$$

$$P_s = A_s f_y$$

By substituting the values of P'_s and P_s in Eq. (C10), and solving for T_u, two conditions are obtained for strength:

$$T_{u_1} = \frac{A'_s f_y (d - d')}{e} \qquad (C11)$$

$$T_{u_2} = \frac{A_s f_y (d - d')}{e'}$$

C2.2 Large Eccentricity

C2.2.1 Compression Steel Yields

This case is similar to bending and axial compression of rectangular section when the compression steel yields.

According to Figure C2(a) and by satisfying force and the moment equilibrium the location of the neutral axis can be found from:

$$T_u = T - C_c - C_s \qquad (C12)$$

$$Te = C_s e' + C_c\left(e_o + d_1 - g - \frac{\beta x}{2}\right) \qquad (C13)$$

where:

$$T = A_s f_y$$

$$C_c = 0.85\, f'_c(\beta.x)t$$

$$C_s = A'_s(f_y - 0.85\, f'_c)$$

Substituting the expressions for T, C_c and C_s into Eqs. [12] and [13] solving for x and arranging the results yield :

$$x^2 - F_1 x + F_2 = 0$$

where:

$$F_1 = \frac{2[d_1 - g + e_o]}{\beta}$$

$$F_2 = \frac{2R_6}{0.85\, f'_c t\beta^2}$$

$$R_4 = A_s f_y - A'_s\,(f_y - 0.85\, f'_c)$$

$$R_5 = T(g - d') + C_s d''$$

$$R_6 = R_4 e_0 - R_5$$

The solution of the above equation is given by:

$$x = \frac{F_1 + \sqrt{F_1^2 - 4F_2}}{2} \qquad (C15)$$

With x known, all other equations are readily determined.

C2.2.2 Compression Steel Does Not Yield

In this case internal force resultants are:

$$T = A_s f_y$$

$$C_s = A_s' f_s'$$

$$C_c = 0.85\, f_c' (\beta x) t$$

From the strain distribution diagram:

$$\frac{\varepsilon_s}{x - d'} = \frac{\varepsilon_y}{d - x}$$

$$f_s' = \frac{f_y (x - d')}{d - x}$$

From force and moment equilibrium:

$$T_u = T - C_s - C_c \qquad (C16)$$

$$T_u e = C_c \left(d_1 - d' - \frac{\beta x}{2}\right) + C_s (d - d') \qquad (C17)$$

By substituting values for T, C_s and C_c into Eqs. (C16) and (C17), solving for x and rearranging the results lead to the position of the neutral axis given by:

$$x^3 - F_1x^2 - F_2x + F_3 = 0 \qquad \text{(C18)}$$

where:

$$F_1 = 2(e + d)$$

$$F_2 = \frac{2R_4}{E_c\epsilon_y t}$$

$$R_4 = A_s f_y e + A'_s f_y (e + d - d')$$

$$F_3 = \frac{2R_5}{E_c\epsilon_y t}$$

$$R_5 = A_s f_y de + A'_s f_y d' (e + d - d')$$